

Anna Katharina Lämmerer, BSc

The Role of Lipid Droplets in Cancer Therapy Response

MASTER´S THESIS

to achieve the university degree of

Diplom-Ingenieurin

Master´s degree program: Biotechnology

submitted to

Graz University of Technology

Supervisor

Assoc. Prof. Dipl.-Ing. Dr. techn. Harald Pichler

Institute of Molecular Biotechnology

Graz, March, 2019

This Master's Thesis was conducted at the

Medical University of Vienna

Department of Medicine I

Institute of Cancer Research

Applied and Experimental Oncology

And was supervised by

Univ. Prof. Dr. Walter Berger

Bernhard Englinger, MSc, PhD

AFFIDAVIT

I declare that I have authored this thesis independently, that I have not used other than the declared sources/resources, and that I have explicitly indicated all material which has been quoted either literally or by content from the sources used.

The text document uploaded to TUGRAZonline is identical to the present master's thesis.

Date

Signature

Abstract

Acquired resistance to chemotherapy as well as targeted therapy with e.g. tyrosine kinase inhibitors (TKIs) represents a major obstacle in the “war against cancer”. Lipid droplets (LDs), initially considered as simple fat depots, are increasingly recognized as highly diverse cell organelles playing an important role in distinct cellular pathways. Several studies pinpoint LDs as cellular reservoir of lipids for the generation of energy and acting as building blocks of membrane structures, but also suggest a role as accumulation site for lipophilic drugs.

This thesis analyzed the underlying molecular mechanisms for the specific accumulation of ponatinib, a multi-targeted lipophilic TKI, to intracellular LDs in fibroblast growth factor receptor 1 (FGFR1)-driven lung cancer cell lines, in order to uncover new targets to by-pass TKI resistance in this cell line. Therefore, we examined the transcriptional distinctions of a lung cancer cell line and their ponatinib-resistant subline. The ponatinib-resistant subline was characterized by higher expression of the microsomal triglyceride transfer protein (*MTTP*, MTP). Moreover, the resistant subline exhibited distinctly higher intracellular lipid levels. Accordingly, MTP was knocked down and pharmacologically inhibited, which resulted in even increased resistance towards ponatinib. Moreover, we studied the impact of a “lipoid” cell compartment on cancer cell survival upon ponatinib treatment. Ponatinib uptake by adipocytes clearly limited the cytotoxic potential of ponatinib. Also, the effect of chemical ponatinib derivatization on subcellular distribution was investigated. Finally, the impact of the LD status on other anticancer compounds was studied in a cell line panel consisting of nine different cancer cell lines. These data showed that several anticancer compounds were less active in LD-enriched cancer cells which was, however, independent of their lipophilicity.

To conclude, LDs as well as a lipophilic phenotype decreased the activity of ponatinib and might represent promising targets to overcome cancer cell resistance. Moreover, LDs influence not only the activity of lipophilic drugs but also from hydrophilic drugs. Together, the generated data suggests a critical role of lipids in the biodistribution of ponatinib. On the one hand, the lipogenic phenotype of cancer cells may hamper the activity of this drug. On the other hand,

adipose tissue is expected to considerably alter ponatinib pharmacokinetics via direct drug scavenging.

Zusammenfassung

Erworbene Resistenz gegenüber Chemotherapie als auch gezielter Krebstherapie mit z.B. Tyrosinkinase Inhibitoren (TKI) ist ein wesentliches Hindernis im „Kampf gegen Krebs“. Lipid droplets (LD), ursprünglich als einfache Fett-Depots betrachtet, werden jüngst als funktionell diverse Zellorganellen angesehen, die eine wichtige Rolle in verschiedenen zellulären Vorgängen spielen. Mehrere Studien präzisieren die Funktion von LD als Reservoir für lipophile Substanzen, sowie Energiespeicher und Baustofflieferant für Krebszellen.

Die zugrundeliegenden molekularen Mechanismen für die spezifische Anhäufung von Ponatinib, einem lipophilen multi-TKI, in intrazellulären LD einer Fibroblasten-Wachstumsfaktorrezeptor(FGFR1)-getriebenen Lungenkrebszelllinie wurden analysiert, um möglicherweise neue Angriffspunkte zur Überwindung der TKI-Resistenz zu finden. Dafür wurde nach transkriptionellen Unterschieden zwischen der parentalen Lungenkrebszelllinie und ihrer Ponatinib-resistenten Sublinie gesucht. Dies ergab für die Ponatinib-resistente Sublinie eine Überexpression des mikrosomalen Triglyceride-Transferproteins (*MTTP*, MTP). Weiters fanden sich in der resistenten Sublinie ein deutlich erhöhtes Lipidlevel. Folglich wurde MTP pharmakologisch gehemmt und ein Knockdown durchgeführt. Ferner wurde der Einfluss eines fettähnlichen Zellkompartiments auf das Krebszellenüberleben gegenüber Ponatinib erforscht. Der chemische Effekt auf die subzelluläre Verteilung von Ponatinib wurde anhand von Derivaten analysiert. Letztlich wurde der Einfluss des LD Zustands auf andere Krebsmittel in neun verschiedenen Krebszelllinien geprüft.

Zusammengefasst resultierte eine MTP-Inhibierung überraschenderweise in einer intrazellulären Zunahme von Ponatinib und LD in Lungenkrebszellen. Weiters limitierten Adipozyten deutlich die zytotoxische Wirkung von Ponatinib. Die zytotoxische Wirkung als auch die intrazelluläre Verteilung von Ponatinib wurden stark von der chemischen Struktur beeinflusst. Darüber hinaus zeigten mehrere Krebsmittel eine geringere Wirkung in LD-angereicherten Krebszellen.

Abschließend verringerten sowohl LD als auch ein lipophiler Phänotyp die Wirkung von Ponatinib, was vielversprechende Ansatzpunkte repräsentiert, um

eine Resistenz zu umgehen. Überdies wurde gezeigt, dass LD nicht nur die Aktivität von lipophilen, sondern auch von hydrophilen Krebsmitteln hemmen. Die entstandenen Daten deuten also auf eine wichtige Rolle von Lipiden in der Biodistribution von Ponatinib hin. Einerseits ist eine verminderte Ponatinib-Aktivität durch den lipogenen Phänotyp von Krebszellen zu erwarten. Andererseits könnte Fettgewebe die Pharmakokinetik von Ponatinib durch direkte Akkumulation deutlich beeinflussen.

“Life is...a chemical incident.”

(Paul Ehrlich, 1870)

Acknowledgement

First of all, I would like to thank Univ. Prof. Dr. Mag. Walter Berger for giving me the opportunity to work with his great team. I would like to acknowledge especially Börns - Bernhard Englinger, MSc, PhD, for being such a great, cheerful and inspiring mentor! I would also like to thank Claudia Kieler for introducing me to this group. To all other lab members, Dina Baier, Carina Dinhof, Dominik Kirchhofer, Sushilla van Schoonhoven, Lisa Gabler, Daniela Lötsch-Gojo, Christine Pirker, Mirjana Stojanovic, Lukas Uhlik, Patrick Moser, Philipp Kroiss, Brian Parkinson, Alessia Stefanelli, Gerhard Zeitler, Johannes Gojo, Carola Jaunecker, Kerstin Fürnweiger, Magdalena Hübner, Hannah Schmidt, Mery La Franca, Petra Lapsanka, Thomas Mohr and Petra Heffeter, thank you for all the helpful tips and tricks and patient support. It was great working with all of you. I would also like to thank Gerald Timelthaler, who did the Definiens quantification. For synthesizing all derivatives, I would like to thank Dipl.-Ing. Marlene Mathuber and Ass.-Prof. Mag. Dr. Christian Kowol from the Department of Inorganic Chemistry at the University of Vienna. Additionally, I would like to thank Mag. Dr. Clemens Röhrl from the Institute of Medical Chemistry and Pathobiochemistry at the Medical University of Vienna for his lipid analyses.

Furthermore, I am greatly thankful for Assoc. Prof. Dipl.-Ing. Dr. techn. Harald Pichler, who supervised my thesis at Graz University of Technology.

A very special gratitude goes to my parents for giving me the opportunity to study without any financial worries, to study even abroad and, most important, always providing me with home-made care-packages! Furthermore, I would like to thank my brother - my first scientific idol -, for always being the guiding, helping hand I can always count on. You all know how much this thesis focusing on cancer means to me – I am so grateful for all your support!!!

“Graciés” to Miguel for cheering me up, always trying to understand what scientific things I am talking about, standing by my side, motivating me and being here with me.

Table of Contents

AFFIDAVIT	V
Abstract	VII
Zusammenfassung.....	IX
Acknowledgement.....	XIII
1. Introduction	1
1.1. Etiology of cancer	1
1.2. The hallmarks of cancer	2
1.3. Cancer incidence and mortality	4
1.4. Cancer therapy	5
1.4.1. Surgery	6
1.4.2. Chemotherapy	6
1.4.3. Radiotherapy	6
1.4.4. Immunotherapy.....	7
1.4.5. Hormone therapy	8
1.4.6. Targeted therapy	8
1.5. Lung cancer	9
1.5.1. Incidence and mortality of lung cancer	9
1.5.2. Etiology of lung cancer	11
1.5.3. Lung cancer therapy.....	12
1.6. Ponatinib.....	13
1.7. Fibroblast growth factor receptor (FGFR).....	13
1.8. FGFR-signaling pathways	15
1.8.1. Ras-Raf-MAPK pathway.....	15
1.8.2. PI3-AKT pathway.....	16
1.8.3. PLC γ pathway	16
1.8.4. Jak-STAT pathway	16
1.9. Lipid droplets (LDs).....	17
1.9.1. Structure of LDs.....	17
1.9.2. LD formation	18
1.9.3. Function of LDs	19
1.9.4. LDs and cancer cells	21
2. Aim of the study	23
3. Materials and methods.....	24
3.1. Materials	24

3.1.1.	Cell lines.....	24
3.1.2.	Chemicals and solutions for cell culture.....	25
3.1.3.	Chemicals and solutions for transfection experiments.....	26
3.1.4.	Fluorescent stains.....	27
3.1.5.	Drugs.....	28
3.1.6.	Buffers and solutions.....	29
3.2.	Methods.....	32
3.2.1.	Cell culture.....	32
3.2.2.	Cell-conditioning experiments.....	34
3.2.3.	Cell proliferation and viability assay.....	35
3.2.4.	Comparative genomic hybridization.....	38
3.2.5.	Differentiation of 3T3-Fibroblasts into Adipocytes.....	39
3.2.6.	Fatty acid uptake determination.....	39
3.2.7.	Flow cytometry.....	40
3.2.8.	Ponatinib imaging in tissue cryosections.....	42
3.2.9.	Live-cell microscopy.....	43
3.2.10.	Lipid content analysis.....	44
3.2.11.	Microscopy.....	45
3.2.12.	mRNA expression array.....	49
3.2.13.	Protein isolation and determination of concentration.....	49
3.2.14.	RNA isolation and real-time quantitative PCR (qPCR).....	50
3.2.15.	Transfection.....	53
3.2.16.	Western blot analysis.....	54
3.2.17.	Statistical analyses.....	57
4.	Results.....	58
4.1.	Co-culture experiments and ponatinib imaging.....	58
4.1.1.	Generation of mCherry expressing NCI-H1703 cells.....	58
4.1.2.	Ponatinib is fluorescent and accumulates in lipid droplets (LDs).....	59
4.1.3.	Differentiation of fibroblasts (3T3-L1/F) into adipocytes (3T3-L1/A).....	60
4.1.4.	Co-culture experiments of cancer cells with 3T3-L1/F or 3T3-L1/A.....	61
4.1.5.	Cell-conditioning experiments.....	66
4.1.6.	Ponatinib imaging in tissue cryosections.....	71
4.2.	LDs as ponatinib resistance mechanism.....	77
4.2.1.	Lipid levels are increased in ponatinib resistant sublines.....	77
4.2.2.	The role of MTP.....	80
4.3.	Characterization of ponatinib derivatives.....	90
4.3.1.	Effect of chemical modifications on ponatinib toxicity.....	90

4.3.2.	Effect of chemical modifications on subcellular distribution of ponatinib	93
4.4.	LDs as resistance mechanism in other cancer cell lines	98
4.4.1.	Drug-specific effects	98
4.4.2.	Cell-specific effects	106
5.	Discussion	110
5.1.	Adipocytes reduce ponatinib availability and mediate cancer cell survival	111
5.2.	Ponatinib uptake is detectable in cryosections	112
5.3.	Lung cancer cells acquire resistance to ponatinib via a lipogenic phenotype switch and overexpression of MTP	114
5.4.	Ponatinib derivatization strongly influences the intracellular distribution and impairs the cytotoxic activity of ponatinib	116
5.5.	Drug- and cell-specific LD-dependent resistance	117
	List of Figures	119
	List of Tables	127
	Abbreviations	128
	References	133

1. Introduction

1.1. Etiology of cancer

Cancer is a disease of chaos and a collapse of the former biological instruction within the body [1]. The World Health Organization (WHO) defines cancer as a large set of diseases, with more than 100 different cancer entities, characterized by cells showing rapid, bounderless and abnormal growth [2, 3]. Furthermore, cancer cells have the ability to spread throughout the whole body, even to disseminate into surrounding or distant organs and tissues called metastasis [2, 4]. These cell abnormalities are due to specific changes in the genomic sequence that lead to alterations in transcriptional programs which drive cancer cells into endlessly making more copies of themselves [1].

Evolution continually creates new versions of genes by altering the genetic information, to generate maybe advanced and improved phenotypes. A mutation of gene information can happen in germ cells or somatic cells. The first one is characterized by mutation of a gene present in the genome of sperm or egg or in precursors thereof, thus transmitting the mutant alleles from one organism to its offspring. In contrast, somatic mutations affect the relative single somatic cells. In case the systems of damage and repair fail, these mutations will be given on to their descendant cells. In terms of histopathology, tumors are classified as benign or malignant, the latter one being able to metastasize [1]. This metastatic tumor stage accounts for the most cancer-related deaths [4].

Physical, chemical as well as viral agents (e.g. human papilloma virus) can cause cancer [1]. A variety of risk factors for cancer include behavioral exposures like tobacco use, little physical activity, unhealthy diet and alcohol consumption, but also environmental factors [5, 6]. Worldwide different factors are associated with particular risks. While in Africa and Asia potent carcinogens in the food are triggers for the impact of food on cancer incidence, in high-income countries energy-rich food with low physical activity or obesity play a major role [6].

1.2. The hallmarks of cancer

The transformation of normal cells into highly malignant cancer cells is a multistep process, like hastened evolution, driven by genetic alterations that finally dictate growth advantage and further independency [7]. The human body consists of 10^{13} cells highlighting the presumably high chance of alterations in the proliferation of just one cell [1]. For understanding the acquired capabilities responsible for tumor formation and its invasiveness, Hanahan and Weinberg postulated the six essential hallmarks of cancer in the year 2000 [3]. These hallmarks comprise:

- evading growth suppressors
- enabling replicative immortality
- resisting cell death
- sustaining proliferative signaling
- inducing angiogenesis
- activating invasion and metastasis [3]

Mechanisms relevant for this thesis are addressed in the following lines. Cancer cells are characterized by a loss of control in the production and release of growth-enhancing signals. They are capable of producing growth factor ligands by themselves (autocrine proliferative stimulation) or provoke normal cells within their surroundings to supply them. Furthermore, cancer cells can number up receptor proteins on their surface, by changing the structure of the receptor molecule, causing hyper responsiveness for the corresponding growth factor ligand. Ligand independent signaling might also occur by activation of signaling pathway members downstream of the receptor [7].

Furthermore, cancer cells activate neo-angiogenesis (sprouting of new vessels), an integral hallmark, amongst other functions in order to ensure continuous nutrient supply as well as to remove metabolic waste. Chronically elevated expression of members of the fibroblast growth factor (FGF) family leads to maintained angiogenesis of tumors. The transit of cancer cells throughout the human body is enabled by alterations in cell shape and cell-cell adhesion as well as attachment to the extracellular matrix (ECM), which drives the cells to invade and disseminate. For epithelial cells, this program is termed as epithelial-

mesenchymal transition (EMT) and is normally activated during embryogenesis but hijacked by transformed epithelial cells. Crucial for colonization of cancer cells after dissemination is their ability to adapt to new tissue microenvironments [7].

Later on, the two emerging hallmarks, avoiding immune destruction and deregulating cellular energetics, as well as the two enabling hallmarks, tumor-promoting inflammation and genome instability and mutation, were added (Figure 1). The latter involves increased incidence of mutation and increased vulnerability towards mutagenic compounds with simultaneous defects in the maintenance and repair of genomes of cancer cells. The second enabling hallmark, tumor-promoting inflammation, describes the role of the innate immune system as tumor-promotor. By supplying tumors with growth factors, survival signals, proangiogenic elements or EMT-activating signals, inflammatory cells help cancer cells to obtain hallmark capabilities. Furthermore, cancer cells outsmart the immune system by secreting immunosuppressive factors, representing one of the emerging hallmarks. Finally, cancer cells have an altered energy metabolism. By upregulation of glucose transporters for aerobic glycolysis they fuel -amongst other things- the generation of nucleosides and amino acids which function as building blocks for enhanced proliferation [7].

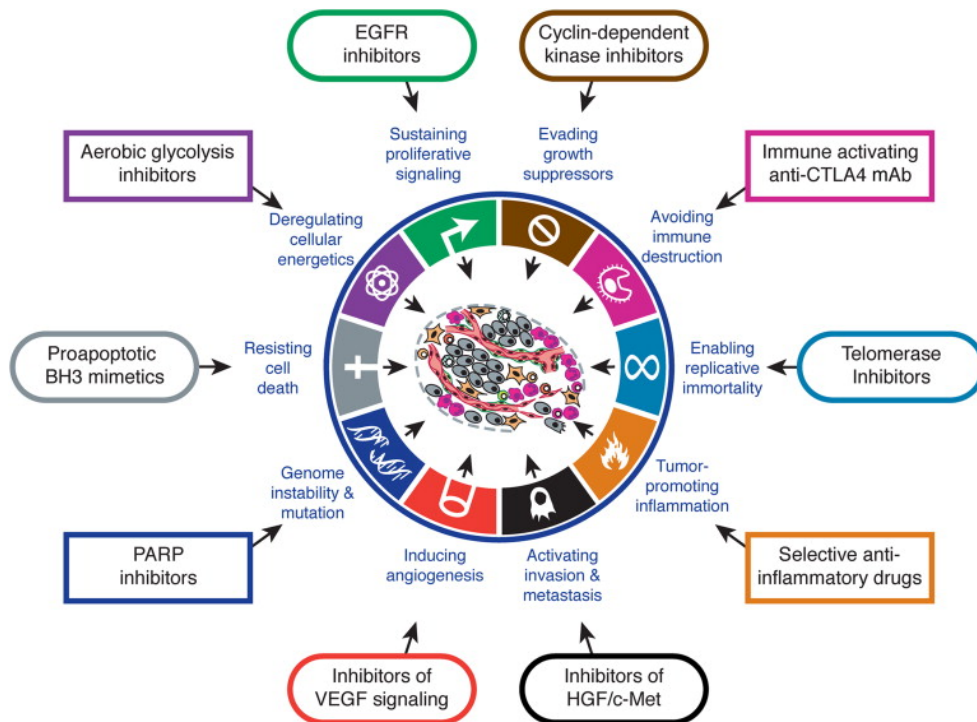


Figure 1: The ten hallmarks of cancer with their respective therapeutic targeting strategies. Illustration of the six hallmarks postulated in 2000 as well as the enabling characteristics and emerging hallmarks defined in 2011. Drugs that target these hallmarks are depicted [7].

1.3. Cancer incidence and mortality

In Austria, the number of new cancer cases (incidence) will increase by the year 2030 to 43,706 (representing an increase by 14 %) [8]. Worldwide, cancer is ranked as the second leading cause of death. For the year 2018, 18 million new cancer cases and 9.6 million cancer-related deaths have been estimated (Figure 2) [2]. In countries with low- or middle income, late-stage diagnosis and poor health care display important factors for worse cancer outcomes [2].

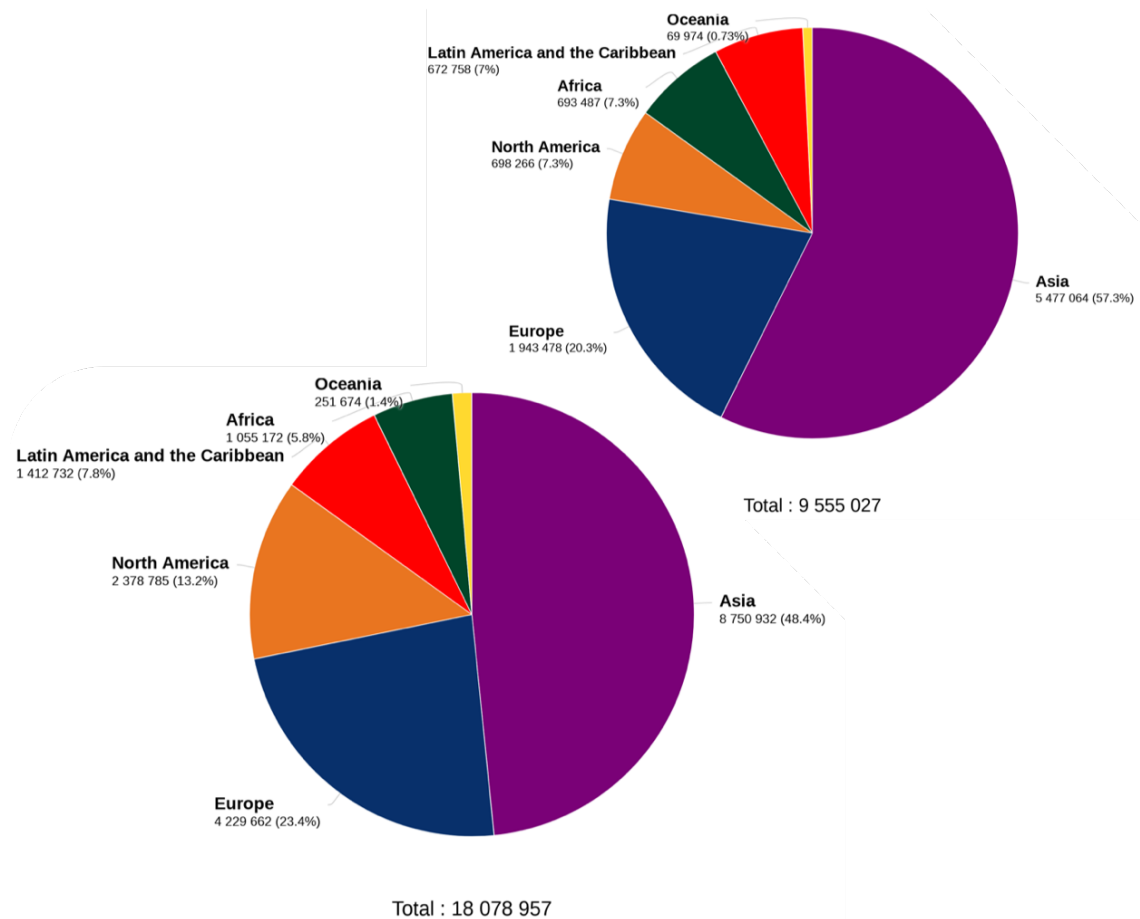


Figure 2: Estimated number of new cases (left) and deaths (right) worldwide in 2018 related to all cancer types, sexes and ages. Adapted from Globocan 2018 [9].

1.4. Cancer therapy

This chapter gives an overview of the classic cancer therapy strategies involving surgery, chemotherapy and radiotherapy, and new treatment approaches. Although all of them aim to eliminate tumors, some of them, especially certain classical chemotherapeutics as well as radiotherapy, turned out to be a double-edged sword, harboring carcinogenic side effects with the potential of leading to second-site tumors. These side effects could often be understood only a long time after the introduction of the respective strategy or compound into the clinic, since the underlying biochemical and cell-biological mechanisms have been discovered late or are still unknown. In contrast to this, the development of new anti-cancer drugs is more precisely, molecularly targeted in order to ensure selective killing of cancer cells while minimizing the damage to healthy tissue [1].

1.4.1. Surgery

Removing small primary tumors before they expand into large tumors is the concept of surgical oncology [1]. Surgery can be performed as cryotherapy, where the cancer tissue is eradicated by extreme cold, or rather the opposite, called hyperthermia (killing by heating), which besides of killing the cancer cells can make them more sensitive to other therapy strategies. Additionally, modern surgery is also complemented by lasers or photodynamic drugs that become activated by a certain type of light [10].

1.4.2. Chemotherapy

For chemotherapy, pharmaceuticals with the ability to kill highly proliferative cancer cells are administered to patients [11]. Chemical analogs, so-called antimetabolites, interfere with biological metabolites and essential cellular enzymatic reactions. Another class of chemotherapeutics disrupts cytoskeleton homeostasis. A very important class is constituted by DNA-interacting or -alkylating agents, leading to an inhibition of transcription and replication. They have often been discovered from products of plants, molds and animals [1]. For example, paclitaxel, approved for AIDS-related Kaposi sarcoma, breast cancer, non-small cell lung cancer (NSCLC) and ovarian cancer, was isolated from the tree *Taxus brevifolia*. Its anti-cancer potency results from its ability to bind to tubulin, thus inhibiting the reassembly of microtubules, which results in a mitotic catastrophe and cell death [1, 12, 13]. Unfortunately, cancer cells have been shown to become resistant to the majority of anti-cancer drugs. Hence, multi-drug protocols have been developed combining various drugs with distinct targets, showing very often synergism with striking results [1].

1.4.3. Radiotherapy

Radiotherapy is used for focused burning down or shrinking of delineated tumors by damaging the tumor DNA or for reducing the risk of metastatic relapse in the area of the tumor after initial surgery or chemotherapy [1, 14]. Radiotherapy can be carried out externally or internally by applying so-called radiopharmaceuticals

(a radiation source) inside of the body. Very often, radiotherapy is combined with other cancer therapies and can be carried out before, during or after these treatments [14].

1.4.4. Immunotherapy

Lately, a huge effort is being made to prime the patient's own immune system for cancer defense. One strategy, so-called active immunotherapy, involves immunization against the tumor via preventive or curative vaccination [1, 15]. Another attractive approach, passive immunotherapy, comprises supplementation with antibodies, that specifically bind to neo-antigens present on the abnormal cell surface and recruit phagocytic or killer cells that further lead to the destruction of this cell [1, 15]. An example for the latter strategy is trastuzumab, approved for early HER2-positive breast cancer. It targets HER2, a transmembrane receptor which is found at abnormally high numbers in breast cancer cells. Trastuzumab is a monoclonal antibody specifically targeting HER2, and shows eminent efficacy, however, it is recommended to administer the antibody in combination with chemotherapy or postoperative [16].

Attempts are also being made to design smart antibodies, consisting of antibody molecules that are joined with chemotherapeutic drugs or radioactive particles. Another approach is to link antibodies with enzymes capable of activating simultaneously injected pro-drugs in the tumor mass [1, 15]. A fascinating form of immunotherapy are the so-called CAR-T cells, therapeutic, genetically engineered T-lymphocytes (specialized cytotoxic cells belonging to the adaptive arm of the cellular immune system) expressing synthetic chimeric antigen receptors (CARs). These CARs have an antigen-binding domain linked to T-cell activating elements [1, 17]. Anti-CD19 CAR-T cell therapy reached almost 80 % remission in hematological cancer types like refractory acute lymphoblastic leukemia (ALL) and diffuse large B-cell lymphoma [17].

Other examples for passive immunotherapy are immune checkpoint inhibitors. The immune system disposes of various inhibitory mechanisms (checkpoints) that downregulate immune responses. Some of them are hijacked by cancer cells for immune resistance. One immune-inhibitory pathway associated protein is the

programmed cell death protein 1 (PD1), which is activated by ligands (PDL1) from cancer cells to avoid activation of T-cells. Elevated expression of PDL1 is known for lung cancer cells, as well as other cancer types [18].]. Drugs that block PDL1 or the corresponding PD1 on T-cells depict a highly effective approach to boost the immune system in regard to antitumor response and has resulted in significantly improved patient outcome in several cancer types [18, 19]. Tasuku Honjo, who discovered PD1 and worked on its blockade, and James P. Allison, who studied another immune checkpoint, CTLA-4, were awarded the Nobel Prize in 2018 [20].

1.4.5. Hormone therapy

If a cancer type strongly depends on hormones, hormone therapy can make the tumors shrink or destroy them. Additionally, hormone therapy can be applied as adjuvant therapy by reducing the risk of the cancer recurrence [21]. Especially, breast and prostate cancer may be highly driven by the steroid hormones estrogen and testosterone. Hormone therapy, either preventing steroid biosynthesis or inhibiting the respective receptor function, has become a standard therapy for receptor-positive cancer types [22].

1.4.6. Targeted therapy

Targeted therapy is often administered to patients with cancers that are inoperable or resistant to chemo- and/or radiotherapy and is a precision medicinal approach [23, 24]. A variety of targeted drugs are cytostatic and block the tumor cell division. In contrast to standard chemotherapeutics, which kill all rapidly dividing cells, targeted drugs act on proteins that are only present on cancer cells or overactive cellular growth- and survival promoters (oncoproteins), in order to reduce the activity either of the oncoprotein itself or its downstream effectors. Druggable targets are e.g. kinases, which often act as oncoproteins and have targetable catalytic clefts of their respective kinase domains. Especially, tyrosine kinases play a major role in many cancer types [1, 24, 25]. Targeted therapy modalities are small-molecule inhibitors, targeting molecules inside the cell, or monoclonal antibodies (e.g. trastuzumab see chapter 1.4.4 Immunotherapy)

which are used in hormone- and immunotherapy [24]. However, resistance to targeted inhibitors represents an urgent problem of cancer therapy. Hence, combining targeted drugs with other agents may improve their efficacy [23].

FGFRs (see chapter 1.7 Fibroblast growth factor receptor (FGFR)) are dysregulated in cancer cells, being aberrantly hyperactivated via e.g. overexpression and activating mutations, and, thus, representing an attractive candidate oncoprotein for targeted therapy. Small molecule FGFR kinase inhibitors are currently the most used modality for targeting FGFR and are classified into FGFR1/2/3 inhibitors, selective FGFR4 inhibitors, pan- or multi-kinase FGFR inhibitors [23].

1.5. Lung cancer

1.5.1. Incidence and mortality of lung cancer



Figure 3: Illustration of environmental and lifestyle factors as major contributors to lung cancer development by Russel Cobb. Adapted from [26].

Worldwide, lung cancer accounts for most of the cancer-related deaths (Figure 4) [9]. As a sadly fact, this cancer type is also the most preventable one, with

tobacco smoking being strongly linked to the epidemic of lung cancer and for instance associated with the deaths of at least 3,000 people per day in China [26, 27]. As early as 1950, R. Doll and A. B. Hill reported a higher risk of lung cancer for heavy smokers than for nonsmokers [28]. Lung cancer incidence reaches its highest point in the elderly due to the fact that the disease manifests decades after smoking initiation [29]. Tobacco is used by 1.3 billion people all over the world, mostly men. While the number of smokers in most high-income countries is declining, the number is estimated to rise in middle- and low-income countries [6]. In comparison to other European countries, Austria has one of the highest smoking rates. Especially in women, smoking prevalence is increasing [6, 30]. While lung cancer incidence and mortality in Austria over the last 30 years have declined in men, incidence and mortality remain on the rise in women, reflecting the later onset of both smoking and cessation among women [29, 30]. Lung cancer is also occurring among nonsmokers, albeit at greatly reduced rates. Also, air pollution, comprising coal smoke, asbestos, dust and transportation contamination as well as genetic factors are potent triggers [26]. This is illustrated by the fact that about 25 % of lung cancer patients worldwide smoked less than 100 cigarettes throughout their lives. There is evidence that fine particles with diameters less than 2.5 micrometers play a major role as carcinogen [26].

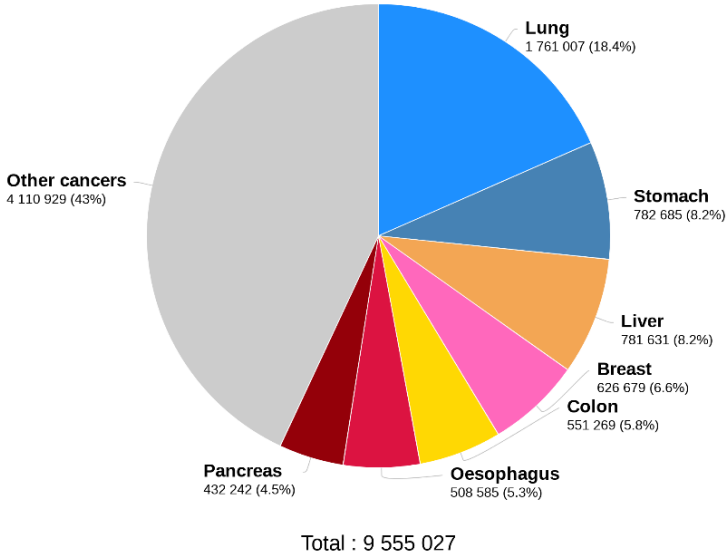


Figure 4: Estimated number of cancer-caused deaths worldwide in 2018 related to tissue of origin. Adapted from Globocan 2018 [9].

1.5.2. Etiology of lung cancer

Lung cancer is classified into non-small-cell lung cancer (NSCLC), accounting for approximately 85 % of all cases, and small-cell lung cancer (SCLC) [26, 31, 32]. There exist further three subcategories of NSCLC: adenocarcinoma, squamous cell carcinoma and large cell carcinoma [26]. In Austria, adenocarcinomas, arising from secreting epithelial cells, are surpassing squamous cell carcinomas, generated by epithelial cells forming protective layers [1, 30, 31]. Non-smokers are often diagnosed with adenocarcinoma, while squamous cell carcinoma and SCLC are strongly associated with smoking. In addition, lung cancer of never-smokers bears less mutational load. In many cases the epidermal growth factor receptor (EGFR) is mutated in non-smokers, and these patients respond better towards small-molecule tyrosine kinase inhibitors. Nevertheless, also never-smokers are frequently diagnosed at late stage of cancer, at least partially owing to the extended unspecific symptoms in the course of disease progression in combination with infrequent routine medical exams [26].

NSCLC is described as cancer with genetic heterogeneity and of cellular diversity. In squamous cell carcinoma, amplification of fibroblast growth-factor receptor 1 (FGFR1) has been identified [33]. Furthermore, genes for transcription and splicing factors can be altered in NSCLCs [31]. For the highly lethal SCLC, exhibiting a 5-year survival rate of 5 %, several somatic mutations have been described. For instance, FGFR1 amplification occurs in 6 % of SCLC cases [34].

Interaction with the ECM, immune cells, fibroblasts or other cells in the tumor microenvironment is essential for lung cancer cells [31]. It was revealed that tumor-associated macrophages foster lung cancer cells neovascularization by release of angiogenesis-promoting factors [35, 36]. Other immune cells support cancer progression by degradation of matrix proteins [36]. Further, there exist tumor-associated fibroblasts, which secrete factors that promote growth of the tumor [37]. This dynamic tumor microenvironment is in focus of many ongoing targeted therapies [19]. Another theory suggests that lung stem cells with their high proliferative capacity might be prototumorigenic, lacking only a permanent mutation that transforms them into tumor cells. However, better understanding of

these cells and involved processes is necessary for targeted-therapy development [27].

1.5.3. Lung cancer therapy

The most effective method to reduce lung cancer mortality is early diagnosis. The potential of lung cancer screening with low-dose computed tomography is currently analyzed in the European NELSON trial [19]. Standard treatment of SCLC and NSCLC involves surgical resection at early disease stage and platinum-based chemotherapy [31, 38]. For SCLC, chemoradiotherapy with cisplatin or carboplatin, as well as etoposide is the standard of care [38]. However, after an initially good response, SCLC especially rapidly becomes therapy-resistant, leading to high relapse rates [32, 38].

Genomic profiling studies like The Cancer Genome Atlas (TCGA) Research Network and targeted mutation analyses, in combination with the growing list of targeted drugs, have introduced advanced and personalized treatment strategies [19]. Subsets of SCLC and NSCLC have been reported to bear genetic amplification of FGFR1 [31, 38]. Specific targeted inhibitors have been developed, e.g. the clinically approved multi-TKIs nintedanib (approved for NSCLC in Europe), ponatinib (approved for BCR-ABL-positive leukemia, compare chapter 1.6 Ponatinib), or several preclinical compounds such as PD173074, showing good results *in vitro* and *in vivo* [34]. However, there is evidence that chronic treatment with targeted inhibitors often results in acquired resistance development. Moreover, the common belief that targeted inhibitors might have less side effects and are less harmful does not appear to match reality, due to the fact that many targeted pathways are not only crucial in malignant cells but also for the proper functioning of normal cells. Hence, finding new strategies for these resistant tumors, targeting rather the tumor-promoting microenvironment such as the tumor vasculature or tumor associated fibroblasts or immune cells, depict important research topics [31]. Success of immunotherapy has already been reported for NSCLC with at least 50 % PD1-expressing tumor cells. The human monoclonal PD1-antibody, pembrolizumab, showed significantly longer overall survival than platinum-based chemotherapy

[39]. Potent new integrated treatment strategies combine a combination of immunotherapy with anti-angiogenic drugs, targeted metabolic inhibitors, and also with classical chemotherapeutic agents [31, 40].

1.6. Ponatinib

Ponatinib, imidazo[1,2-b]pyridazine or commercially called Iclusig, is a Food and Drug Administration (FDA)-approved highly potent, multi-targeted tyrosine kinase inhibitor (TKI) for leukemia with the Philadelphia chromosome (Ph). More precisely, ponatinib is indicated for patients with ALL, that is Ph-positive and carries the T315I mutation and for patients suffering chronic myelogenous leukemia (CML) that also has the T315I mutation [12, 13, 41-44].

Ponatinib was discovered by computational and structure-based drug designing [43]. A phase II study revealed adverse effects of ponatinib, like thrombocytopenia (37 %), with an increased risk of bleeding and vascular occlusion (23 %). Serious adverse effects included increased lipase (2 %) and fatal liver failure. This led to an abrupt, temporal suspension of the clinical development of ponatinib. However, at the moment, for many patients, there is no alternative drug as potent as ponatinib for the above-mentioned indications. Because ponatinib targets the BCR-ABL fusion protein that often confers resistance to other TKIs, the drug was finally reintroduced to the market as a third line drug for patients for whom no other TKIs show efficacy [41, 42, 44].

Ponatinib also showed activity against 40 other kinases, e.g. kinase domains of FGFRs. Ponatinib was able to inhibit the growth of 14 different, FGFR-dysregulated cancer cell lines, including lung cancer cells. Consequently, ponatinib is also tested in clinical trials for its activity in adenocarcinoma, SCLC and NSCLC [44].

1.7. Fibroblast growth factor receptor (FGFR)

The formation of tissues and organisms requires intercellular communication, based on cells emitting biological messages in form of signaling peptides or proteins (e.g. growth factors) to other cells. Recipient cells sense these signals

via receptor proteins which become activated and convey the signal into the cell interior through biochemical modification of effector proteins, e.g. via phosphorylation of cytoplasmic proteins by tyrosine kinases [1]. Fibroblast growth factors (FGFs), 22 in number, bind to FGFR and activate their intracellular tyrosine kinase domains, which elicits cellular responses such as fibroblast proliferation and others. In general, FGF signaling is diverse in ligands and receptors and regulates important functions like embryonic development, tissue homeostasis, wound healing and tissue regeneration. Abnormal FGF signaling is typical in lung, breast, bladder and prostate cancer [45]. Enhanced FGFR signaling is achieved by mutations (mediating constitutive activation), receptor amplification (leading to FGFR overexpression) and chromosomal translocations (oncogenic fusions resulting in hyper activated receptors via ligand dependent or -independent mechanisms). Furthermore, autocrine (by the tumor cell itself) and paracrine (by stromal cells) signaling plays an important role [46, 47].

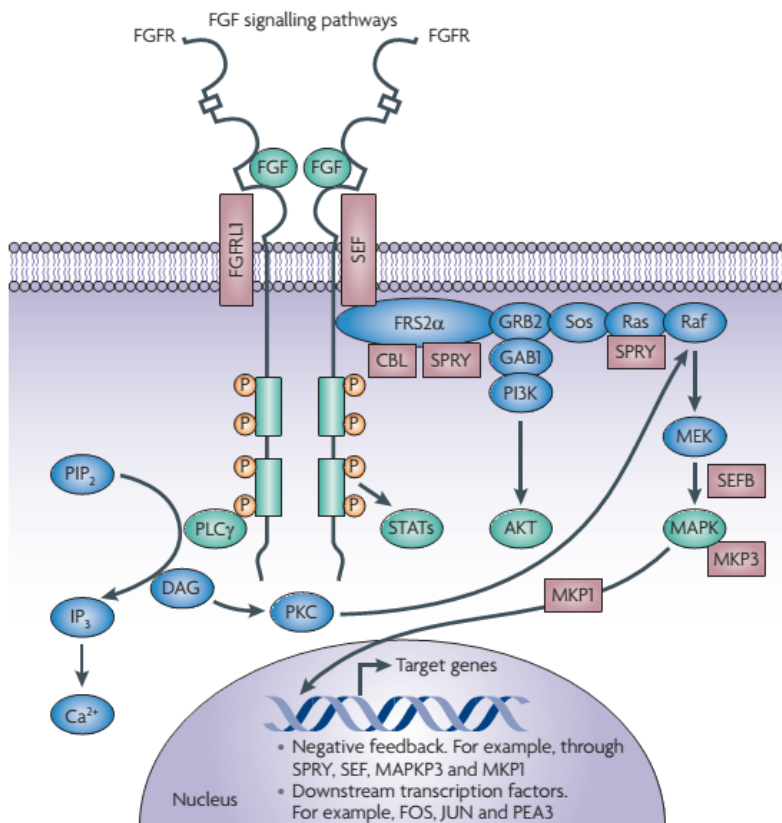


Figure 5: Fibroblast growth factor (FGF) signaling pathways. FGFs bind to FGF receptor (FGFR) and induce receptor dimerization, cross-phosphorylation of the kinase domains and binding of several proteins that activate downstream pathways (RAS-RAF-MAPK, PI3-AKT, STAT and PLCγ). Adapted from [47].

The FGFRs belong to the immunoglobulin family and form a group of four transmembrane receptor tyrosine kinases (FGFR1-4) that have an extracellular domain for FGF (ligand) binding, a transmembrane domain and an intracellular tyrosine kinase domain [45, 46, 48]. Upon binding of FGF, dimerization causes a conformational change and cross-phosphorylation of the kinase domains is promoted. Hence, the downstream effector molecule FGFR substrate 2 (FRS2) binds via its phosphotyrosine-binding domain (Scr-homology, Sh2 domain) to the phosphorylated sites and gets phosphorylated itself. Consequently, the complex of sevenless (SOS) and growth factor receptor-bound 2 (GRB2) binds to phosphorylated FRS2 and activates a cascade of intracellular events (Figure 5) [46, 47]. After activation, the signaling is negatively regulated, e.g. via tyrosine phosphatases and FGFR are internalized for further degradation or recycling [47].

1.8. FGFR-signaling pathways

Downstream of FGFR, a cascade of intracellular events and the following pathways are activated: Ras-Raf-MAPK, PI3-AKT, PLC γ and Jak-STAT [45, 46].

1.8.1. Ras-Raf-MAPK pathway

SOS becomes anchored to FGFR via GRB2, thus getting well positioned nearby membrane-anchored Ras, which consequently gets activated. Ras, a small GTPase (G protein), having the ability to bind and hydrolyze guanosine nucleotides. In its inactivated state, Ras binds to a GDP molecule, while when it exchanges the GDP for a GTP molecule, Ras becomes activated and its effector loop can interact with Raf kinase (MAPKKK). Thereby, Raf proceeds to phosphorylate MEK kinase (MAPKK), which further activates extracellular signal-related kinases 1 and 2 (Erk1 and Erk2, MAPKs). Phosphorylated Erk 1 and Erk 2 can further phosphorylate cytoplasmic substrates or translocate to the nucleus for transcription factor activation. This kinase cascade, where phosphorylation results in a functional activation of a kinase, is called mitogen-activated protein kinase (MAPK) pathway [1]. The downstream signaling of MAPK results predominantly in cell proliferation [47].

1.8.2. PI3-AKT pathway

Eukaryotic cells exploit a special phospholipid from the membrane as second messenger. By addition of phosphate groups to phosphatidylinositol, the resulting molecules can be used to attract cytosolic proteins. Phosphatidylinositol-3-kinase (PI3K) phosphorylates phosphatidylinositol-(4,5)diphosphate (PIP2) to phosphatidylinositol-(3,4,5)-trisphosphate (PIP3). Akt or also called protein kinase B, a serine/threonine kinase, recognizes PIP3 and binds to it via a pleckstrin homology (PH) domain. Hence, Akt becomes activated and phosphorylates several downstream proteins. One important function of this pathway is its pro-survival activity. Hence, Akt inhibits cell death by deactivating apoptosis-stimulating proteins [1].

1.8.3. PLC γ pathway

Phospholipase C- γ (PLC γ) is able to cleave PIP2 into two potent cell proliferation stimulating molecules: diacylglycerol (DAG) and inositol (1,4,5)-triphosphate (IP3). This occurs, when PLC γ is brought into close proximity with the plasma membrane through tethering to its receptor via its Sh2 domain [1].

1.8.4. Jak-STAT pathway

Tyrosine kinases of the Janus kinase (Jak) class are not covalently bound to the receptor molecule. Once the receptor dimerizes upon ligand binding, the Jaks cross-phosphorylate each other and the C-terminal parts of the receptor. This attracts STATs (signal transducers and activators of transcription) which, as a consequence, also become phosphorylated by Jaks. Further, this leads to dimerization of STATs and the dimers translocate to the nucleus, directly acting as transcription factors [1].

1.9. Lipid droplets (LDs)

1.9.1. Structure of LDs

Lipid droplets (LDs), also called lipid bodies, fat bodies or adiposomes, are present in nearly all organisms, from bacteria up to mammals. Hepatocytes, heart and skeletal muscle cells may contain high numbers of LDs [49, 50]. LD size ranges from less than 1 μM in yeasts to 10-100 μM in adipocytes [51]. They are heterogeneous in terms of composition and function [49]. However, they were mainly believed to serve as reservoir of lipids for membrane synthesis and energy storage. This storage function is of great importance when fatty acids are present in high concentrations, which could make them potentially toxic detergents unless they are esterified [49, 51]. LDs have a protein-decorated, amphipathic phospholipid monolayer, with phosphatidylcholine as abundant phospholipid in mammalian cells, and a neutral lipid core (Figure 6) [49, 52]. This hydrophobic interior contains mostly triacylglycerols (TAG) and sterol esters. LD-associated proteins contain amphipathic α -helices and/or hydrophobic hairpins in their structure [51]. Caveolin and diacylglycerol acetyltransferase 2 (DGAT2) represent decorative proteins that localize on one hand to the lipid droplets and on the other to the plasma membrane or endoplasmic reticulum (ER) membrane, respectively [49]. Also other proteins, like members of the PAT family (perilipin, adipose differentiation related protein/ADRP and tail-interacting protein of 47 kDa/Tip47) localize to LDs: whereas Tip47 is found on diminutive droplets, perilipin, expressed in adipocytes and steroid producing cells, localizes to large LDs [49, 52, 53]. Additionally, several membrane trafficking proteins (Rabs), lipid synthesizing (acetyl CoA carboxylase) or lipid hydrolyzing enzymes (lipases) and signaling proteins can be located on LDs, highlighting the active role of LDs in cellular homeostasis [50, 54]. Recently, the protein-décor in various organisms was estimated to exist of approximately 200 different proteins [50].

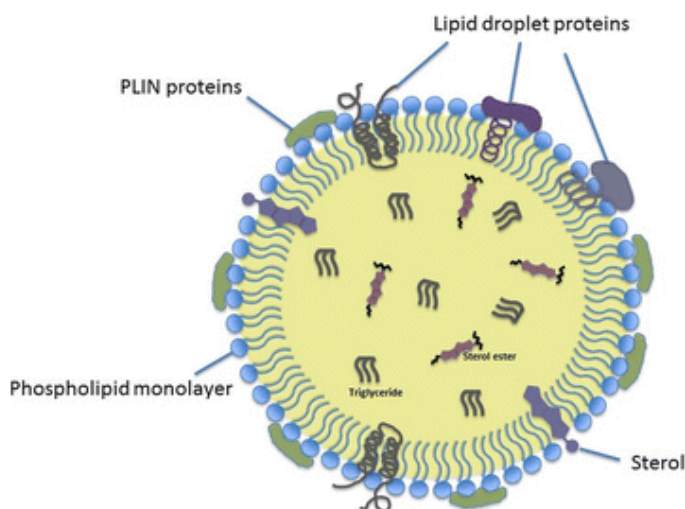


Figure 6: Structural composition of lipid droplets (LDs). LDs have a phospholipid monolayer decorated with proteins e.g. perilipin (termed PLIN proteins) and a core containing neutral lipids (triglycerides and sterol esters). Adapted from [50].

1.9.2. LD formation

When cells are exposed to elevated fatty acid (FA) levels, LDs are generated rapidly [53]. In eukaryotes, the ER seems to play an important role as LD-birthplace. As mentioned before, DGAT2, an enzyme catalyzing TAG synthesis, is localized to the ER, pointing towards the ER as hotspot for lipid transfer and synthesis. But also, mitochondria and mitochondria-associated membranes, which are often found close to LDs, may provide NADPH for TAG synthesis and LD formation [49, 55]. Beside the ER and mitochondria, LDs are also found close to endosomes, lysosomes, autophagosomes and the plasma membrane [54, 56]. Free FAs get activated by acyl-CoA synthetase. The resulting fatty-acyl-CoA is converted by glycerol-3-phosphate acyltransferase (GPAT) into MAG, and by acylglycerophosphate acyltransferase (AGPAT) and phosphatidic acid phosphatase (PAP) into DAG. In a final step, a TAG is synthesized by DGAT [50, 54]. In contrast, sterols are endocytosed or obtained from lysosomally degraded lipoproteins [54].

Further, there are several models for LD biogenesis. The leading theory represents formation of LDs as a result of accumulated neutral lipids in the ER membrane, finally leading to budding of a droplet. Another model postulates that LDs are excised from the ER as bicelle, however leaving the question how the integrity of the ER membrane is restored remains unresolved. There exists also

the concept of vesicular budding, in which LDs are formed within small bilayer vesicles in a certain domain of the ER. Remaining parts of the vesicle could then fuse with the outer layer or be included within the droplet, representing an explanation for the evidence of hydrophilic proteins in the hydrophobic core. LDs then grow either through fusion or with help of ER-located proteins like DGAT2, which favors an increase in the volume, or the microsomal triglyceride transfer protein (*MTTP*, MTP), which moderates the transfer of neutral lipids in the ER [49]. When LDs are not connected to the ER, growth occurs by proteins and lipids that are transported to the LDs [54].

In mammalian cells, adipocytes represent a highly specialized form of LDs. While in mature adipocytes LDs appear rather static, they appear highly dynamic in other systems [49, 53]. Several of the proteins found on LDs have functions in vesicular transport and cytoskeletal mobility [53]. LDs can move through interactions with the ER and other compartments via GTPases, Rabs and caveolins. Their movement is also facilitated by microtubules and happens in a coordinated way [49, 53].

1.9.3. Function of LDs

When FAs are rare, LDs get dispersed and neutral lipids are metabolized or liberated for membrane synthesis [51, 53]. To generate energy (ATP), neutral lipids get hydrolyzed into FAs (Figure 7) which can further be activated to acyl-CoA and oxidized in the mitochondria [49, 54]. Intracellular lipases balance the amount of neutral lipids in LDs and are regulated by lipolytic and antilipolytic hormones [49, 57]. This lipolysis happens at basal levels but can be increased by phosphorylation of perilipin and hormone-sensitive lipase (HSL) via cyclic-AMP-dependent protein kinase A (PKA) [49, 53, 54]. Besides this lipolysis-promoting capacity, perilipin also protects triglycerides from hydrolysis in its non-phosphorylated condition [52]. Recently, also another lipase, the adipose triglyceride lipase (ATGL) was discovered to be localized to adipocytic LDs. This ATGL gets activated by a cofactor that depends on phosphorylation of perilipin and converts a TAG into a DAG. Consequently, the DAG is hydrolyzed by HSL to monoacylglycerol (MAG), which is in a final step hydrolyzed to glycerol and a

FA by the MAG lipase (MGL). Sterol esters are converted by HSL [51, 57]. While ATGL seems to be constitutively present on LDs, HSL is recruited to the LD surface from the cytoplasm [57].

LDs also play an important role in regulating the cholesterol level by storing excess cholesterol as cholesterol esters [53]. In obesity, characterized by exorbitant number of accumulated fats, excess numbers and increased sizes of LDs occur. This is also observed for type 2 diabetes, hepatic steatosis, atherosclerosis and other diseases [49, 57].

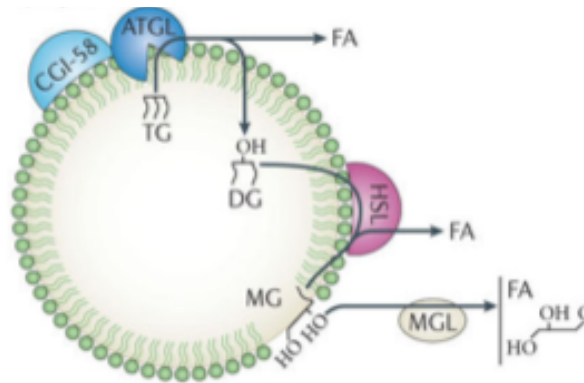


Figure 7: Lipolysis of lipid droplets (LDs). Triacylglyceride (TAG) hydrolysis is catalyzed by adipose triglyceride lipase (ATGL), which leads to release of free fatty acids (FA) and diacylglycerol (DAG). Subsequently, DAG hydrolysis is catalyzed by hormone-sensitive lipase (HSL), which leads to free FA and monoacylglycerol (MAG). In turn, MAG lipase (MGL) hydrolyses MAG into free FA and glycerol. Adapted from [51].

In the liver and intestinal cells, secretion of lipoproteins filled with triglycerides is mediated by apolipoprotein B (apoB). ApoB is essential for the formation of very-low density lipoprotein 2 (VLDL2) and gets lipidated by MTP in the ER lumen. It is thought that cytosolic LDs present in the lumen of involved pathways fuse with apoB, in order to further lipidate VLDL2 into VLDL1 in the Golgi apparatus before it gets secreted. Thus, the accumulation of cytosolic LDs is strongly related to the formation of VLDL1 (Figure 8) [52].

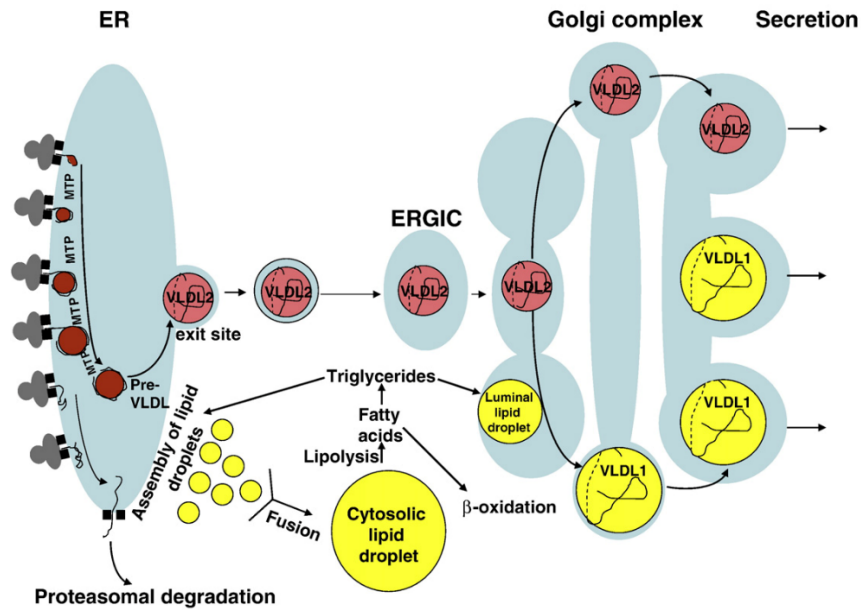


Figure 8: Assembly and secretion of very-low density lipoprotein (VLDL). Apolipoprotein B (ApoB) is lipidated in the endoplasmic reticulum (ER) by the microsomal triglyceride transfer protein (MTP) to form primordial lipoprotein (pre-VLDL). Pre-VLDL is further lipidated and exits the ER. In the ER Golgi intermediate compartment (ERGIC) the VLDL2 is sorted and further promoted to enter the secretory pathway. Cytosolic lipid droplets (LDs) provide triglycerides for further lipidation to VLDL1 before it is secreted. Adapted from [52].

Apart from serving as reservoir for lipophilic drugs, LDs store unfolded proteins and fat-soluble vitamins, suggesting for autophagy pathways in LDs [50, 51, 54]. Also, histones, which are required in early embryogenesis, were identified as major LD proteins in *Drosophila* embryos. There is also evidence that LDs are hijacked as platforms for the replication of hepatitis C virus, dengue virus and *Chlamydia trachomatis*. Thus, LDs represent also a therapeutic target [49, 50]. Insufficient or increased lipid storage is also typical in neurodegenerative diseases and cancer development [56]. Finally, in plant science, LDs are also of great interest for the industrial production for foods and biofuels [49].

1.9.4. LDs and cancer cells

Cancer cells might compensate their need for lipids as biomass and building blocks by increased generation of LDs [58]. Count and volume of LDs are a biomarker for breast cancer aggressiveness. Thus, alterations in LD content in tumors can be considered as hallmark of breast cancer aggressiveness [59, 60]. The number and size of LDs as well as ADRP expression are increased in various

CHAPTER ONE: INTRODUCTION

cancer types [60]. Moreover, *de novo* lipid synthesis, leading to lipid saturation in the plasma membrane, is associated with chemoresistant cancer cells. Prostate, breast and ovarian cancer have been shown to be highly dependent on LDs, which contribute to resistance towards paclitaxel and platinum-containing drugs as well as hormone-related drugs [61-63]. One explanation for this chemoresistance might be drug sequestration in LDs. Recently, it was also observed that LDs in colon cancer were associated with resistance towards erlotinib [64]. Measuring the LD load in tumors might thus represent an emerging tool for predicting treatment response in patients [59].

2. Aim of the study

Resistance of cancer cells towards chemo- and targeted therapy is a main obstacle of anticancer therapy. LDs, the major lipid storage organelle, serves as central hub between membrane biosynthesis and energy homeostasis. In various cancer types, lipid metabolic reprogramming and increased LD amounts are associated with aggressiveness and chemo-resistance. Preliminary results from our lab point to a selective accumulation of the lipophilic multi-RTK ponatinib in LDs, underpinning the role of LDs in cancer therapy resistance.

The aim of this thesis was to identify the underlying mechanisms determining compartmentalization of ponatinib to intracellular LDs. Furthermore, the role of the tumor microenvironment, in particular “lipoid” cells, on ponatinib activity was investigated. Moreover, ponatinib derivatives were synthesized in order to investigate the effect of chemical derivatization on the cellular distribution and anticancer activity. A special focus was laid also on the impact of the LD status in a selected cancer cell line panel on the efficacy of other anticancer compounds.

Methods included co-culture experiments to investigate whether “lipoid” cell types (adipocytes) foster cancer cell survival upon ponatinib treatment. Further, the distribution of ponatinib was studied in tissue cryosections of orally treated mice. Transcriptional distinctions of a parental FGFR1-driven lung cancer cell line and its ponatinib-resistant subline were assessed by whole-genome expression analysis and qRT-PCR. The cell killing potential of ponatinib derivatives was assessed in MTT assays. Subcellular distribution of these derivatives was investigated with CLSM. Additionally, the physico-chemical properties of anticancer compounds found in databases were compared to their cell viability response in various LD-induced cancer cell lines, in order to pinpoint key parameters for LD accumulation.

3. Materials and methods

3.1. Materials

3.1.1. Cell lines

The following table gives an overview of human cancer cell lines and the murine cell line used in this study.

Table 1: List of distinct human cancer cell lines and the murine cell line utilized during this study.

Cell Line	Tissue	Specification	Company
A2780	Human ovarian carcinoma		Sigma-Aldrich
CAPAN-1	Human pancreas carcinoma		ATCC
DMS114	Human small cell lung carcinoma		ATCC
DMS114/PON	Human small cell lung carcinoma	Ponatinib-resistant subline	ICR
HCT116	Human colon carcinoma		ATCC
HeLa	Human cervix carcinoma		ATCC
HepG2	Human hepatoblastoma		ATCC
HT1376	Human urinary bladder carcinoma		ATCC
MCF7	Human mamma carcinoma		ATCC
NCI-H520	Human non-small cell lung carcinoma		ATCC
NCI-H1703	Human non-small cell lung carcinoma		ATCC
NCI-H1703/PON	Human non-small cell lung carcinoma	Ponatinib-resistant subline	ICR

Cell Line	Tissue	Specification	Company
NCI-H1703/ mCherry	Human non-small cell lung carcinoma	pQCXIP-mCherry-IRES-Puro plasmid transfected subline	ICR
PC3	Human prostate adeno carcinoma		ATCC
U87MG	Human glioblastoma		ATCC
3T3-L1	Mouse embryonic fibroblasts	Chemical-inducible differentiation into adipocytes	ATCC

ATCC: American Type Culture Collection, Manassas, USA; ICR: Institute for Cancer Research, Vienna, Austria; Sigma-Aldrich, St. Louis, USA;

3.1.2. Chemicals and solutions for cell culture

Listed in Table 2 are all chemicals and solutions used during this thesis project for cell culture.

Table 2: Chemicals utilized for differentiation of 3T3-L1 fibroblasts into adipocytes, for lowering lipids and induction or reduction of lipid droplet formation in different cell lines.

Compound	Remarks	Usage	Company
3-Isobutyl-1-Methylxanthine (IBMX)	inhibits cAMP and cGMP phosphodiesterase, leading to decreased proliferation, increased differentiation, and induction of apoptosis	pro-differentiative agent for 3T3-L1 fibroblasts	Sigma-Aldrich
Dexamethasone	anti-inflammatory glucocorticoid	pro-differentiative agent for 3T3-L1 fibroblasts	Sigma-Aldrich

Compound	Remarks	Usage	Company
Insulin	stimulates lipogenesis and supports adipocyte differentiation <i>in vitro</i> ^{a)}	pro-differentiative agent for 3T3-L1 fibroblasts	Sigma-Aldrich
Lomitapide	inhibits microsomal triglyceride transfer protein (MTP)	MTP inhibitor	Sigma-Aldrich
Oleic Acid-Albumin from bovine serum	solubilized form of oleic acid	induction of lipid droplets	Sigma-Aldrich
Triacsin C	inhibits long fatty acid acyl-CoA synthetase	compromises formation of lipid droplets	Biomol

Biomol: Biomol GmbH, Hamburg, Germany; Sigma-Aldrich, St. Louis, USA

^{a)} Klemm, D. J. *et al.*, Insulin-induced adipocyte differentiation. Activation of CREB rescues adipogenesis from the arrest caused by inhibition of prenylation. *The Journal of biological chemistry* 276, 28430-28435, doi:10.1074/jbc.M103382200 (2001).

3.1.3. Chemicals and solutions for transfection experiments

Table 3 lists the small interfering ribonucleic acids (siRNAs) and plasmids used for knockdown experiments during this master thesis project.

Table 3: siRNAs and plasmids used for transfection of cancer cells.

siRNA/plasmid	Specification	Company
siGENOME Non-Targeting siRNA Pool #1	negative control siRNA that targets no known genes in human, mouse, or rat	Dharmacon
ON-TARGETplus Human MTP siRNA	siRNA for silencing MTP (Microsomal triglyceride transfer protein)	Dharmacon

siRNA/plasmid	Specification	Company
pQCXIP-mCherry-IRES-Puro plasmid	plasmid carrying a red fluorophore and a puromycin resistance cassette	ICR

Dharmacon, Colorado, USA; ICR: Institute for Cancer Research, Vienna, Austria

Indicated in Table 4 are the reagents necessary for each transfection method used for this thesis.

Table 4: List of transfection reagents used for this study and their respective provider.

Reagent	Transfection method	Company
Xfect transfection polymer + reaction buffer	Lipofection	Clontech
Lipofectamine 2000 reagent	Lipofection	Invitrogen

Clontech: Clontech Laboratories, Inc.; Mountain View, USA; Invitrogen, Carlsbad, USA

3.1.4. Fluorescent stains

Fluorescent stains that were used throughout this study are given in Table 5.

Table 5: Fluorescent dyes that were used for specific staining of cells.

Stain	Specification	Company
Bodipy 493/503	green fluorescent dye for lipids, membranes and other lipophilic compounds	Thermo Fisher
Propidium iodide solution	nuclear counterstain	Sigma-Aldrich
TRITC-labeled phalloidin	actin cytoskeleton stain	Sigma-Aldrich

Sigma-Aldrich, St. Louis, USA; Thermo Fisher Scientific, Waltham, USA

3.1.5. Drugs

In this study, chemotherapeutics were classified into antimetabolites, DNA-interacting agents, spindle poisons, molecularly targeted agents and topoisomerase inhibitors. Indicated in Table 6 are all drugs used during this study.

Table 6: Classification of drugs used in this study and their respective provider.

Drug	Company
Antimetabolites	
5-Fluorouracil (Adrucil)	Ebewe Pharma
Gemcitabine (Gemzar)	ChemWerth Inc.
Methotrexate (Trexall)	Ebewe Pharma/Flukatec
DNA-interacting agents	
Cisplatin (Platinol)	Ebewe Pharma
Cyclophosphamide (Cytophosphane)	Sigma-Aldrich
Dacarbazine	Sigma-Aldrich
Doxorubicin (Adriamycin)	Ebewe Pharma
Oxaliplatin (Eloxatin)	Selleckchem
Temozolomide (Temodar)	Selleckchem
Trabectedin (Yondelis)	PharmaMar
Spindle poisons	
Docetaxel (Taxotere)	LC Laboratories
Paclitaxel (Taxol)	Sigma-Aldrich

Drug	Company
Molecularly targeted agents	
Crizotinib (Xalkori)	LC Laboratories
Gefitinib (Iressa)	LC Laboratories
Lapatinib (Tykerb)	LC Laboratories
Olaparib (Lynparza)	LC Laboratories
Ponatinib (Iclusig)	Selleckchem
Regorafenib (Stivarga)	Selleckchem
Sorafenib (Nexavar)	LC Laboratories
Temsirolimus (Torisel)	Selleckchem
Topoisomerase inhibitor	
Irinotecan (Camptosar)	LC Laboratories

ChemWerth, Woodbridge, USA; Ewebe Pharma Ges.m.b.H. Nfg.KG, Austria; LC Laboratories, Woburn, USA; PharmaMar, Madrid, Spain; Selleckchemicals, Houston, USA; Sigma-Aldrich, St. Louis, USA

3.1.6. Buffers and solutions

10 x TBS

120 g Tris

90 g NaCl

Filled up to 1 L with ddH₂O

pH adjusted to 7.6

1 x TBST

100 mL 10 x TBS

Filled up to 1 L with ddH₂O

1 mL Tween-20

CHAPTER THREE: MATERIALS AND METHODS

Tris-HCl 1.5 M pH 8.8

18.2 g Tris

Filled up to 100 mL with ddH₂O

pH adjusted to 8.8

Tris-HCl 0.5 M pH 6.8

3 g Tris

Filled up to 50 mL with ddH₂O

10 x Lämmli buffer

30 g Tris

144 g Glycine

10 g SDS

Filled up to 1 L with ddH₂O

PBS

9.5 g Na₂HPO₄ x 2 H₂O

3.2 g Na₂HPO₄ x H₂O

4.4 g NaCl

Filled up to 1 L with ddH₂O

4 x Sample loading buffer

4 mL 10 % glycine

2 mL 2-mercaptoethanol

0.92 g (9.2 %) SDS

2.5 mL 1 M Tris-HCl (pH 6.8)

Filled up to 10 mL with ddH₂O

Aliquots stored at -20 °C

Lysis buffer

50 mM Tris

300 mM NaCl

0.5 % Triton X-100

50 µL Phospho Stop (phosphatase inhibitor, Roche) per mL buffer

25 µL Complete (protease inhibitor, Roche) per mL buffer

10 µL PMSF (serine protease inhibitor, Roche) per mL buffer

Bjerrumbuffer + methanol

5.82 g Tris

2.93 g Glycine

200 ml Methanol

Filled up to 1 L with ddH₂O

Bjerrumbuffer + SDS

5.82 g Tris

2.93 g Glycine

0.375 g SDS

Filled up to 1 L with ddH₂O

4 % Paraformaldehyde (PFA)

2 mg PFA

50 mL PBS

Dropwise NaOH (until solution
clears),

pH adjusted to 7.4 with HCl

Ponceau S staining solution

0.1 % w/v Ponceau S

5 % (v/v) Acetic acid

Filled up to 1 L with ddH₂O

**Electrochemiluminescent
detection solution**

5 mL 1 M Tris-HCl (pH 8.8)

125 µL 80 mM p-coumaric acid in
DMSO

Adjusted to 50 mL with ddH₂O

Crystal violet staining

1 g Crystal violet

10 mL Ethanol

Diluted 1:1000 with PBS

3.2. Methods

3.2.1. Cell culture

The following table gives an overview of the human and murine cell lines and the media they were cultured with. Cell lines were grown at 37 °C and 5 % CO₂. Cells were cultured in T25 and T75 culture flasks (CytoOne® Tissue culture treated flasks with vented filter caps, Starlab International GmbH, Hamburg, Germany). Adherent cells were detached using trypsin/EDTA (Sigma Aldrich, St. Louis, USA). Puromycin (Puromycin 2 HCl; Selleckchemicals, Houston, USA) was added to the respective growth medium at 0.75 µg/mL to select for NCI-H1703/mCherry transfectants.

Table 7: Human cell lines and the murine cell lines with their respective culture media used in this study.

Cell line	Culture medium
A2780	RPMI-1640 supplemented with 10 % fetal calf serum (FCS)
CAPAN-1	RPMI-1640 + 10 % FCS
DMS114	RPMI-1640 + 10 % FCS
DMS114/PON	RPMI-1640 + 10 % FCS
HCT116	McCoy's 5A + 10 % FCS and L-Glutamine
HeLa	RPMI-1640 + 10 % FCS
HepG2	Minimum Essential Medium with non-essential amino acids and pyruvate, supplemented with 10 % FCS
HT1376	Minimum Essential Medium with non-essential amino acids, supplemented with 10 % FCS
MCF7	Dulbecco's modified Eagle's Medium + 10 % FCS
NCI-H520	RPMI-1640 + 10 % FCS
NCI-H1703	RPMI-1640 + 10 % FCS
NCI-H1703/PON	RPMI-1640 + 10 % FCS

Cell line	Culture medium
NCI-H1703/ mCherry	RPMI-1640 + 10 % FCS, containing 0.75 $\mu\text{g}/\text{mL}$ Puromycin
PC3	Kaighn's Modification of Ham's F-12 Medium + 10 % FCS
U87MG	Dulbecco's modified Eagle's Medium + 10 % FCS
3T3-L1	Dulbecco's modified Eagle's Medium + 10 % FCS

Table 8 lists the media used for differentiation of 3T3-L1 fibroblasts (3T3-L1/F) into adipocytes (3T3-L1/A). Dexamethasone and 3-Isobutyl-1-Methylxanthine were freshly dissolved in their specific solvent before addition to the respective medium.

Table 8: Composition of the culture media for differentiation of 3T3-L1 fibroblasts into adipocytes.

Media	Composition
Growth Medium	Dulbecco's modified Eagle's Medium + 10 % FCS, penicillin, streptomycin and 1 % L-Glutamine stock [0.58 g/L]
Differentiation Medium	Growth Medium with 7.65 μM Dexamethasone, 200 μM 3-Isobutyl-1-Methylxanthine and 1 $\mu\text{g}/\text{mL}$ Insulin final concentration.
Post-differentiation Medium	Growth Medium with 1 $\mu\text{g}/\text{mL}$ Insulin final concentration.

3.2.2. Cell-conditioning experiments

In order to address the accumulation potential of 3T3-L1/F and 3T3-L1/A for ponatinib, cell conditioning experiments were conducted. Therefore, different concentrations of ponatinib were added to 3T3-L1/F and 3T3-L1/A, or cell culture medium only. The next day, the supernatant/medium was transferred onto lung cancer cells.

3.2.2.1. Method

For cell conditioning experiments, 3T3-L1/F and 3T3-L1/A were first differentiated/seeded in 6-well plates (6-well CytoOne® plate, Starlab International GmbH, Hamburg, Germany) at a density of 4×10^4 cells per mL in 2 mL of the respective culture media (Table 7, Table 8), as described in 3.2.5 Differentiation of 3T3-Fibroblasts into Adipocytes, p. 39. Control wells were filled only with Dulbecco's modified Eagle's Medium supplemented with 10 % fetal calf serum (FCS). All plates were incubated at 37 °C and 5 % CO₂. The following day, $1.2\text{--}2.5 \times 10^5$ lung cancer cells per 500 µL of RPMI-1640 supplemented with 10 % FCS were seeded in separate 6-well plates. In parallel, 3T3-L1/F, 3T3-L1/A and empty wells were treated with increasing concentrations of ponatinib in RPMI-1640 supplemented with 10 % FCS. Cells were incubated for 24 h at 37 °C and 5 % CO₂. Thereafter, supernatants of 3T3-L1/F, 3T3-L1/A or drug-containing medium from wells without cells were passed on to the cancer cell plates (Figure 9). For Western blot analysis proteins were isolated after 1 h (see 3.2.13 Protein isolation and determination of concentration, p. 49). For flow cytometry experiments, cells were analyzed after 1 h of incubation with ponatinib-containing supernatants (see 3.2.7.4 Flow cytometry for measuring ponatinib uptake from 3T3-L1/F, 3T3-L1/A-pre-exposed NCI-H1703 cells, p. 41). Cell conditioning experiments were also performed as colony formation assay (see 3.2.3.2 Colony formation assay, p. 36).

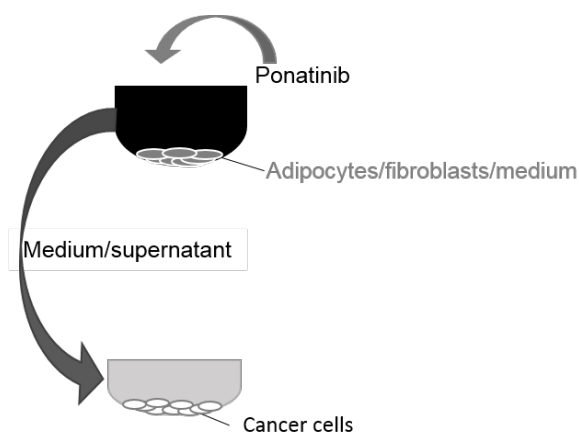


Figure 9: Cell conditioning experiment processing scheme.

3.2.3. Cell proliferation and viability assay

3.2.3.1. Cell viability assay

The 3-(4,5- dimethylthiazol-2-yl)-2,5-diphenyltetrazolium bromide (MTT)-vitality assay was used for all cell viability experiments. This high throughput screening assay determines the enzymatic activity of viable cells, which are exposed to anticancer drugs [65]. In this assay, living cells are able to reduce tetrazolium to formazan crystals, which is catalyzed by dehydrogenases from the mitochondria or other enzymes occurring for example in the endoplasmic reticulum [66]. The quantity of accumulated, purple colored formazan inside of the cells as well as in the medium, is determined by colorimetrically changes in the absorbance [65].

Method

To determine cell viability, cells were seeded in 96-well plates (96-well CytoOne® plate, Starlab International GmbH, Hamburg, Germany) at a density of 5×10^4 per mL in 100 μL of the respective culture media per well (Table 7). Due to their highly proliferative behavior, Capan-1 cells were seeded to a cell density of 3×10^4 per mL. Cells were left to adhere for 24 h at 37 °C and 5 % CO_2 . The next day, cells were checked for confluency and exposed to several drugs (Table 6). Therefore, the compounds were diluted in 100 μL of the respective growth media (Table 7) at the indicated concentrations, corresponding to 2-fold concentrated stocks, to achieve a final volume of 200 μL per well. For combination drug

experiments, the compounds were diluted in 50 μL of the respective growth media (Table 7) at the indicated concentrations, corresponding to 4-fold concentrated stocks. Drug exposure lasted for 72 h at 37 °C and 5 % CO_2 . The amount of viable cells was determined by MTT assay, according to the manufacturer's instructions (EZ4U, Biomedica, Vienna, Austria). Briefly, cell supernatant was aspirated and replaced by 100 μL of EZ4U solution per well. The plates were gently shaken prior to the measurement and color intensity was measured on a plate reader (Tecan Infinite 2000 pro, Lifesciences, Switzerland) at 450 nm, using 620 nm as reference wavelength. Data analysis was performed using GraphPad Prism 5 software (La Jolla, USA). Half maximal inhibitory concentrations (IC_{50} values), meaning 50 % reduced viability of cells compared to untreated controls, were calculated by non-linear regression line curve-fitting.

3.2.3.2. *Colony formation assay*

The basic principle of a colony formation assay is to determine differences in the capacity of treated cells, seeded at low-density, to form colonies compared to untreated controls. In general, a cell line seeded to an appropriate number in the culture vessel is exposed to cytotoxic agents or other treatments and incubated for a certain time. Consequently, the cells are fixed and stained [67].

Method

For the colony formation assay, 3T3-L1/F and 3T3-L1/A were first differentiated/seeded in 24-well plates (24-well CytoOne® plate, Starlab International GmbH, Hamburg, Germany) at a density of 6×10^4 cells per mL in 500 μL of the respective culture media (Table 7, Table 8), as described in 3.2.5 Differentiation of 3T3-Fibroblasts into Adipocytes, p. 39. An extra 24-well plate was filled only with Dulbecco's modified Eagle's Medium supplemented with 10 % FCS. All plates were incubated at 37 °C and 5 % CO_2 . The following day 5×10^3 lung cancer cells per 500 μL RPMI-1640 supplemented with 10 % FCS were seeded in additional 24-well plates. In parallel, 3T3-L1/F, 3T3-L1/A and empty wells were treated with increasing concentrations of ponatinib in RPMI-1640 supplemented with 10 % FCS. Cells were incubated for 24 h at 37 °C and 5 %

CO₂. Thereafter, supernatants of 3T3-L1/F, 3T3-L1/A or drug-containing medium from wells without cells were passed on to the cancer cells. Plates were incubated for 96 h at 37 °C and 5 % CO₂. Medium was discarded and plates were left upside down for drying overnight. Each well was gently fixed with 250 µL of ice-cold methanol for 15 min at 4 °C. The wells were further washed with 300 µL of PBS. 250 µL of crystal violet were added, followed by gentle shaking of the plates for 10 min. Surplus crystal violet was removed and each well was washed with water. The plates were left for drying upside down. Photos of each well were taken with a Nikon D3200 (Tokyo, Japan). For cell quantification, crystal violet staining was re-dissolved overnight in 2% sodium dodecyl sulfate- polyacrylamide (SDS, Sigma-Aldrich, St. Louis, USA) in PBS and pipetted into 96-well plates. Absorbance was measured at 560 nm on a plate reader. Analysis was performed in triplicates.

3.2.3.3. *Co-culture assay*

Co-culture experiments provide a suitable system to mimic and investigate cell-cell interactions in heterogeneous cell populations. Co-cultures can be fundamental for drug research, as they more closely resemble *in vivo* situation for instance with respect to pharmaceutical behavior of tested compounds [68].

Method

For co-culture experiments, 3T3-L1/F and 3T3-L1/A were first differentiated/seeded in 24-well plates at a density of 6×10^4 cells per mL in 500 µL of the respective culture media (Table 7, Table 8), as described in 3.2.5 Differentiation of 3T3-Fibroblasts into Adipocytes, p. 39. An extra 24-well plate was filled only with Dulbecco's modified Eagle's Medium supplemented with 10 % FCS. All plates were incubated at 37 °C and 5 % CO₂. The following day, transparent PET membrane inserts with pores (8 µM, Falcon, Starlab, UK) were placed into each well and lung cancer cells were seeded at a density of 5×10^4 per mL in 200 µL of the respective culture medium (Table 7) per insert (Figure 10). After 24 h, ponatinib was added at indicated concentrations to the bottom well compartment, containing either 3T3-L1/F, 3T3-L1/A or medium). Plates were

incubated for 120 h at 37 °C and 5 % CO₂. Thereafter, medium was discarded and each insert was left upside down for drying overnight. The following day, the inserts were transferred into a new 24-well plate and gently fixed with 200 µL of ice-cold methanol for 15 min at 7 °C. Furthermore, the inserts were washed with 300 µL of PBS. 150 µL of crystal violet were added, following gentle shaking of the plates for 10 min. Excess crystal violet was removed and each well was washed carefully with water. The inserts were left for drying upside down. Pictures were taken with a Nikon D3200 and crystal violet staining was re-dissolved overnight for cell quantification in 2 % SDS in PBS and pipetted into 96-well plates. Absorbance was measured at 560 nm on a plate reader. Analysis was performed in triplicates.

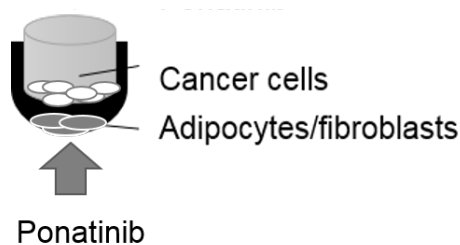


Figure 10: Co-culture assembling scheme.

3.2.4. Comparative genomic hybridization

Comparative genomic hybridization of treatment-naïve and ponatinib-resistant DMS114 cells was performed by B. Englinger, MSc, PhD. For the aim of this thesis, data were analyzed for gene copy numbers of the *MTTP* gene.

Method

Direct array comparative genome hybridization (aCGH) was conducted using 4x44K oligonucleotide microarrays (Gene Expression Microarray, Aligent, Santa Clara, USA), as described previously [69]. The ponatinib resistant subline of DMS114, DMS114/PON, as well as parental DMS114 cells were compared to healthy, diploid human reference DNA. Labeling and hybridization of genomic DNA was performed according to the manufacturer's procedure.

3.2.5. Differentiation of 3T3-Fibroblasts into Adipocytes

3T3-L1 pre-adipocyte cells are murine fibroblast clones that can be differentiated into adipocytes under specific cell culture conditions. When entering a resting state, the cells accumulate lipids in multiple intracellular droplets. This is due to metabolic changes, resulting in an increased synthesis of triglycerides from fatty acids, acetate and glucose [70].

Method

3T3-L1 fibroblasts (3T3-L1/F) were thawed in fresh Dulbecco's modified Eagle's Medium supplemented with 10 % FCS. When the cells reached 70 % confluency, cells were detached by trypsinization and seeded in the desired culture plates (cell density for 24-well plates: 6×10^4 ; 6-well plates: 4×10^4 per mL; 8-chambers: 1×10^5 per mL). After 48 and 96 h, cells were fed with growth medium. After 48 h, differentiation of cells was induced by adding differentiation medium (Table 8). Two days later, differentiation medium was replaced with post-differentiation medium (Table 8), which was further fed to cells every 48 h for the next four days.

3.2.6. Fatty acid uptake determination

The effect of ponatinib treatment on fatty acid uptake was analyzed by experiments that were performed by Mag. Dr. Clemens Röhrl (Institute of Medical Chemistry and Pathobiochemistry, Medical University of Vienna). This analysis was performed in untreated parental cells and ponatinib-selected cells.

Method

DMS114 cells and their ponatinib resistant subline DMS114/PON were plated in 12-well plates at a density of 1×10^5 in 1 mL of RPMI-1640 supplemented with 10 % FCS.

3.2.7. Flow cytometry

The use of flow cytometry enables simultaneous determination of multiple characteristics, including size, granularity and fluorescent labeling of single cells in heterogeneous cell suspensions. Both quantity and quality parameters can be assessed. Briefly, the cell fluid is drawn into a stream in such a way that one cell at a time passes through a laser beam and the scattered light gets detected and digitized [71].

3.2.7.1. Flow cytometry for lipid droplet (LD) quantification

Lipid droplet (LD) quantification with flow cytometry was performed for DMS114 and DMS114/PON cells for studying the impact of MTP inhibition with lomitapide and MTP siRNA knockdown on LD formation. Lomitapide pre-treatment was with 2 μ M for 72 h, MTP siRNA knockdown was with 50 nM for 48 h (see 3.2.15.1 Transfection of DMS114/PON cells with MTP siRNA, p. 53). Cells were seeded in FACS tubes (Corning™ Falcon™ 5 mL test tube with cell strainer snap cap, VWR International, Radnor, USA) at a density of $5-6 \times 10^5$ per mL in 200-300 μ L of serum-free RPMI-1640 medium. For lomitapide experiments 500 nM of Bodipy 493/503 were added to the samples 15 min prior to measurement, whereas for MTP knockdown experiments a total volume of 100 μ L of Bodipy 493/503 diluted in the same medium at indicated concentrations, corresponding to 3-fold concentrated stocks, was added to the samples 30 min before measurement. The tubes were incubated at 37 °C and 5 % CO₂ for 30 min. Measurement was performed at a LSRFortessa flow cytometer (BD Biosciences, New Jersey, USA), all samples were kept on ice. Bodipy 493/503 fluorescence was determined using 488 nm laser excitation wavelength and 530/30 nm (FITC) bandpass emission filter. Data analysis was performed with Flowing Software (University of Turku, Finland) and GraphPad Prism 5 software. Fluorescence intensities were depicted as arbitrary units (a.u.).

3.2.7.2. Flow cytometry for characterization of ponatinib derivatives

NCI-H1703 cells were seeded in FACS tubes at a density of 5×10^5 per mL in 300 μ L of serum-free RPMI-1640 medium. A total volume of 100 μ L of ponatinib

or ponatinib derivatives (MMAT057-2, MMAT077-3, MMAT066-2, MMAT040-3, MMAT081-1 and MMAT095-6), corresponding to 4-fold concentrated stocks, was added to each tube for 30 min and 3 h. Measurement was performed at the LSRFortessa flow cytometer, all samples were kept on ice. Ponatinib and ponatinib derivatives fluorescence was determined using 355, 405, 488 and 640 nm laser excitation wavelengths and 450/40 (DAPI), 519/40 (Indo-1); 450/40 (Horizon V450), 610/20 (Qdot 605), 660/20 (Qdot 655); 530/30 (FITC), 575/26 (PE-A), 630/30 (PE-Texas Red), 670/30 (PE-Cy5), 780/60 (PE-Cy7); 660/20 (APC-A), 720/40 (Alexa Fluor-700) and 780/60 (APC-Cy7) bandpass emission filters. Data analysis was performed with Flowing Software and GraphPad Prism 5 software. Fluorescence intensities were depicted as arbitrary units (a.u.).

3.2.7.3. Flow cytometry for quantification of ponatinib in DMS114 cells

Ponatinib quantification was performed in DMS114 and DMS114/PON cells for studying the impact of MTP inhibition with lomitapide and MTP siRNA knockdown on cellular ponatinib uptake. Lomitapide pre-treatment was with 2 μ M for 72 h, MTP siRNA knockdown was with 50 nM for 48 h (see 3.2.15.1 Transfection of DMS114/PON cells with MTP siRNA, p. 53). Cells were resuspended in FACS tubes at a density of 6×10^5 per mL in 200 L of serum-free RPMI-1640 medium. A total volume of 100 μ L of ponatinib diluted in the same medium at the indicated concentrations, corresponding to 3-fold concentrated stocks, was added to each tube. The tubes were incubated at 37 °C and 5 % CO₂. Measurement at the LSRFortessa flow cytometer was performed 30 min after drug exposure and all samples were kept on ice. Ponatinib fluorescence was determined using 405 nm laser excitation wavelength and 450/40 nm (Horizon V450) bandpass filter emission. Data analysis was performed with Flowing Software and GraphPad Prism 5 software. Fluorescence intensities were depicted as arbitrary units (a.u.).

3.2.7.4. Flow cytometry for measuring ponatinib uptake from 3T3-L1/F, 3T3-L1/A-pre-exposed NCI-H1703 cells

To measure ponatinib uptake in cancer cells from media pre-exposed to 3T3-L1/F, 3T3-L1/A or drug-containing medium (see 3.2.2 Cell-conditioning

experiments, p.34), flow cytometry experiments were performed. After 1 h of incubation with supernatants of 3T3-L1/F, 3T3-L1/A or drug-containing medium from wells without cells, cancer cells were trypsinized with 0.5 mL per well and were collected in 15 mL falcon tubes. Tubes were stored on ice until detachment was completed for all samples. After centrifugation at 280 x g for 10 min, each cell pellet was resuspended in 300 μ L of serum-free RPMI-1640 and kept on ice until intracellular drug accumulation was measured using a LSRFortessa flow cytometer. Ponatinib fluorescence was determined using 405 nm laser excitation wavelength and 450/40 nm (Horizon V450) bandpass filter emission. Data analysis was performed with Flowing Software and GraphPad Prism 5 software. Fluorescence intensities were depicted as arbitrary units (a.u.).

3.2.8. Ponatinib imaging in tissue cryosections

In order to study the fluorescence of ponatinib *in vivo*, mice were injected with ponatinib. Subsequently, organs were collected, embedded, sliced and analyzed for ponatinib fluorescence.

3.2.8.1. *In vivo ponatinib administration and organ preparation*

The *in vivo* fluorescence of ponatinib was tested in two male severe combined immunodeficient (SCID) mice. These mice were injected subcutaneously into the right flank with lung cancer cells when they were four weeks old. All procedures were approved by the Ethic Review Board of the Medical University of Vienna and performed following the Federation of Laboratory Animal Science Associations (FELASA) guidelines. Solvent was given orally for 2 h to the control mouse, whereas the other one was treated with 30 mg ponatinib per kg weight, dissolved in ddH₂O containing 10 % Chremophor (Sigma-Aldrich, St. Louis, USA), 10 % dimethylsulfoxide (DMSO, Sigma-Aldrich, St. Louis, USA) and 5% ethanol (Sigma-Aldrich, St. Louis, USA), for the same time period. Animals were sacrificed and the following organs were collected and embedded in cryomolds: adipose tissue in OCT (optimal cutting temperature) medium (Tissue-Tek® O.C.T. Compound, Sakura Finetek Europe, Netherlands) and formalin (Formalin solution, neutral buffered, 10 %, Sigma-Aldrich, St. Louis, USA), kidney, liver,

lung, tumor and swiss roles of small intestine and colon in OCT medium only. 5 slices (with a thickness of 10 μM) per organ were prepared with a cryomicrotome (Thermo Fisher Scientific, Waltham, USA) and stored at $-80\text{ }^{\circ}\text{C}$ on microscopic slides (Superfrost Plus microscope slides, Thermo Fisher Scientific, Waltham, USA). Tissue slices were then imaged on CLSM (see 3.2.11.5 CLSM imaging of ponatinib in tissue cryosections, p. 46) and digitized with Panoramic Midi Slide Scanner (3DHISTECH, Budapest, Hungary).

3.2.9. Live-cell microscopy

With a live-cell microscope, it is possible to monitor the behavior of living cells without altering physiological and biological conditions, like minimal light exposure and optimum cell culture conditions regarding temperature and CO_2 content [72].

3.2.9.1. *Live-cell microscopy of cancer cell-3T3-L1/F,3T3-L1/A co-cultures*

3T3-L1/F and 3T3-L1/A were first differentiated/seeded in 8-chamber slides (chambered coverslip with 8 wells, ibidi GmbH, Martinsried, Germany) at a density of 1×10^5 per mL in 300 μL of the respective cell culture medium per well (Table 7, Table 8), as described in 3.2.5 Differentiation of 3T3-Fibroblasts into Adipocytes, p. 39. The 8-chamber was incubated at $37\text{ }^{\circ}\text{C}$ and 5 % CO_2 . 24 h after differentiation of 3T3-L1/A was completed and 3T3-L1/F were adherent, media was sucked off and NCI-H1703/mCherry cells were seeded to each well at a cell density of 5×10^4 per mL in 300 μL of RPMI-1640 supplemented with 10 % FCS. The next day, one round of images was taken before 100 μL of ponatinib was spiked into each well directly at the microscope (Visitron Systems live cell microscope, Puchheim, Germany) at indicated concentrations, corresponding to 4-fold stocks, diluted in the same medium. After addition of ponatinib, images were taken every h for a duration of 120 h. A 20 x objective was used. Ponatinib, Bodipy 493/503 and mCherry fluorescence were captured using DAPI, GFP, and RFP channels, respectively. Data analysis was done using ImageJ (Java).

3.2.10. Lipid content analysis

The effect of ponatinib treatment on cellular lipid content was analyzed by gas chromatography. This analysis was performed in untreated parental cells, in parental cells exposed to a single, subtoxic dose of ponatinib, as well as in ponatinib-selected cells.

Method

DMS114, NCI-H1703 cells and their respective ponatinib resistant sublines were cultured in T75 flasks, incubated at 37 °C and 5 % CO₂. Parental and resistant cells were seeded in triplicates in petri dishes (sterile Falcon® Petri discs, 100 mm diameter, VWR International, Radnor, USA) at a cell density of 3 x 10⁵ per mL in 10 mL of culture medium and incubated at 37 °C and 5 % CO₂. Parental and ponatinib-selected cells were treated with 1 µM of ponatinib for 1 h. Untreated parental cells (controls), as well as treated parental and resistant cells were fed with fresh culture media and incubated at 37 °C and 5 % CO₂. The following day, controls (naïve cells) were harvested by washing each dish twice with 5 mL of PBS, trypsinizing with 3 mL, again performing two PBS washing steps and collecting the cells in 15 mL falcon tubes. Consequently, cells were centrifuged at 280 x g for 10 min. The resulting cell pellet was washed again with 2 mL of PBS and centrifuged one more time. The supernatant was discarded and the pellet was stored at -80 °C. After a time period of 48 h, the ponatinib pre-treated parental as well as resistant cells revealed the same confluency as untreated parental cells and were isolated according to the same procedure. Gas chromatography analysis of the cellular lipid content was performed by Mag. Dr. Clemens Röhrl (Institute of Medical Chemistry and Pathobiochemistry, Medical University of Vienna).

3.2.11. Microscopy

3.2.11.1. *Light microscopy*

Monitoring of cells (e.g. progress of 3T3-L1 differentiation) and cell imaging was performed with a Zeiss Primo Vert light microscope (Carl Zeiss, Jena, Germany).

3.2.11.2. *Confocal Laser Scanning Microscopy (CLSM)*

Multi-dimensional structures of fluorescently labelled cells can be captured by using confocal laser scanning microscopy (CLSM). Therefore, a laser scans the specimen point-by-point in multiple wavelength modes, while out-of-focus fluorescence is removed by a pinhole (a special filter). Thus detailed images of biological specimen can be generated [73].

3.2.11.3. *CLSM for characterization of ponatinib and ponatinib derivatives*

NCI-H1703/mCherry cells were seeded in an 8-chamber (Chamber slide with a removable 8-well silicon chamber, ibidi GmbH, Martinsried, Germany) at a density of 5×10^4 per mL in 300 μ L of RPMI-1640 supplemented with 10 % FCS per well. The 8-chamber was incubated at 37 °C and 5 % CO₂. After 24 h, 100 μ L of ponatinib or ponatinib derivatives (MMAT057-2, MMAT077-3, MMAT066-2, MMAT040-3, MMAT081-1 and MMAT095-6), diluted in the same medium at the indicated concentrations, corresponding to 4-fold stocks, were added to each well for 1 h. The 8-chamber was incubated at 37 °C and 5 % CO₂. Staining with 500 nM of Bodipy 493/503, diluted in 50 μ L of cell culture medium, corresponding to a 9-fold concentrated stock, was performed 15 min prior to fixation, incubating the cells at 37 °C and 5 % CO₂. Cells were fixed with 4 % Paraformaldehyde (PFA) for 20 min at room temperature. Thereafter, each well was washed with 300 μ L of PBS and the slide was covered with Vectashield (Vectashield antifade mounting medium H-1000, Vector Laboratories Inc., Burlingame, USA) and a cover glass. After letting the slide rest for some minutes at 4 °C, cells were imaged on a laser scanning microscope (Zeiss LSM 700, Carl Zeiss, Jena, Germany), with a 63 x oil immersion objective and using the appropriate image software

(Zen2010, Carl Zeiss, Jena, Germany). Ponatinib, Bodipy 493/503 and NCI-H1703/mCherry cells were detected using 405 nm, 488 nm and 555 nm solid state laser lines and 500 nm shortpass (DAPI), 602 nm longpass (FITC) and 578 nm longpass (mCherry) emission filters, respectively.

3.2.11.4. CLSM for LD imaging in DMS114 and DMS114/PON cells

DMS114 and DMS114/PON cells were seeded in an 8-chamber with removable chambers at a density of 6×10^4 per mL in 300 μ L of RPMI-1640 supplemented with 10 % FCS per well. The 8-chamber was incubated at 37 °C and 5 % CO₂. After a time period of 24 h, a total volume of 50 μ L of 2 μ M of lomitapide, corresponding to an 8-fold concentrated stock diluted in the same medium, or medium only was added to the cells. A total volume of 50 μ L of 100 μ M of OA, corresponding to an 8-fold concentrated stock, was provided 30 min after lomitapide. Lomitapide and OA exposure lasted for 24 h. Each 8-chamber was incubated at 37 °C and 5 % CO₂. LD staining with 500 nM of Bodipy 493/503, diluted in 50 μ L of cell culture medium, corresponding to a 9-fold concentrated stock, was performed 15 min prior to fixation, incubating the cells at 37 °C and 5 % CO₂. Cells were fixed with 4 % PFA for 20 min at room temperature. Thereafter, each well was washed with 300 μ L of PBS. Actin staining with 30 μ g of phalloidin-TRITC (100 μ g/mL; Sigma-Aldrich, St. Louis, USA) was performed for 30 min, following three washing steps with 300 μ L of PBS. Finally, each slide was covered with Vectashield and a cover glass. After letting the slide rest for some minutes at 4 °C, cells were imaged on a laser scanning microscope, with a 63 x oil immersion objective and using the appropriate image software. Bodipy 493/503 and phalloidin-TRITC were detected using 488 nm and 555 nm solid state laser lines and 568 nm (FITC) and 559 nm longpass (TRITC) emission filters, respectively.

3.2.11.5. CLSM imaging of ponatinib in tissue cryosections

Tissue slices were thawed to room temperature for 2 min and fixed with 4 % PFA for 20 min. After a washing step with PBS, specimen were covered for 30 min at 4 °C with a solution containing 5 mL of PBS, 100 μ g/mL of RNase A (Sigma-

Aldrich, St. Louis, USA) and 5 µg/mL of propidium iodide (PI, Sigma-Aldrich, St. Louis, USA) to counterstain the nuclei. After washing twice with PBS, the slices were left for 5 min at 4 °C. Finally, the tissue slices were covered with Vectashield and imaged on a laser scanning microscope, with a 63 x oil immersion objective and using the appropriate image software. Ponatinib and PI were detected using the 405 nm and 488 solid state laser lines and 420 nm (DAPI) and 617 nm (PI) longpass emission filters, respectively. The generated images were further analyzed using Tissue Studio software (Definiens, Munich, Germany). Ponatinib fluorescence intensity was quantified in simulated single cells from at least three images per tissue. For optical illustration, the ponatinib channel of 8-bit images (pixel intensity values 0-155) was colored according to the Definiens measured intensity ranges, reflecting negative, low, medium, and high intensity. For data presentation and statistical analysis, using GraphPad Prism 5 software, the values were pooled.

3.2.11.6. CLSM of cancer cell-fibroblast/adipocyte co-cultures

3T3-L1/F and 3T3-L1/A cells were first differentiated/seeded in 8-chamber with removable chambers at a density of 1×10^5 per mL in 300 µL of the respective cell culture medium per well (Table 7, Table 8, as described in 3.2.5 Differentiation of 3T3-Fibroblasts into Adipocytes, p. 39). The 8-chamber was incubated at 37 °C and 5 % CO₂. 24 h after differentiation of 3T3-L1/A was completed and 3T3-L1/F were adherent, surplus media was aspirated and NCI-H1703/mCherry cells were seeded to each well at a cell density of 5×10^4 per mL in 300 µL of RPMI-1640 supplemented with 10 % FCS. The next day, co-cultures were exposed for 1 h to ponatinib at indicated concentrations, corresponding to 4-fold stocks, diluted in the same medium. The 8-chamber was incubated at 37 °C and 5 % CO₂. Staining with 500 nM of Bodipy 493/503, diluted in 50 µL of cell culture medium corresponding to a 9-fold concentrated stock, was performed 15 min prior to fixation, incubating the cells at 37 °C and 5 % CO₂. Cells were fixed with 4 % PFA for 30 min and (after removing the 4 % PFA) the slide was covered with Vectashield and a cover glass. Cells were imaged on a laser scanning microscope with a 63 x oil immersion objective, using the appropriate image software. Ponatinib, Bodipy 493/503 and mCherry were detected using 405 nm,

488 nm and 555 nm solid state laser lines and 420 nm (DAPI), 559 nm (FITC) and 578 nm (mCherry) longpass emission filters, respectively. Ponatinib intensity in NCI-H1703/mCherry cells was quantified using Image J (Java). Cancer cells were defined by drawing regions of interest (ROI) around mCherry positive regions. In each of this ROIs in ponatinib treated co-cultures, blue (ponatinib) pixel intensities were measured subtracting background fluorescence of ROIs of the respective untreated controls. The ponatinib intensities were plotted using GraphPad Prism 5 software.

3.2.11.7. Slide scanner

Histology images of the cryosections were digitized on a Pannoramic Midi Slide Scanner (3DHISTECH, Budapest, Hungary) using Pannoramic Viewer software (3DHISTECH).

3.2.11.8. Hematoxylin/Eosin staining

For Hematoxylin/Eosin staining tissue slices were thawed to room temperature for 2 min and fixed with 4 % PFA for 20 min. The slides were then dipped in PBS and further stained as indicated in Table 9. After completing dipping in 100 % ethanol, the slices were taken in n-butyl-acetate and covered with Entellan and a cover glass.

Table 9: Used solutions for hematoxylin/eosin staining of organ slices in their applied order, including washing steps in-between. All solutions were prepared by the Filipits lab group.

Solution	Incubation time
4 x ddH2O	4 x 1 min
Hematoxylin	7 min
*	-
Sott's solution	45 sec
**	5 min
***	5 min
****	-
Eosin	1 min
*****	-

Solution	Incubation time
Ethanol, 70 %	dip 3 x
Ethanol, 96 %	1 min
Ethanol, 96 %	1 min
Ethanol, 100 %	1 min
Ethanol, 100 %	1 min

- * Rinsing in tap water, 3 water cuvettes
- ** Rinsing in warm tap water
- *** Rinsing in floating water
- **** Rinsing in ddH₂O
- ***** Rinsing in ddH₂O, dipping 6 x in two water cuvettes

3.2.12. mRNA expression array

Whole-genome gene expression was performed by B. Englinger, MSc, PhD. In frame of this thesis, data were analyzed regarding transcription factors for the *MTTP* promotor region.

Method

4x44K oligonucleotide mRNA expression arrays (Gene Expression Microarray, Aligent, Santa Clara, USA) were used for gene expression analysis, as previously described [74, 75]. Raw intensity values were read into R, background-corrected and normalized applying the normexp and loess algorithm of limma [76]. With gene set enrichment analysis (GSEA), enrichment of differentially expressed genes in distinct functional genesets (Kyoto Encyclopedia of Genes and Genomes, KEGG) were investigated (<http://www.broadinstitute.org/gsea/msigdb/index.jsp>).

3.2.13. Protein isolation and determination of concentration

Method

Adherent cell cultures were scratched into the respective growth medium (Table 7) and each well was washed with 1 mL of PBS. The cells were collected in 15 mL Falcon tubes and centrifuged for 10 min at 280 x g. Each cell pellet was washed one more time with 1 mL of PBS and centrifuged again. Consequently,

pellets were dissolved in 30-50 μL of lysis buffer and incubated for 30-45 min on ice, pipetting the pellets up and down vigorously. The cell lysates were treated with ultrasound for 5 min and centrifuged at $23.748 \times g$ for 15 min at 4°C . The protein-containing supernatants were collected and 2.5 μL of the lysates were separated for determining the protein concentration. The Pierce BCA Protein Assay Kit (Thermo Fisher Scientific, Waltham, USA) was used for measuring the protein concentration. A standard curve was obtained by using series of bovine serum albumin (BSA) dilutions (Thermo Fisher Scientific, Waltham, USA).

3.2.14. RNA isolation and real-time quantitative PCR (qPCR)

3.2.14.1. RNA isolation

Method

DMS114 cells and their ponatinib resistant subline DMS114/PON were seeded in 6-well plates at a density of 5×10^5 cells per well in a total volume of 2 mL of RPMI-1640 supplemented with 10 % FCS. The 6-well plate was incubated at 37°C and 5 % CO_2 . The next day, total RNA was isolated by liquid-liquid extraction. Therefore, medium was sucked off, cells were lysed with 500 μL of Trizol (Life technologies, Carlsbad, USA) per well, collected in 1.5 mL tubes and incubated for 5 min at room temperature. In order to obtain a separation of the homogenate, 100 μL of chloroform (Sigma-Aldrich, St. Louis, USA) were added. Each tube was inverted for 15 sec and incubated for 10 min at room temperature, before another centrifugation at $12\,000 \times g$ for 15 min at 4°C was performed. The mixture was separated into a clear, aqueous phase containing RNA, an interphase, and an organic phase. The RNA was transferred into a fresh tube, the volume [μL] was noted down and precipitated with half of the volume of isopropanol, inverted for 15 sec and incubated for 10 min at room temperature. Another centrifugation at $18,200 \times g$ for 10 min at 4°C was performed. Subsequently, the precipitated RNA was washed with two 80 % ethanol washing steps, each followed by a centrifugation at $18,200 \times g$ for 15 min at 4°C . Any left ethanol was sucked off carefully using a 100 μL pipet and the pellet was left for drying at room temperature for 20 min. The dried RNA pellet was re-dissolved in RNase-free

water and stored at $-80\text{ }^{\circ}\text{C}$. Quality and quantity of the RNA were measured by Nanodrop (NanoDrop ND-1000, Thermo Fisher Scientific). The 260 nm/280 nm and the 260/230 nm ratios provide a measure for sample purity.

3.2.14.2. Reverse transcription

A total amount of $1\text{ }\mu\text{g}$ of RNA was diluted in RNase-free water for transcription into complementary DNA (cDNA). By heating the sample up to $70\text{ }^{\circ}\text{C}$ for 10 min any remaining double-stranded RNA structures were denatured. The samples were immediately transferred onto ice. The reverse transcription master mix was added to each sample (Table 10), as was $1\text{ }\mu\text{L}$ of the Revert Aid Reverse Transcriptase (Revert Aid Transcriptase M-MuLV RT, Thermo Fisher Scientific, Waltham, USA). Incubation was for 90 min at $42\text{ }^{\circ}\text{C}$. Part of the obtained cDNA product was diluted 1:25 with RNase-free water and stored at $-20\text{ }^{\circ}\text{C}$.

Table 10: Composition of the master mix for mRNA transcription.

mRNA transcription master mix
4 μL 5x transcription buffer (Thermo Fisher Scientific)
1 μL Hexanucleotide [20 ng/ μL] (Random Primer 3 $\mu\text{g}/\mu\text{L}$, Invitrogen #48190-011)
1 μL dNTP of a 10 mM dNTP mix, (GE Healthcare Life Sciences)
2 μL Dithiothreitol (DTT) [100 mM] (Sigma-Aldrich)
A total volume of 8 μL was prepared for each sample

GE Healthcare Life Sciences, Little Chalfont, UK; Sigma-Aldrich, St. Louis, USA; Thermo Fisher Scientific, Waltham, USA

3.2.14.3. Quantitative real-time PCR (qRT-PCR)

mRNA expression of several LD-associated genes was analyzed in a quantitative way with quantitative real-time polymerase chain reaction or qPCR. This is a diverse, multistep technology and involves template denaturation, primer annealing, and amplification using quantifiable fluorescent probes [77]. Unlike normal PCR, the qPCR reaction can be monitored under real-time conditions with the help of an excitation light source and a fluorescence detection system [77, 78].

The preliminary step of qPCR involves conversion of RNA to cDNA. Subsequently, the cDNA template is amplified by a DNA polymerase. Primers used for qPCR have to be specific for their target and thus their design should take into account, besides the need for 100 % sequence complementarity, also factors such as length and ratio/position of purine/pyrimidine bases, which influence hybridization efficiency [77]. For qPCR, there exist further two different approaches: one involving double-stranded DNA (dsDNA) intercalating molecules like SYBR Green, the other one using fluorescent oligonucleotides for monitoring the increasing amount of amplified DNA. While fluorescent dsDNA binding dyes lead to the detection of both specific and non-specific PCR products as well as primer dimers, fluorophore-labeled oligonucleotides only detect specific amplification products [78].

In this study, SYBR Green was used for detection of PCR products. When SYBR Green binds to dsDNA, its fluorescence increases and the resulting complex emits green light, which can be detected each PCR cycle. To ensure correctness of the amplified PCR products, a melting curve analysis after the qPCR is crucial, because non-specific products and primer dimers are denatured at lower temperatures [78].

Method

All primers (100 μ M stocks, Eurofins Genomics, Luxemburg) were 1:10 diluted in RNase-free water. Per gene, 0.1 μ L of both forward and reverse primer (Table 11) were mixed with 5 μ L of GoTag qPCR Master Mix (Promega, Wisconsin, USA). In a 96-well plate (Hard-Shell 96-well PCR plates, Bio-Rad Laboratories Inc., Hercules, USA), a final volume of 5.2 μ L of this master mix was added per well. Importantly, an excess of master mix was prepared for reverse pipetting. Subsequently, 5 μ L of the 1:25 diluted cDNA were pipetted in triplicates onto the 96-well plate. The plate was sealed with a sheet, kept on ice until the measurement was performed and centrifuged before the PCR was started. mRNA expression of each gene was measured, using *ACTB* for normalization. Negative controls, containing RNase-free water instead of cDNA, were measured in order to exclude any contamination. qPCR was performed at the C1000 Touch Thermal Cycler (CFX96 Real time system, Bio-Rad Laboratories Inc., Hercules,

USA) and analyzed by the proper software (CFX Maestro, Bio-Rad Laboratories Inc., Hercules, USA). The obtained results were processed according to the following formula and normalized to the control (by further division with the $2^{-\Delta CT}$ value of DMS114 cells):

$$2^{-\Delta CT} = 2^{-(Cq \text{ target} - Cq \text{ housekeeping})}$$

Table 11: List of used primers.

Target gene (protein)	Forward primer 5'-3'	Reverse primer 5'-3'
ACTB (β -actin)	GGATGCAGAAGGAGATCACTG	CGATCCACACGGAGTACTTG
MTTP (MTP)	ACAAGCTCACGTACTCCACTG	TCCTCCATAGTAAGGCCACATC
PLIN1 (Perilipin)	CCTGCCTTACATGGCTTGTT	CCTTTGTTGACTGCCATCCT
PLIN2 (ADRP)	GGCTAGACAGGATTGAGGAGAG	TCACTGCCCCTTTGGTCTTG
PLIN3 (Tip47)	GGTCCTAAGCCTGATGGAAA	CTGGCCTTCCACCAGCTTCT

ADRP: Adipose differentiation-related protein; MTP: Microsomal triglyceride transfer protein; Tip47: Mannose-6-phosphate receptor binding protein 1

3.2.15. Transfection

Introducing foreign nucleic acids into cells is a powerful tool to study the function and regulation of gene products [79]. For this study, small interference RNA (siRNA) was used for knocking-down the *MTTP* gene product MTP in DMS114 cells and their ponatinib resistant subline DMS114/PON. Moreover, a plasmid carrying a fluorescent mCherry protein was introduced in NCI-H1703 cells to make them visible for various experimental applications.

3.2.15.1. Transfection of DMS114/PON cells with MTP siRNA

Ponatinib resistant DMS114 cells were transfected with non-targeting (scrambled siRNA) and *MTP* siRNA using Xfect Transfection Reagent (Clontech, Mountain

View, USA) according to the manufacturer's recommendations. Subsequently, cells were seeded in a 6-well plate at a cell density of 5×10^5 in 2 mL. The next day, Xfect Polymer was vortexed and added to 50 nM of each siRNA diluted in Xfect Reaction Buffer. The whole transfection complex was vortexed for 10 seconds and added dropwise to adherent cells after 20 min. Fresh medium was fed to the cells after 4 h. Knockdown of protein expression was determined after 48 and 72 h by Western blot. Cells were further used for cell viability assays and FACS experiments (see 3.2.7.3 Flow cytometry for quantification of ponatinib in DMS114 cells, p. 41), after 24 and 48 h of transfection, respectively.

3.2.15.2. Transfection of NCI-H1703 cells with an mCherry expression plasmid

Transfection of NCI-H1703 cells with pQCXIP-mCherry-IRES-Puro plasmid DNA (Institute of Cancer Research of the Medical University Vienna, Austria), carrying a puromycin resistance gene and the gene encoding red fluorescent mCherry, was performed with Lipofectamine2000 (Thermo Fisher Scientific, Waltham, USA), according to the manufacturer's instructions. Briefly, Lipofectamine 2000 reagent was diluted to a final volume of 4 % in RPMI-1640 supplemented with 10 % FCS. The Plasmid [360 ng/ μ L] was diluted separately to a final amount of 5 μ g in the same medium. The dissolved plasmid was then added dropwise to dissolved Lipofectamine 2000 reagent (1:1), and after 20 min of incubation, the transfection complex was added with 3 mL of medium to the adherent cells in T25 flasks. The following day, transfectants were selected with media containing 0.75 μ g/mL Puromycin. Transfection efficiency was monitored by a Nikon Ti Eclipse fluorescent inverted microscope.

3.2.16. Western blot analysis

Western blot analysis enables determination of expression levels of specific proteins as well as posttranslational modifications (e.g. phosphorylation). Therefore, cellular protein lysates are separated by gel electrophoresis and further transferred to a membrane. Specific proteins can then be detected by using protein targeting antibodies [80].

Method

Western blotting experiments were performed to determine the expression of proteins after siRNA transfection and cell conditioning experiments. Therefore, 4 x sample loading buffer was added to 15 µg of each protein sample diluted in lysis buffer. All samples were loaded into the 15 slots of the stacking gel and the proteins were further separated according to their molecular weight on a 10 % sodium dodecyl sulfate polyacrylamide electrophoresis (SDS-PAGE) gel (Table 12) at a constant of 90 V in an electrophoresis chamber filled with 1 x Lämmli buffer. Six µL of marker (Precision Plus Protein marker, Bio-Rad Laboratories Inc., Hercules, USA) were used as molecular weight reference.

Table 12: SDS-PAGE ingredient recipe for a stacking (4.5 %) and separation gel (10%). Polymerization of each gel lasted for 30 min.

Ingredient	Stacking gel (4.5 %)	Separation gel (10 %)
ddH₂O	1.56 mL	3.65 mL
Acrylamid	0.281 mL	1.875 mL
Tris HCl [0.5 M] pH 6.8	0.625 mL	-
Tris HCl [1.5 M] pH 8.8	-	1.875 mL
20 % SDS	25 µL	75 µL
10 % APS	12.5 µL	25 µL
TEMED	2.5 µL	5 µL

Consequently, proteins were blotted semi-dry onto a 6 cm x 9 cm polyvinylidene fluoride transfer (PVDF) membrane (Immun-Blot LF PVDF Membrane, Bio-Rad Laboratories Inc., Hercules, USA) by using a Trans-Blot Turbo (Bio-Rad Laboratories Inc., Hercules, USA). The order of filters, gel and membrane is illustrated in Figure 11.

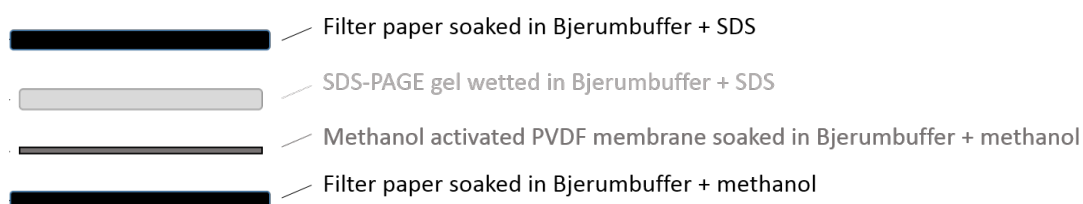


Figure 11: The order (top to bottom) of filters, gel and membrane for Western blotting.

Staining the membranes with Ponceau solution after blotting revealed separation quality and possible unequal loading. Red staining was removed by several washing steps with 1 x Tris-buffered saline/Tween (TBST) solution and the blots were further incubated for 1 h in 1 x TBST containing 1 % fat-free milk powder and 0.5 % BSA (Albumin fraction V, Carl Roth, Karlsruhe, Germany) to prevent unspecific binding. Subsequently, blots were again washed in 1 x TBST and incubated with the chosen primary antibody (Table 13) at 4 °C overnight. Beta-actin was always used as loading control. Three washing steps with 1 x TBST were performed and a horseradish peroxidase (HRP)-conjugated secondary antibody (Santa Cruz Biotechnology, Dallas, USA), that binds to the Fc domain of the primary antibody, was added for 1 h followed by three more washing steps with 1 x TBST. The signal was assessed by applying the electrochemiluminescent (ECL) detection solution, which causes a chemiluminescent reaction that was visualized on X-ray films (Amersham Hyperfilm™ ECL, GE Healthcare, UK).

Table 13: List of primary antibodies that were used for Western blot analysis.

Antigen	Antibody source	Dilution	Size [kDa]	Company
β-actin	Mouse monoclonal	1:5000-1:10 000	42	Sigma-Aldrich
Akt (pan) C67E7	Rabbit	1:1000	60	Cell Signaling
Erk1/2 (p44/42 MAPK)	Rabbit	1:1000	42, 44	Cell Signaling
MTP (C-1)	Mouse monoclonal	1:100-1:1000	97	Santa Cruz
Phospho-Akt (Ser473, D9E)	Rabbit monoclonal	1:1000	60	Cell Signaling
Phospho-Erk (p44/42 MAPK, Thr202/Tyr204)	Rabbit	1:1000	42, 44	Cell Signaling

Cell Signaling: Cell Signaling Technology, Danvers, USA; Santa Cruz Biotechnology, Dallas, USA; Sigma-Aldrich, St. Louis, USA

3.2.17. Statistical analyses

Statistical analyses were performed using GraphPad Prism 5 software. Throughout this study significance levels are marked as following: ***= $p < 0.001$; **= $p < 0.01$ and *= $p < 0.05$. Non-significant values are abbreviated as “n.s.”.

For triplicate values Gaussian distribution was assumed. To assess Gaussian or non-Gaussian distributions of more than three replicates, the D’Agostino and Pearson omnibus normality test was performed. If the data was Gaussian distributed, a student’s t-test was used to compare the means of two groups (e.g. parental cell line and resistant subline). For non-Gaussian data, the Mann-Whitney test was used to compare two groups. Statistical significance of two or more groups defined by two factors (e.g. crystal violet absorbance or drug fluorescence between co-culture conditions, as well as IC_{50} values for a drug between cell lines) were analyzed using two-way ANOVA statistics with Bonferroni post test.

4. Results

4.1. Co-culture experiments and ponatinib imaging

4.1.1. Generation of mCherry expressing NCI-H1703 cells

For microscopic experiments, NCI-H1703 cells were transfected with pQCXIP-mCherry-IRES-Puro plasmid DNA using Lipofectamine2000 transfection reagent. Transfectants were constantly selected with 0.75 $\mu\text{g}/\text{mL}$ puromycin, a harmful dosage for non-transfected cells (Figure 12A). Transfection efficiency was observed as cells that appeared red when illuminated with an RFP laser on a fluorescent microscope (Figure 12B).

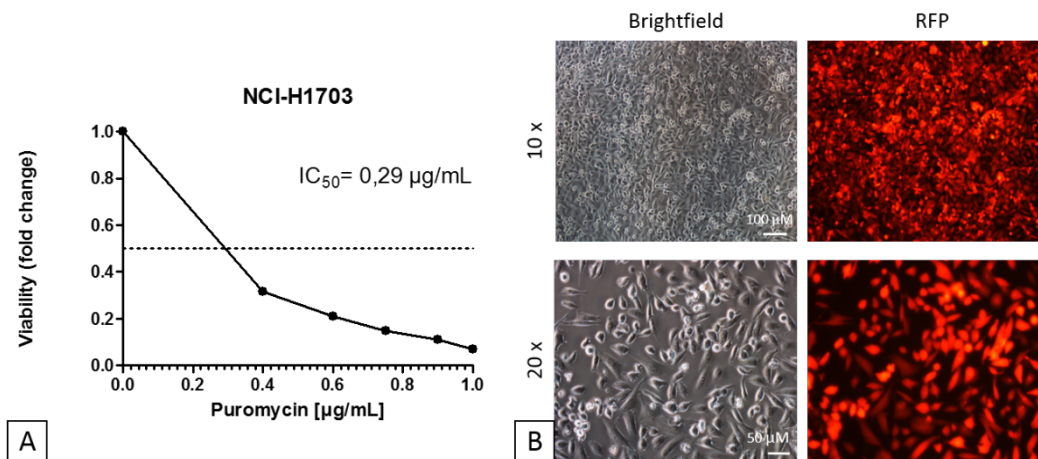


Figure 12: Transfection efficiency of NCI-H1703 cells with pQCXIP-mCherry-IRES-Puro plasmid DNA. Cells were exposed for 4 h to plasmid and Lipofectamine2000 reagents. Transfectants were constantly selected with 0.75 $\mu\text{g}/\text{mL}$ puromycin. A) Toxicity of puromycin in non-transfected NCI-H1703 cells. Cells were exposed to increasing concentrations of puromycin for 72 h and viability was determined with MTT assay. B) Transfection efficiency was determined 20 days after transfection by fluorescence microscopy using the RFP channel and brightfield.

4.1.2. Ponatinib is fluorescent and accumulates in lipid droplets (LDs)

Previous studies performed by B. Englinger, MSc, PhD, revealed intrinsic fluorescence of ponatinib and accumulation in lipid droplets (LDs). Indeed, confocal laser scanning microscopy (CLSM) of NCI-H1703/mCherry cells incubated with 1 μ M of ponatinib for 1 h confirmed fluorescence of ponatinib in the DAPI channel (Figure 13). Furthermore, co-staining of ponatinib with Bodipy 493/503 displayed overlapping fluorescence signals, demonstrating drug accumulation in LDs (Figure 14).

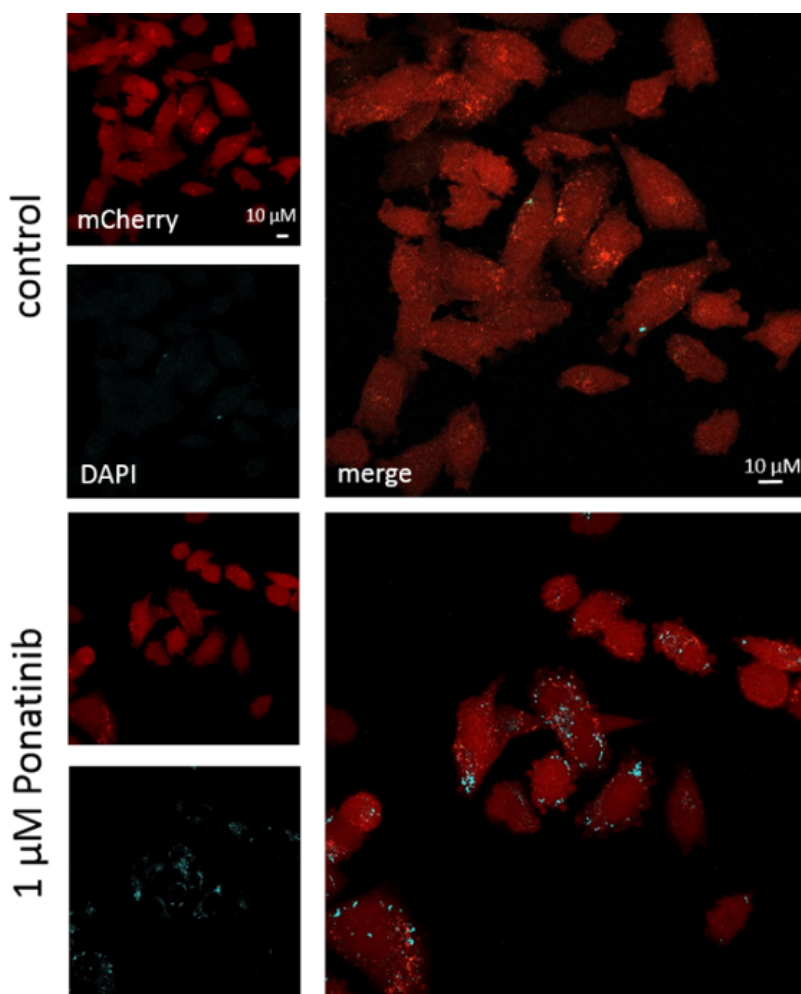


Figure 13: Ponatinib fluorescence is detectable in cultured lung cancer cells. Fluorescence activity of ponatinib in NCI-H1703/mCherry cells was analyzed by CLSM using DAPI and mCherry channels. Cells were incubated with 1 μ M of ponatinib for 1 h. Scale bars indicate 10 μ M.

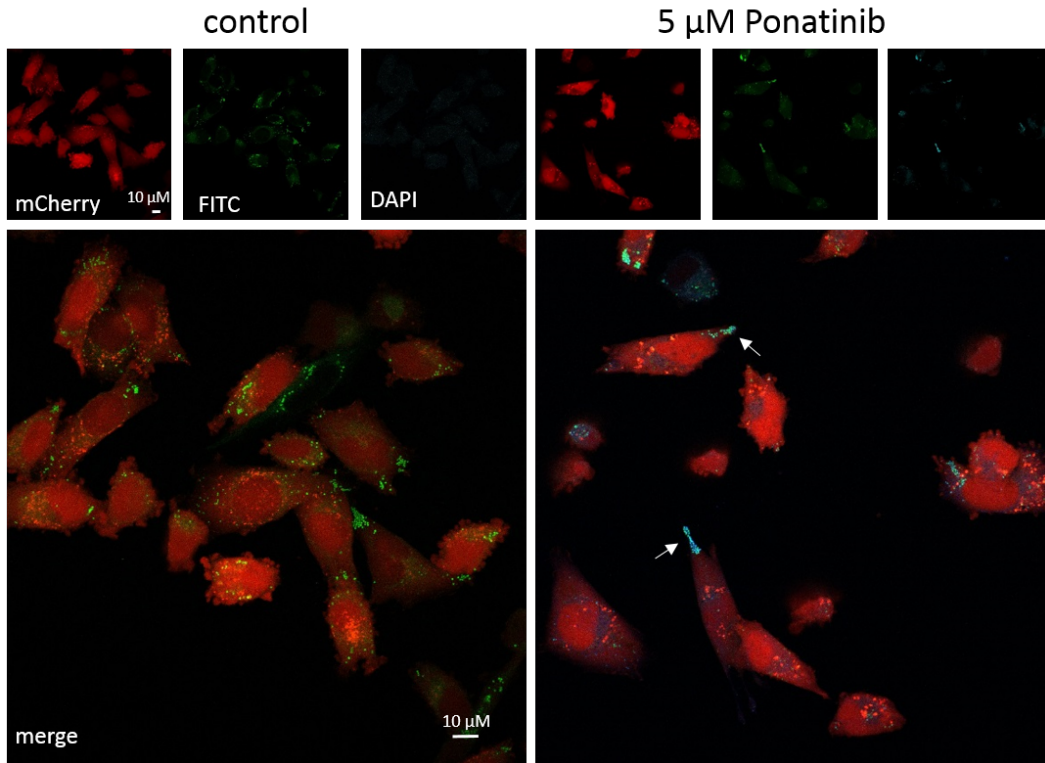


Figure 14: Ponatinib accumulates in LDs in cancer cells. Subcellular localization of ponatinib in NCI-H1703/mCherry cells was determined by CLSM using mCherry, FITC and DAPI channels. Cells were incubated with 5 μM of ponatinib for 1 h. 500 nM Bodipy 493/503 was used as marker for LDs. Scale bars indicate 10 μM .

4.1.3. Differentiation of fibroblasts (3T3-L1/F) into adipocytes (3T3-L1/A)

Fibroblasts (3T3-L1/F) accumulated fat during 6-10 days of culture in differentiation medium (supplied on day 2) and post differentiation medium (from day 4 onwards). Visible as light refractory intracellular spots, these fatty drops became increasingly prominent upon further cultivation in post differentiation medium (e.g. up to day 23, Figure 15).

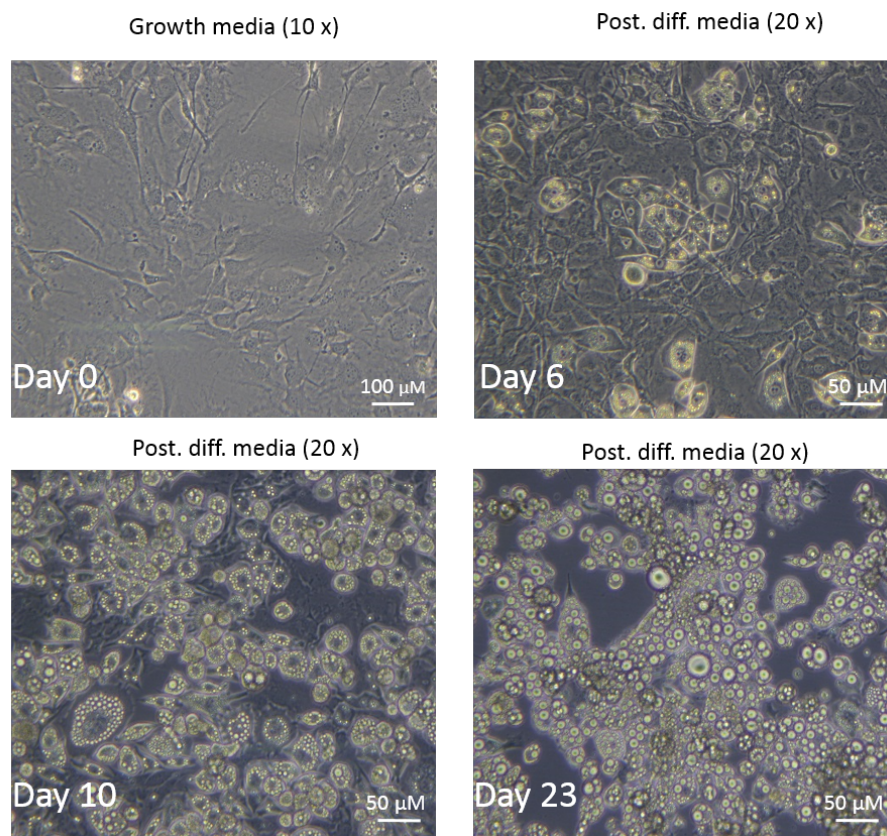


Figure 15: Changes of morphology of fibroblast (3T3-L1/F) upon differentiation into mature adipocytes (3T3-L1/A). 3T3-L1 mouse embryonic fibroblasts were thawed in Dulbecco's modified Eagle's Medium supplemented with 10 % fetal calf serum (FCS) and allowed to differentiate for 23 days. Composition of the differentiation media is listed in Table 8.

4.1.4. Co-culture experiments of cancer cells with 3T3-L1/F or 3T3-L1/A

To assess the role of a lipid compartment in cancer cell survival upon treatment with ponatinib, co-culture experiments were conducted. Therefore, the isogenic cell lines 3T3-L1/F and 3T3-L1/A were chosen for representing a non-lipoid and lipid cell phenotype, respectively. Experiments were performed with DMS114, NCI-H520 and NCI-H1703 cells. Furthermore, NCI-H1703/mCherry cells were used for microscopic co-culture experiments. Initially, co-culture experiments were conducted within the same well. However, long-time live-cell microscopy revealed bad survival of NCI-H1703/mCherry cells upon contact with 3T3-L1/A cells (Figure 16).

CHAPTER FOUR: RESULTS

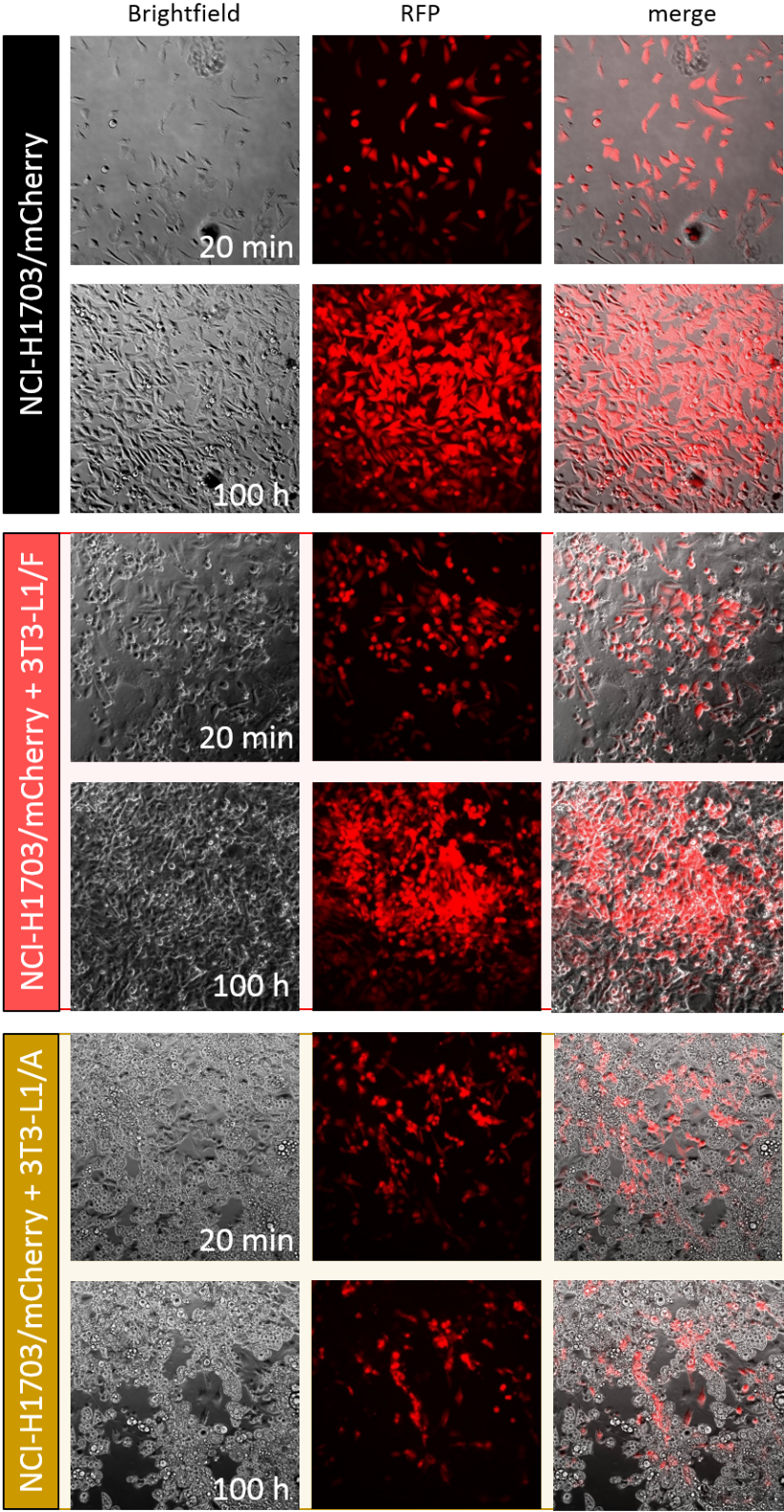


Figure 16: NCI-H1703/mCherry lung cancer cells do not tolerate long-time co-culturing with 3T3-L1/A cells. NCI-H1703/mCherry cells were co-cultured with fibroblasts or adipocytes. Photographs were taken in brightfield, DAPI and RFP settings, using a live-cell imaging system with 20x objective. Indicated are time points 20 min and 100 h representing the start and end of the experiment.

On the contrary, short-time microscopic co-culture experiments revealed less ponatinib content in NCI-H1703/mCherry cells that were cultured with 3T3-L1/A cells as compared to those cultured with 3T3-L1/F cells (Figure 17). In line with this, interactive co-culture assays, where cancer cells were separated in inserts from 3T3-L1/A, 3T3-L1/F cells, or medium, NCI-H520 cells showed better survival in presence of 3T3-L1/A cells (Figure 18). In contrast, quite the opposite was observed for NCI-H1703 cells (Figure 19). However, together with the observations in Figure 16, this indicates that NCI-H1703 cells do not tolerate long-term co-culturing with adipocytes, independently of the presence of ponatinib.

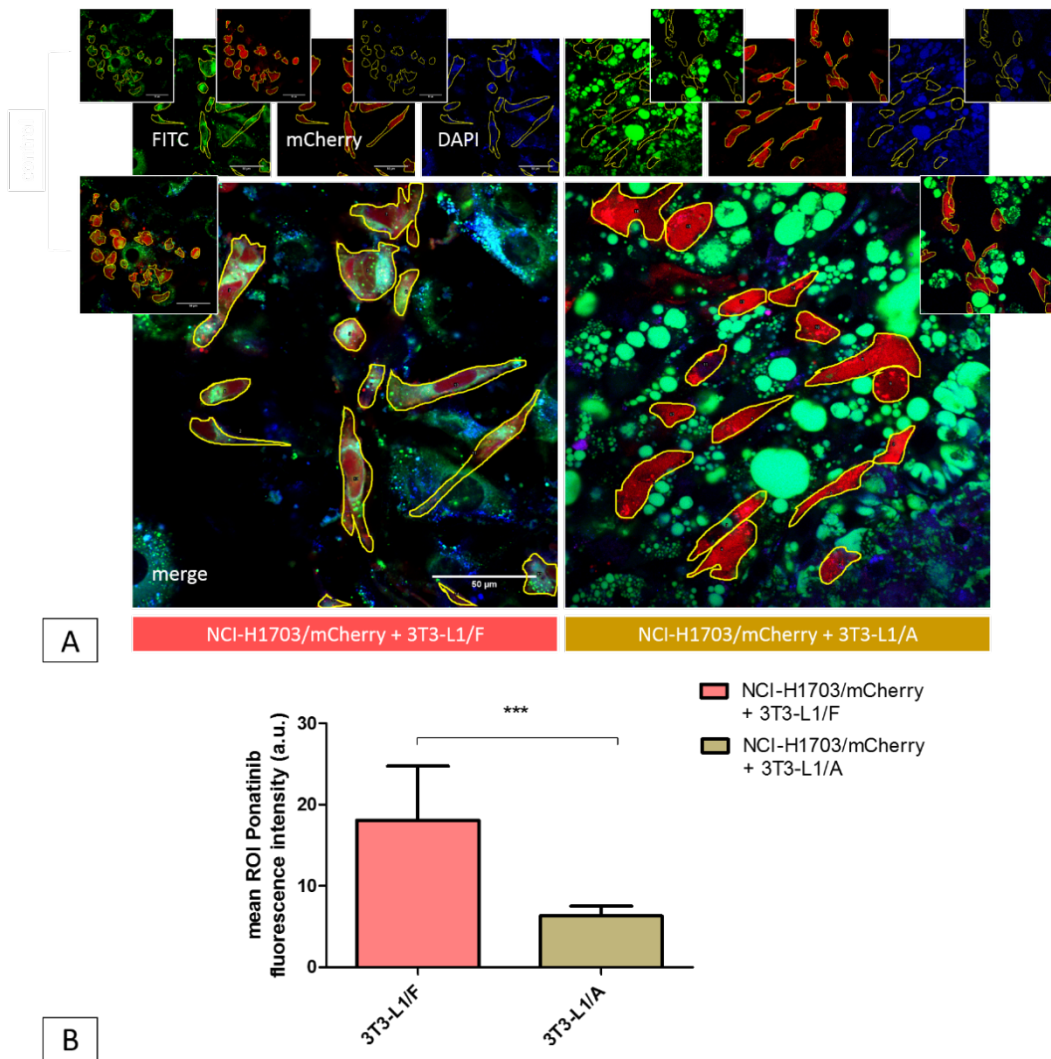


Figure 17: Ponatinib uptake in cancer cells is diminished in the presence of adipocytes. NCI-H1703/mCherry cells were exposed to ponatinib short-time in the presence of 3T3-L1/F or 3T3-L1/A cells. A) Photomicrographs were taken by CLSM using FITC, mCherry and DAPI channels. Bodipy 493/503 was used as marker for LDs. Cells were incubated with 2.5 μ M of ponatinib for 1 h. Scale bars indicate 50 μ M. Regions of interests (ROIs) were created by marking mCherry-positive areas in ImageJ. B) Ponatinib was quantified by measuring pixel intensities in the DAPI channel of each mCherry-positive ROI, subtracting the fluorescence of the respective untreated control images. Significance was calculated using D'Agostino and Pearson omnibus normality test, followed by Mann-Whitney test (***=p<0.0001).

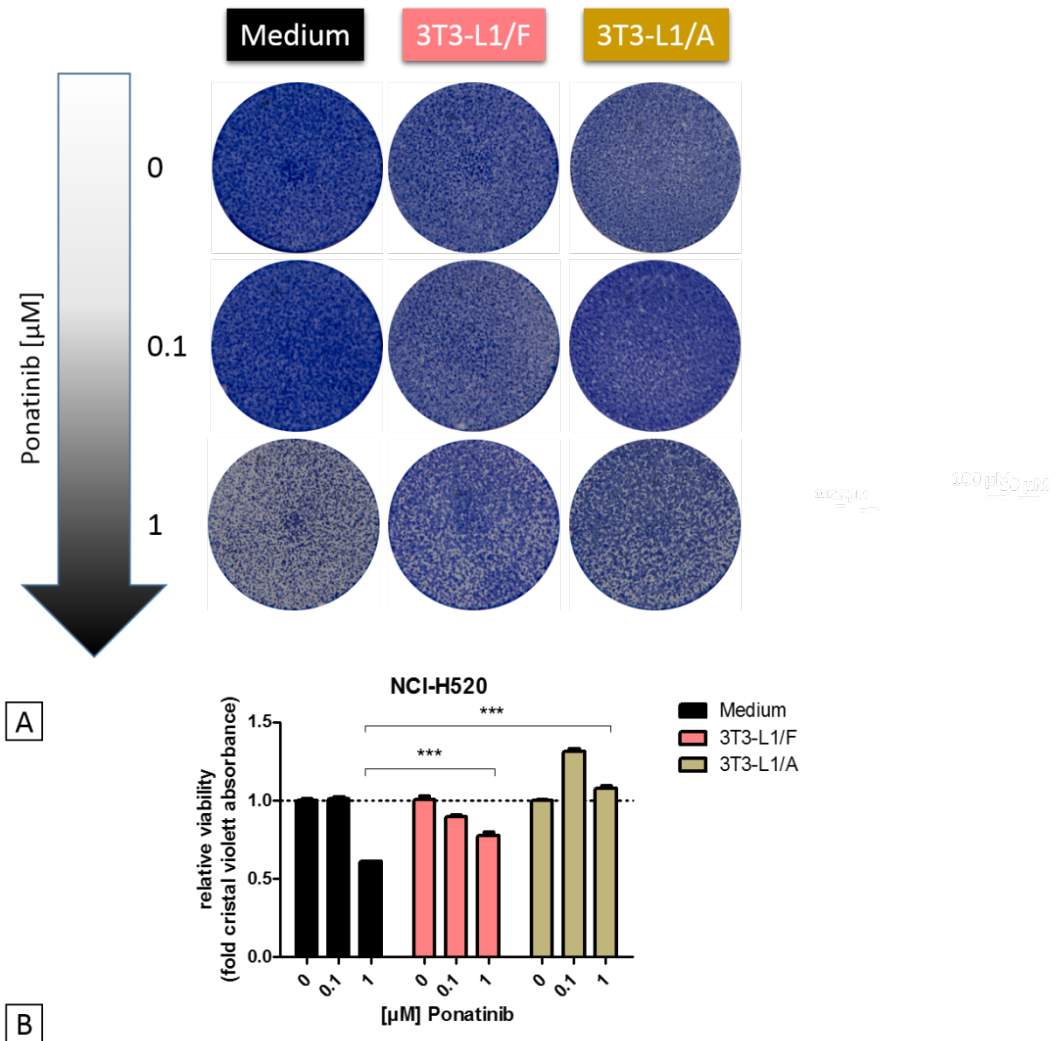


Figure 18: Adipocytes mediate cancer cell survival. A) NCI-H520 cells were cultured in transwells in a co-culture assay with ponatinib containing medium or ponatinib-exposed 3T3-L1/F or 3T3-L1/A cells and stained after 5 days with crystal violet. B) Relative viability of NCI-H520 cells determined by measuring re-dissolved crystal violet absorbance at 560 nm. Results were normalized according to the corresponding untreated controls, set to 1. Significance was calculated using two-way ANOVA with Bonferroni post-test (***=p<0.001).

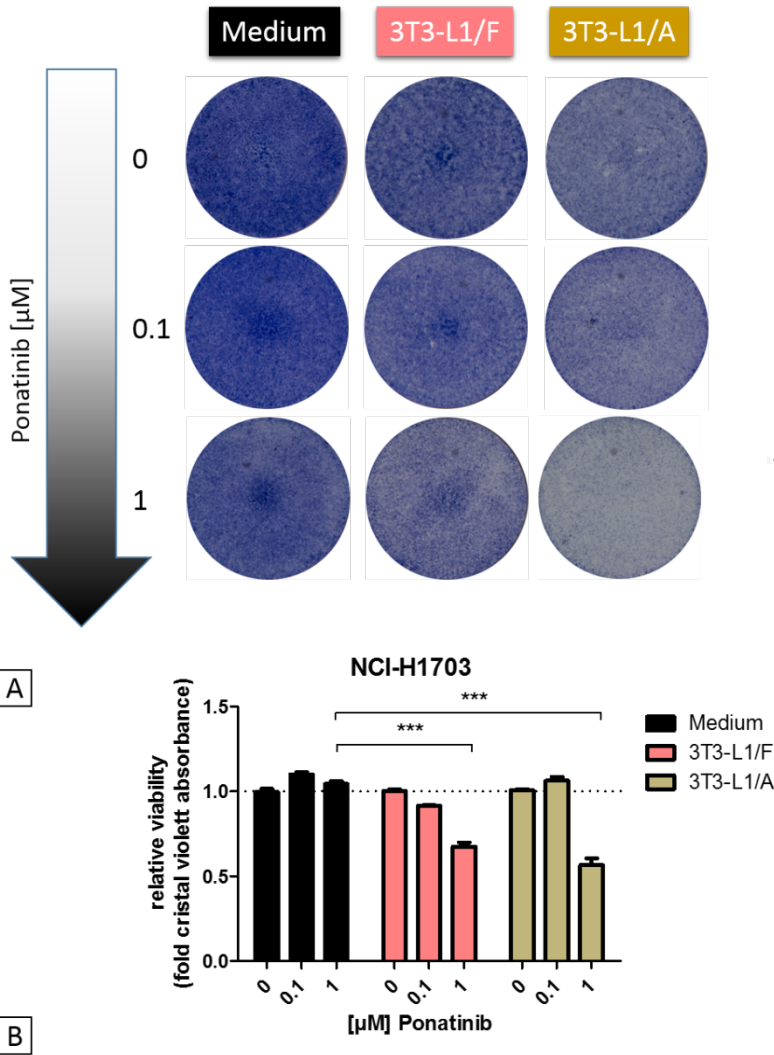


Figure 19: NCI-H1703 cells do not tolerate direct co-culturing with adipocytes in transwell chambers. A) NCI-H1703 cells were cultured in transwells in a co-culture assay with ponatinib containing medium or ponatinib-exposed 3T3-L1/F or 3T3-L1/A cells and stained after 5 days with crystal violet. B) Relative viability of NCI-H1703 cells determined by measuring re-dissolved crystal violet absorbance at 560 nm. Results were normalized according to the corresponding untreated controls, set to 1. Significance was calculated using two-way ANOVA with Bonferroni post-test (**= $p < 0.001$).

4.1.5. Cell-conditioning experiments

As mentioned previously (chapter 4.1.4 Co-culture experiments of cancer cells with 3T3-L1/F or 3T3-L1/A), live-cell experiments revealed that NCI-H1703/mCherry cells did not tolerate long-lasting co-culturing with 3T3-L1/A cells. Hence, cell conditioning experiments with no direct cell-cell contact were established. The obtained results showed increased colony formation capacity of NCI-H1703 (data not shown), NCI-H520, and DMS114 cells, when exposed to

supernatant of ponatinib-treated adipocytes as compared to that of fibroblasts (Figure 20 and 21, A and B). To test whether adipocytes scavenge ponatinib to an extent that leads to diminished inhibitory potential in cancer cells, Western blot analysis was performed. Indeed, these experiments demonstrated that DMS114 cells incubated with adipocyte pre-exposed supernatant containing increasing ponatinib concentrations, showed sustained Erk phosphorylation in comparison to both fibroblast pre-exposed and unexposed media (Figure 21C). In line with this, intracellular fluorescence of ponatinib, quantified by flow cytometry, was distinctly decreased in NCI-H1703/mCherry cells incubated with adipocyte-conditioned, ponatinib containing media (Figure 22).

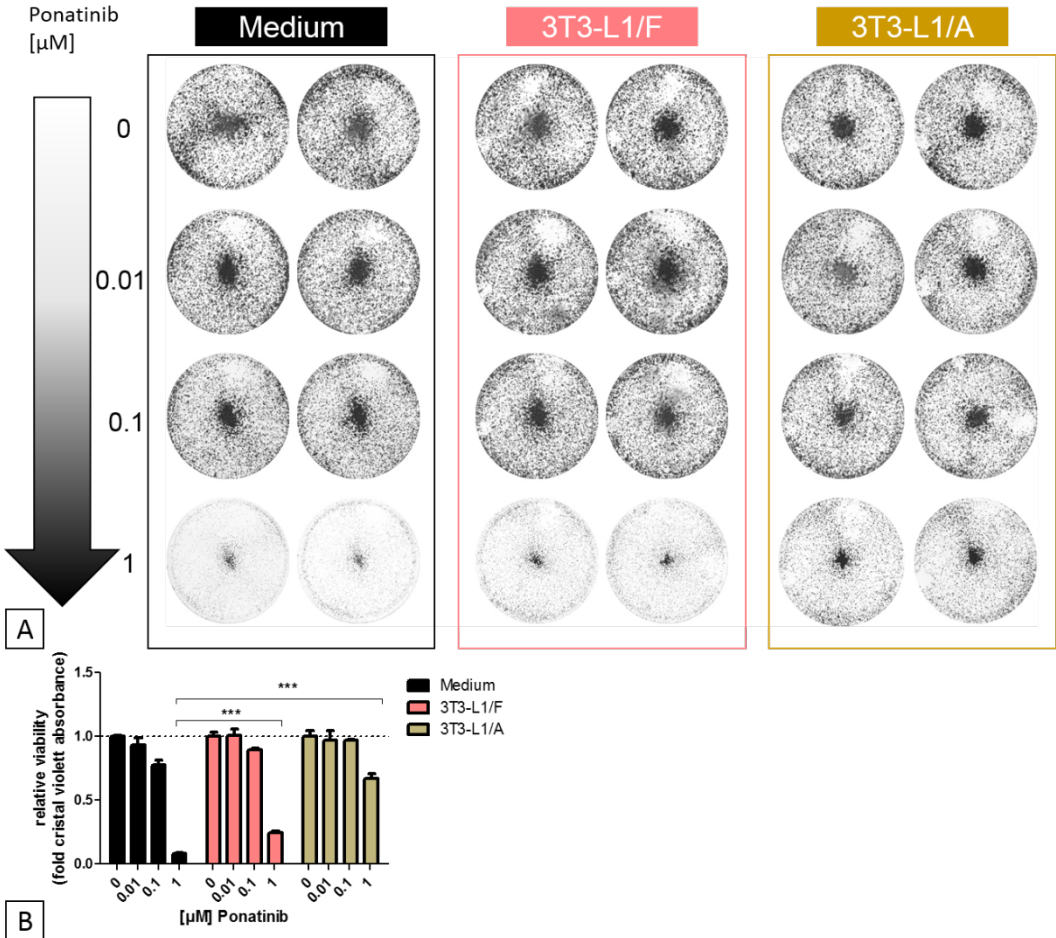


Figure 20: Adipocyte pre-exposure diminishes the cytotoxic activity of ponatinib towards cancer cells. Effect of ponatinib containing medium or fibroblast/adipocyte-pre-exposed supernatant on NCI-H520 cancer cell survival. A) Colony formation capacity of NCI-H520 cells upon conditioning with medium or supernatant of ponatinib treated 3T3-L1/F and 3T3-L1/A cells. Ponatinib incubation of fibroblasts/adipocytes was for 24 h, conditioning of NCI-H520 cells lasted for 4 days. B) Cell quantification was performed by measuring re-dissolved crystal violet absorbance at 560 nm. Results were normalized according to the corresponding untreated controls, set to 1. Significance was calculated using two-way ANOVA with Bonferroni post-test (**= $p < 0.001$).

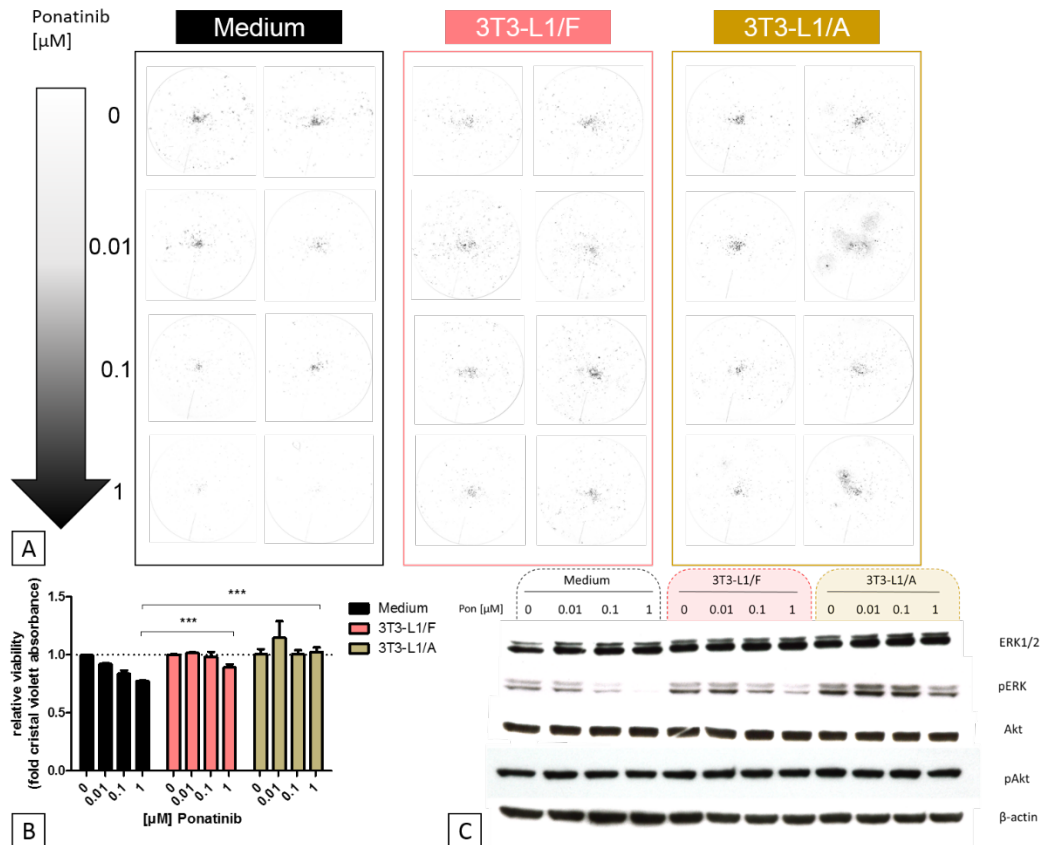


Figure 21: Adipocyte pre-exposure diminishes the cytotoxic activity of ponatinib towards cancer cells. Effect of ponatinib containing medium or fibroblast/adipocyte-pre-exposed supernatant on DMS114 cancer cell survival. A) Colony formation capacity of DMS114 cells upon conditioning with medium or supernatant of ponatinib treated 3T3-L1/F and 3T3-L1/A cells. Ponatinib incubation of fibroblasts/adipocytes was for 24 h, conditioning of DMS114 cells lasted for 4 days. B) Cell quantification was performed by measuring re-dissolved crystal violet absorbance at 560 nm. Results were normalized according to the corresponding untreated controls, set to 1. Significance was calculated using two-way ANOVA with Bonferroni post-test ($***=p<0.001$). C) Ponatinib inhibitory potential on MAPK and Akt signaling pathways in DMS114 cells following 24 h pre-exposure to fibroblasts/adipocytes was determined by Western blot. β -actin served as loading control.

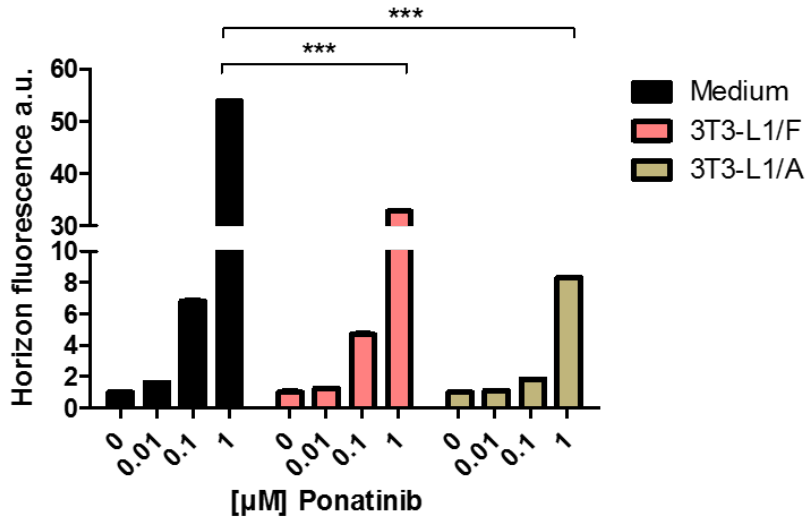


Figure 22: Intracellular ponatinib fluorescence is decreased in NCI-H1703/mCherry cells exposed to adipocyte-conditioned media. Ponatinib incubation of medium, 3T3-L1/F or 3T3-L1/A cells lasted for 24 h, followed by exposure to NCI-H1703/mCherry cells for 1 h. Ponatinib fluorescence was quantified by flow cytometry, using the Horizon V450 channel. Significance was calculated using two-way ANOVA with Bonferroni post-test (**= $p < 0.001$).

4.1.6. Ponatinib imaging in tissue cryosections

Having observed fluorescence of ponatinib *in vitro*, CLSM was conducted in order to study fluorescence of ponatinib in mouse tissue cryosections. Therefore, SCID mice, carrying subcutaneous A549 lung cancer xenografts, were treated orally with 30 mg/kg ponatinib or solvent only. After 2 h, mice were sacrificed and organs and tumors were frozen in cryomolds containing Optimal Cutting Temperature (OCT) medium. Consecutive cryosections were generated on a cryotome (Thermo Fisher Scientific, Waltham, USA). Tissue slides were stained with Hematoxylin/Eosin (H/E) for histo-morphological analysis. Strong ponatinib fluorescence was observed in colon and small intestine samples (Figure 23 and 24). Strikingly, drug fluorescence was also found in liver and tumor tissue, although to a lesser extent (Figure 25 and 26).

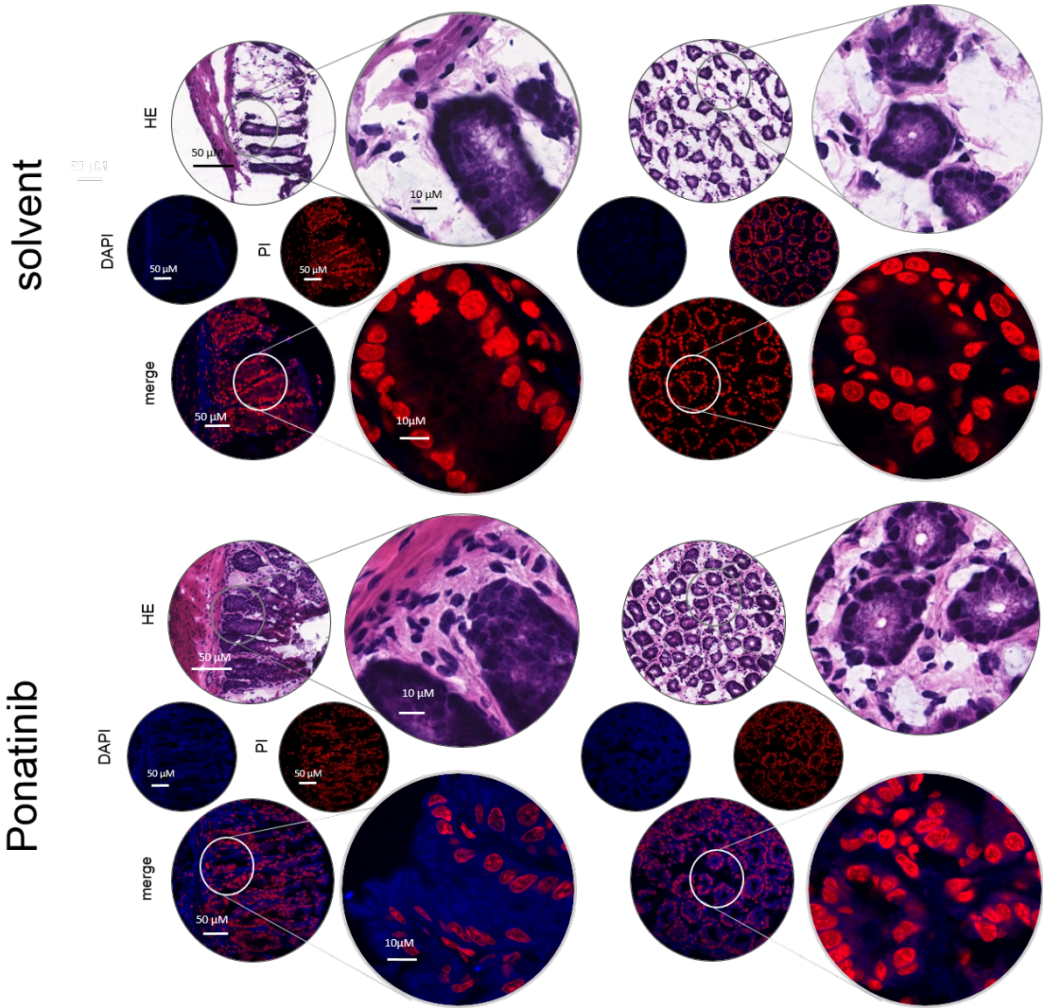


Figure 23: Ponatinib uptake is detectable in colon cryosections from orally treated mice. SCID mice, bearing lung tumor xenografts, were treated orally with 30 mg ponatinib per kg weight for 2 h. Mice were sacrificed and consecutive cryosections were generated. Ponatinib fluorescence was imaged by CLSM using DAPI and PI channels. Propidium iodide (PI) was used as nuclear counterstain. H/E staining was used as histologically control.

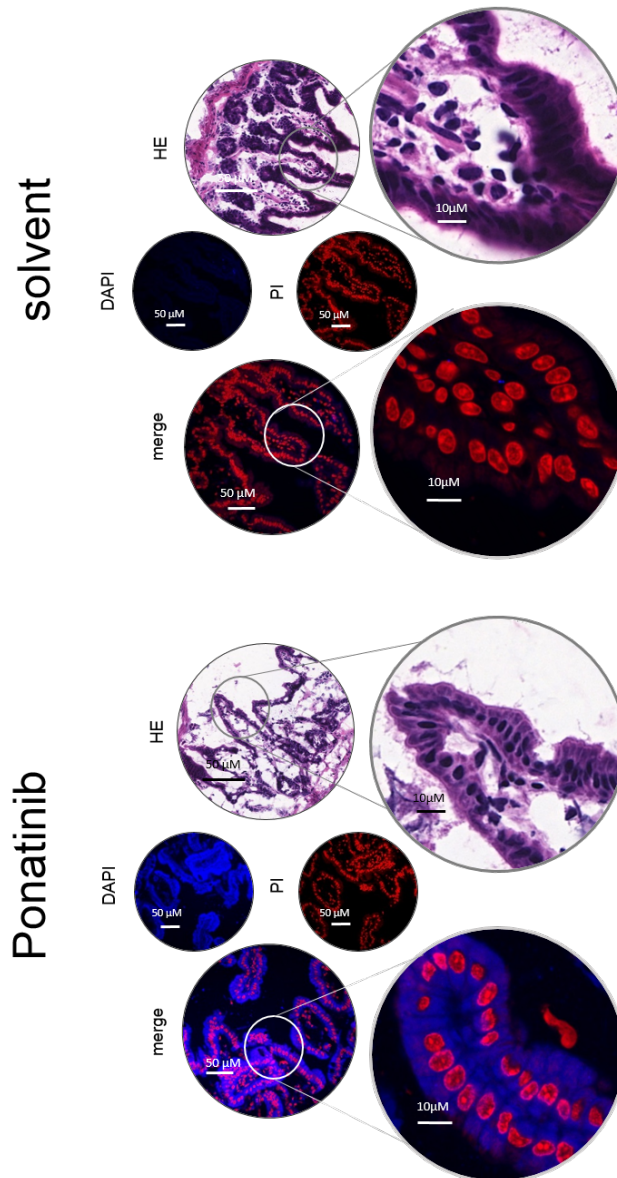


Figure 24: Ponatinib uptake is detectable in small intestine cryosections from orally treated mice. SCID mice, bearing lung tumor xenografts, were treated orally with 30 mg ponatinib per kg weight for 2 h. Mice were sacrificed and consecutive cryosections were generated. Ponatinib fluorescence was imaged by CLSM using DAPI and PI channels. Propidium iodide (PI) was used as nuclear counterstain. H/E staining was used as histologically control.

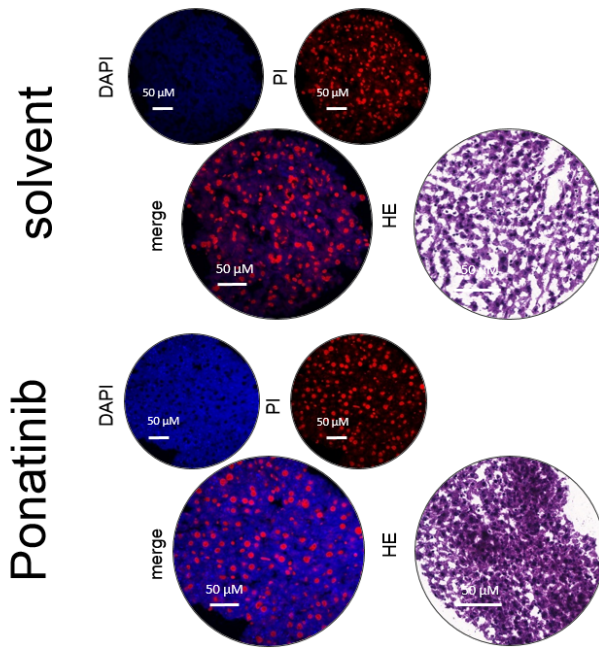


Figure 25: Ponatinib uptake is detectable in liver cryosections from orally treated mice. SCID mice, bearing lung tumor xenografts, were treated orally with 30 mg ponatinib per kg weight for 2 h. Mice were sacrificed and consecutive cryosections were generated. Ponatinib fluorescence was imaged by CLSM using DAPI and PI channels. Propidium iodide (PI) was used as nuclear counterstain. H/E staining was used as histologically control.

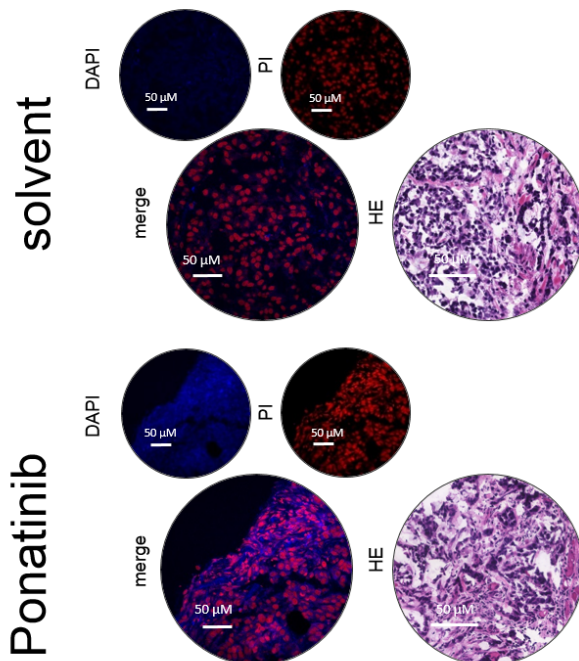


Figure 26: Ponatinib uptake is detectable in tumor cryosections from orally treated mice. SCID mice, bearing lung tumor xenografts, were treated orally with 30 mg ponatinib per kg weight for 2 h. Mice were sacrificed and consecutive cryosections were generated. Ponatinib fluorescence was imaged by CLSM using DAPI and PI channels. Propidium iodide (PI) was used as nuclear counterstain. H/E staining was used as histologically control.

In adipose tissue (Figure 27), kidney and lung cryosections (data not shown) no ponatinib fluorescence was detectable, due to high auto-fluorescence of these tissue types.

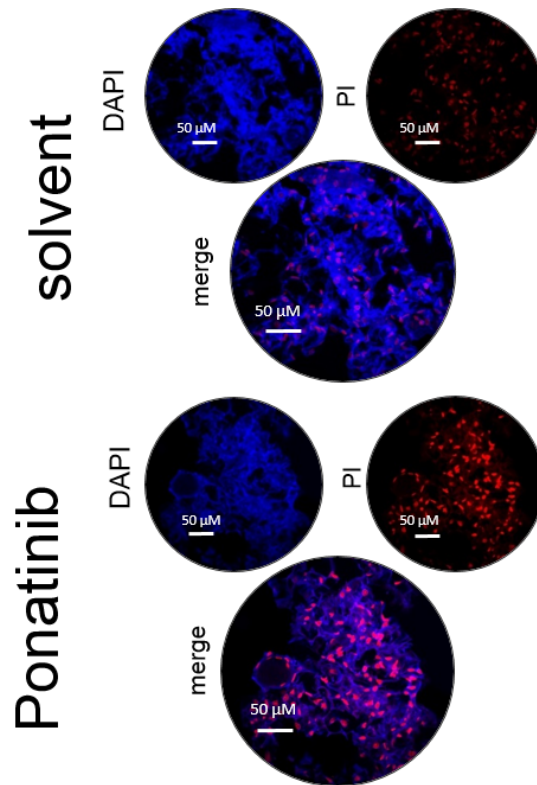


Figure 27: Ponatinib imaging in adipose tissue cryosections is hampered by tissue auto-fluorescence. SCID mice, bearing lung tumor xenografts, were treated orally with 30 mg ponatinib per kg weight for 2 h. Mice were sacrificed and consecutive cryosections were generated. Ponatinib fluorescence was imaged by CLSM using DAPI and PI channels. Propidium iodide (PI) was used as nuclear counterstain.

For each tissue slice, the ponatinib fluorescence intensity in simulated single cells was quantified using Tissue Studio software. Figure 28 shows the coloring of the ponatinib channel of colon, small intestine and tumor samples according to the measured intensity ranges. Strong drug fluorescence was observed in the small intestine tissue, as compared to colon and tumor (Figure 28).

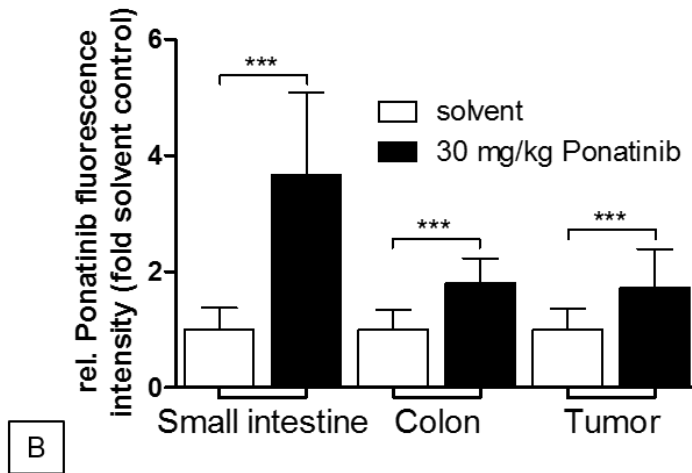
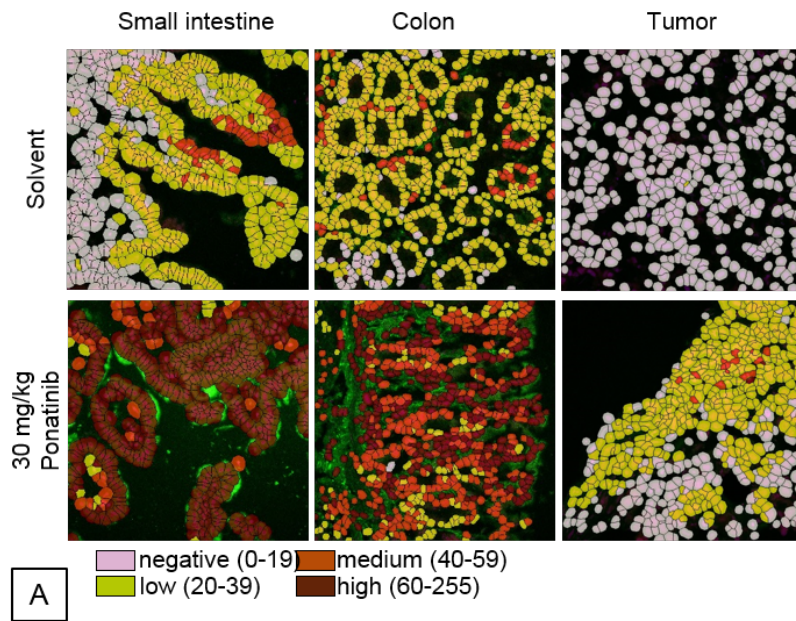


Figure 28: Strong ponatinib-fluorescence intensity is detectable in simulated single cells of small intestine. SCID mice, bearing lung tumor xenografts, were treated orally with 30 mg ponatinib per kg weight for 2 h. Mice were sacrificed and consecutive cryosections were generated. Ponatinib fluorescence was quantified with Tissue Studio software. A) The DAPI channels of small intestine, colon and tumor 8-bit images were divided and colored in respect to the measured intensity ranges, given below the figure. B) Quantification of ponatinib fluorescence intensity in simulated single cells of small intestine, colon and tumor cryosections. Significance was calculated using D'Agostino and Pearson omnibus normality test, followed by two-tailed Mann-Whitney test (**= $p < 0.001$).

4.2. LDs as ponatinib resistance mechanism

As mentioned earlier (chapter 4.1.2 Ponatinib is fluorescent and accumulates in lipid droplets (LDs)), ponatinib accumulates specifically in LDs. Pharmacological induction (by oleic acid, OA) or depletion (by triacsin c, TC) of LD formation revealed strong dependence of NCI-H1703 cell ponatinib sensitivity on the LD status (Figure 29A). This was also observed for HeLa cervix carcinoma cells upon LD induction with OA (Figure 29B).

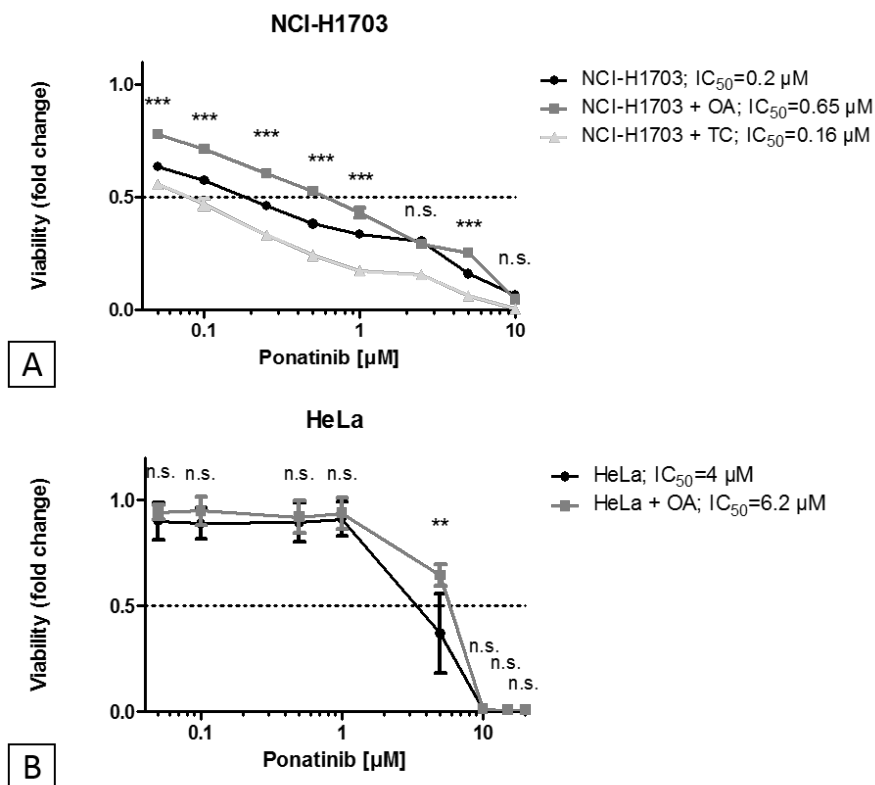


Figure 29: The LD status influences the sensitivity of two cancer cell lines towards ponatinib. A) NCI-H1703 lung cancer and B) HeLa cervix carcinoma cells were exposed to increasing concentrations of ponatinib for 72 h. Depletion of LDs was with 0.1 μM TC for 72 h, induction of LDs was with 100 μM OA for 72 h. Viability was determined with MTT assay. Each data point represents the mean \pm SD of triplicate values of a representative experiment, performed in three times. Significance was calculated using two-way ANOVA with Bonferroni post-test (**=p<0.01; ***=p<0.001).

4.2.1. Lipid levels are increased in ponatinib resistant sublines

To further define the mechanisms responsible for ponatinib accumulation in LDs, DMS114 and NCI-H1703 cells were constantly exposed to low doses of ponatinib in order to establish ponatinib-resistant sublines (DMS114/PON and NCI-

CHAPTER FOUR: RESULTS

H1703/PON). As expected, the ponatinib-resistant sublines showed decreased sensitivity towards ponatinib in viability assays (Figure 30). Importantly, lipid content analysis, analyzed by flow cytometry of Bodipy 493/503-stained cells revealed increased overall LD content in DMS114/PON cells despite a tendency towards decreased fatty uptake levels (Figure 31A, B). In addition, triglyceride- and cholesterol levels were distinctly elevated in DMS114/PON cells as compared to parental cells, as determined by gas chromatography (Figure 31C). Strikingly, also in NCI-H1703/PON cells elevated lipid content was observed (Figure 31D)

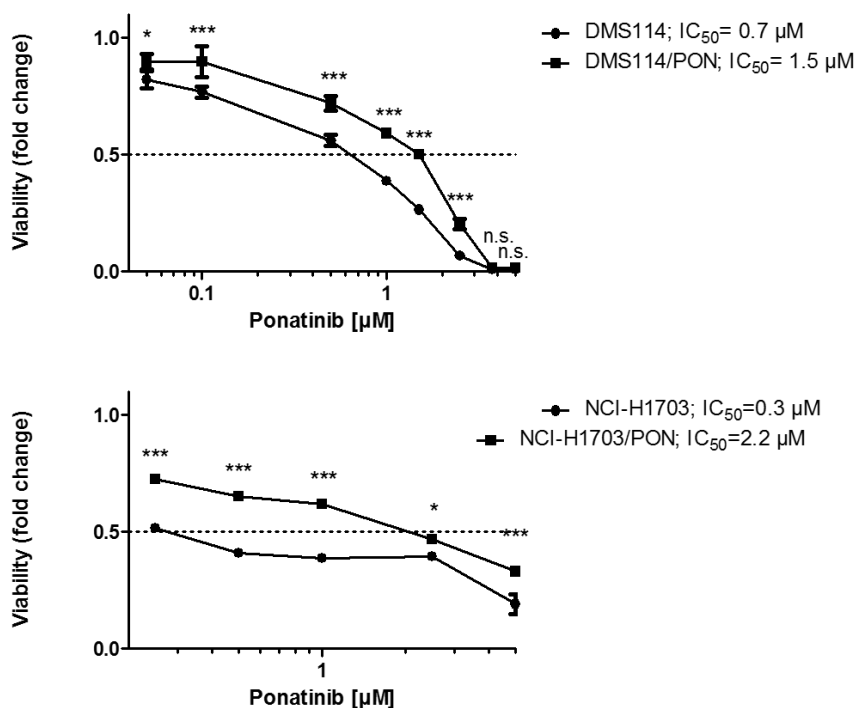


Figure 30: Ponatinib-resistant sublines of lung cancer cells show increased resistance towards ponatinib. DMS114 and NCI-H1703 parental- and ponatinib-resistant cells were exposed to increasing concentrations of ponatinib for 72 h. DMS114/PON and NCI-H1703/PON cells were exposed to ponatinib (10 µM and 3 µM, respectively) in constant intervals. Viability was determined with MTT assay. Each data point represents the mean \pm SD of triplicate values of a representative experiment, performed in three times. Significance was calculated using two-way ANOVA with Bonferroni post-test (*= $p < 0.05$; ***= $p < 0.001$).

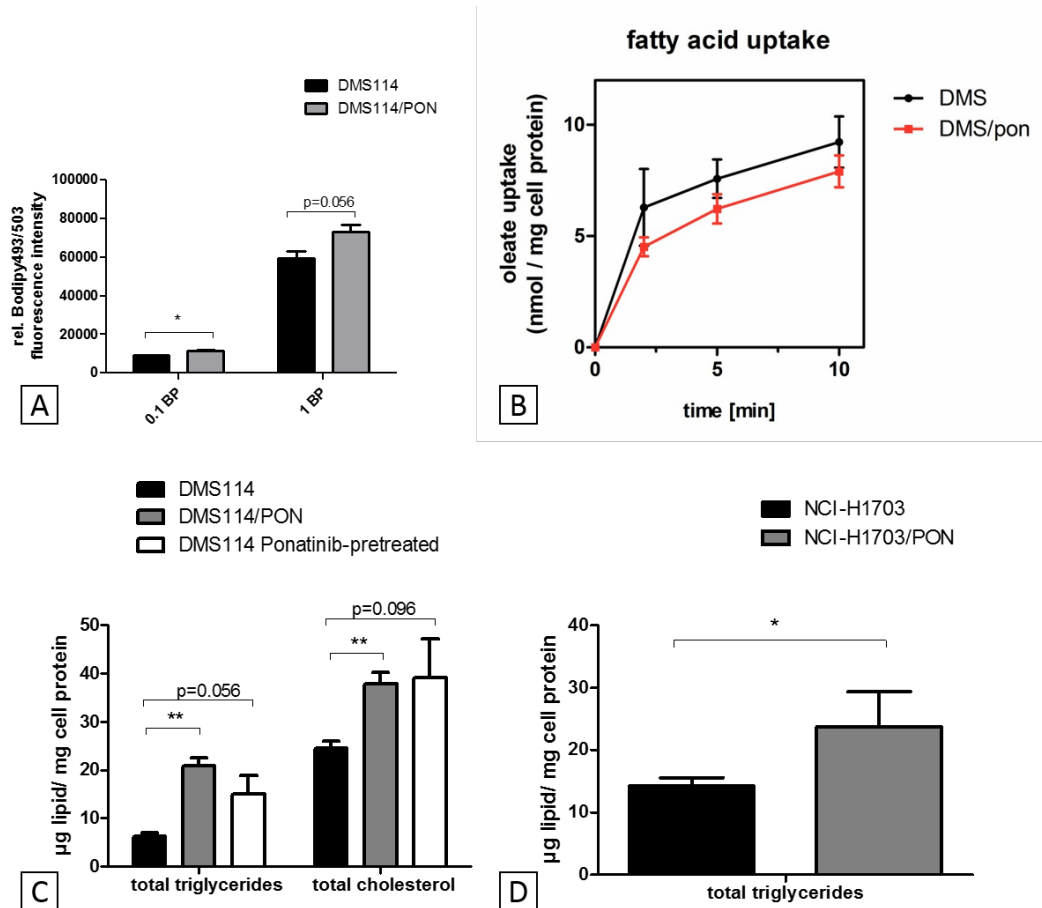


Figure 31: Ponatinib-resistant lung cancer cells show alterations in lipid content and fatty acid uptake. A) Lipid droplet content of trypsinized DMS114 and ponatinib-resistant DMS114/PON cells was quantified by flow cytometry, using FITC channel. Bodipy 493/503 served as LD marker. DMS114/PON cells were exposed to 10 μM of ponatinib in constant intervals. Significance was calculated using student's t-test (*= $p < 0.05$). B) Fatty acid uptake of DMS114 and DMS114/PON cells was measured by GC analysis. C) Total triglyceride and cholesterol content in ponatinib-naïve, -pretreated and -resistant DMS114 cells was determined by GC analysis. Ponatinib pre-treatment was with 1 μM for 1 h. DMS114/PON cells were exposed to 10 μM of ponatinib in constant intervals and also pre-treated 5 days prior to GC analysis with 1 μM of ponatinib. Significance was calculated using student's t-test (**= $p < 0.01$). D) Total triglyceride content in ponatinib-resistant NCI-H1703 and ponatinib-naïve NCI-H1703 cells was determined by GC analysis. Ponatinib pre-treatment was with 1 μM for 1 h. NCI-H1703/PON cells were exposed to 3 μM of ponatinib in constant intervals and also pre-treated 5 days prior to GC analysis with 1 μM of ponatinib. Significance was calculated using student's t-test (**= $p < 0.05$).

Interestingly, an elevated ponatinib uptake in the ponatinib resistant subline DMS114/PON was observed by flow cytometry, pointing towards a direct correlation between LD content and ponatinib resistance (Figure 32).

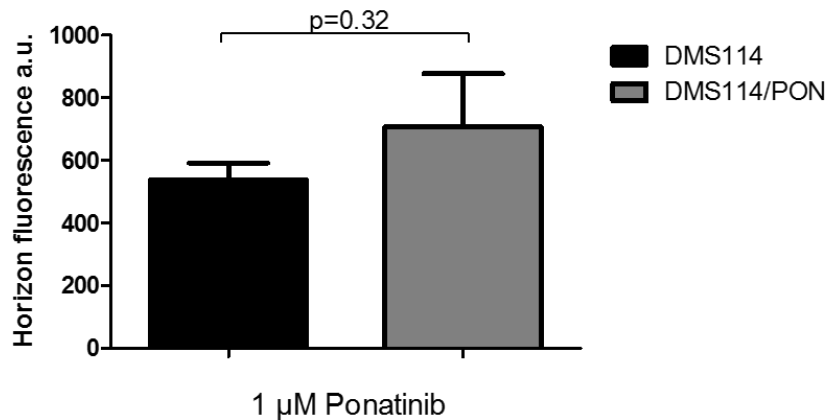


Figure 32: Ponatinib-resistant lung cancer cells show an increased ponatinib uptake. DMS114 and DMS114/PON cells were exposed to 1 μ M of ponatinib for 30 min. Intracellular ponatinib content of DMS114 and DMS114/PON cells was quantified by flow cytometry of trypsinized cells, using Horizon V450-A channel. Significance was calculated using student's t-test.

4.2.2. The role of MTP

In order to gain insights into transcriptional deregulations on the course of ponatinib resistance generation of DMS114 cells, a previous whole-genome gene expression analysis performed by B. Englinger, MSc, PhD, was analyzed *de novo*. This revealed upregulated expression (16-fold) of the gene encoding microsomal triglyceride transfer protein (*MTTP*, MTP) in DMS114/PON cells (Figure 33A). However, aCGH analysis revealed no amplification of the *MTTP* gene locus on chromosome 4 (4q23) in DMS114/PON cells in comparison to DMS114 cells, suggesting alternative mechanisms for MTP upregulation (Figure 33B). Hence, expression of putative transcription factors binding to the *MTTP* promoter was analyzed, identifying NR2F2 as upregulated (4-fold) in DMS114/PON cells (Figure 33C,D). Finally, a MTP-containing colored KEGG pathway was analyzed, based on differentially expressed genes of DMS114/PON cells compared to DMS114 cells to illustrate the central role of MTP in cellular lipid homeostasis. Red color indicates upregulated gene expression in the ponatinib-resistant cell line, while blue color stands for downregulated gene expression compared to the parental cell line (Figure 34).

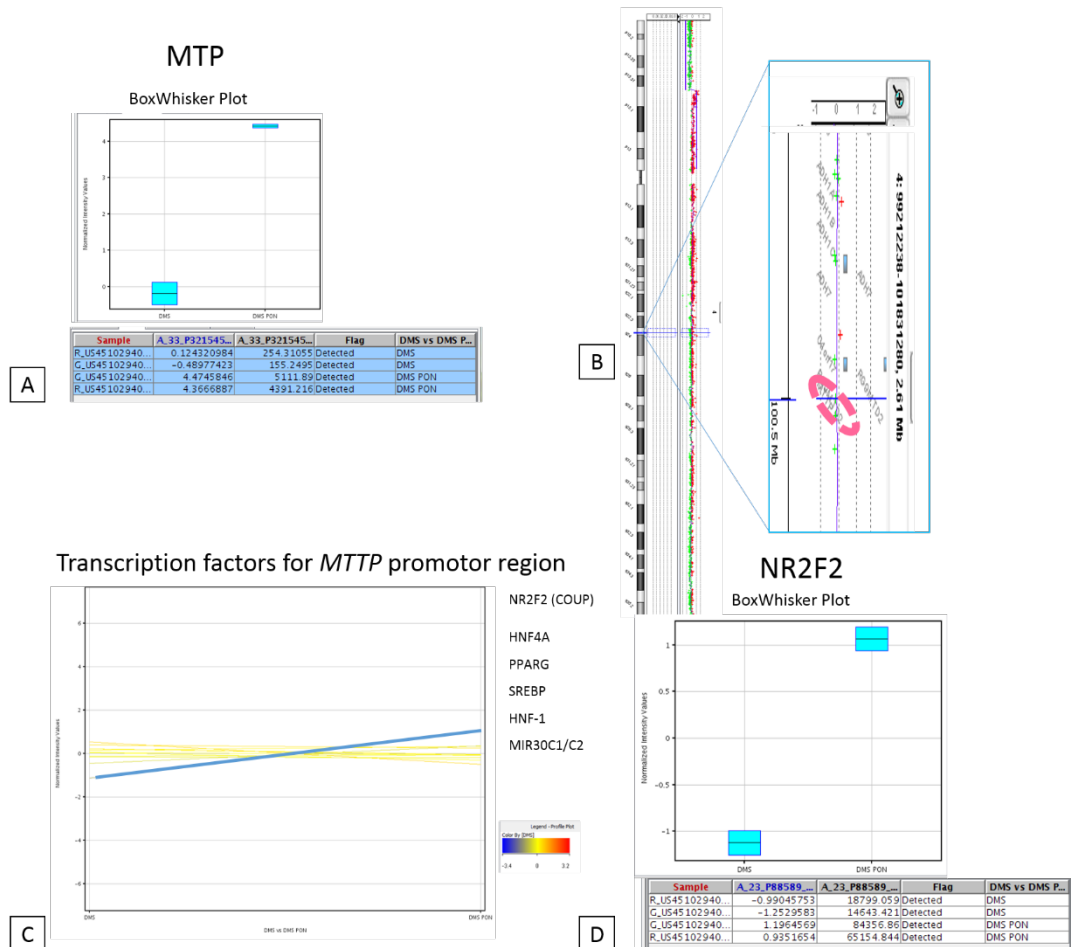


Figure 33: Elevated levels of MTP and NR2F2 expression in ponatinib-resistant lung cancer cells. A) Whole-genome gene expression revealed upregulated expression (16-fold) of MTP in DMS114/PON cells. B) Array comparative genomic hybridization (aCGH) showed normal copy number of *MTTP* (pink circle) on chromosome 4 (4q23) in DMS114/PON cells. C) Listed up- and deregulated alternative transcription factors for *MTTP* promoter region in DMS114/PON cells. D) Whole-genome gene expression revealed upregulated expression (4-fold) of NR2F2 in DMS114/PON cells, indicated by the blue line. aCGH and whole-genome expression array were performed by Bernhard Enginger, MSc, PhD.

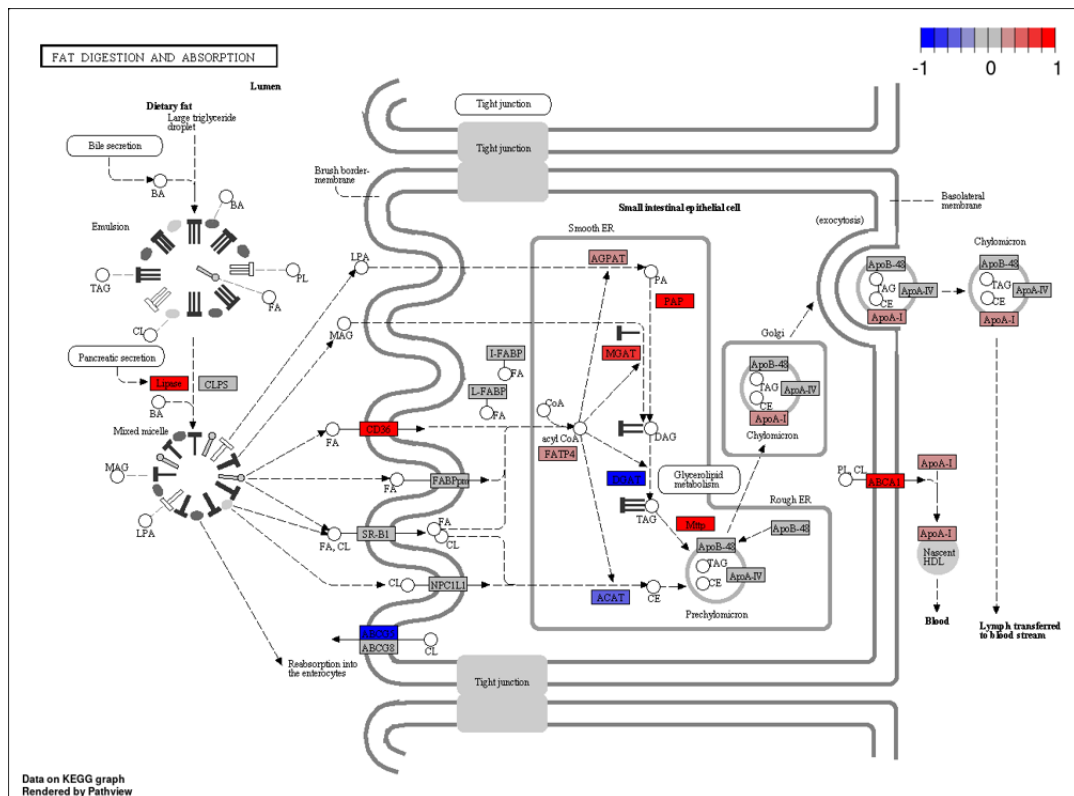


Figure 34: MTP has a central role in cellular lipid homeostasis. *MTTP* gene expression in DMS114/PON vs. DMS114 cells and the relation to lipoprotein homeostasis. The “fat digestion and absorption” KEGG pathway was colored using the Search&Color KEGG pathway mapping tool. The red color illustrates upregulated *MTTP* expression in DMS114/PON cells as compared to DMS114 cells.

Additionally, mRNA expression levels of *MTTP* and three other LD-associated genes (*PLIN1* (Perilipin), *PLIN2* (ADRP), *PLIN3* (Tip47)) were quantified with real-time quantitative polymerase chain reaction (qRT-PCR). This qRT-PCR revealed massive upregulation of *MTTP* mRNA in DMS114/PON cells as compared to DMS114 cells (Figure 35A). In contrast to this, mRNA levels of ADRP, Tip47 and Perilipin were decreased in DMS114/PON cells (Figure 35B). Subsequently, MTP was shown to be also overexpressed on a protein level in DMS114/PON cells (Figure 36).

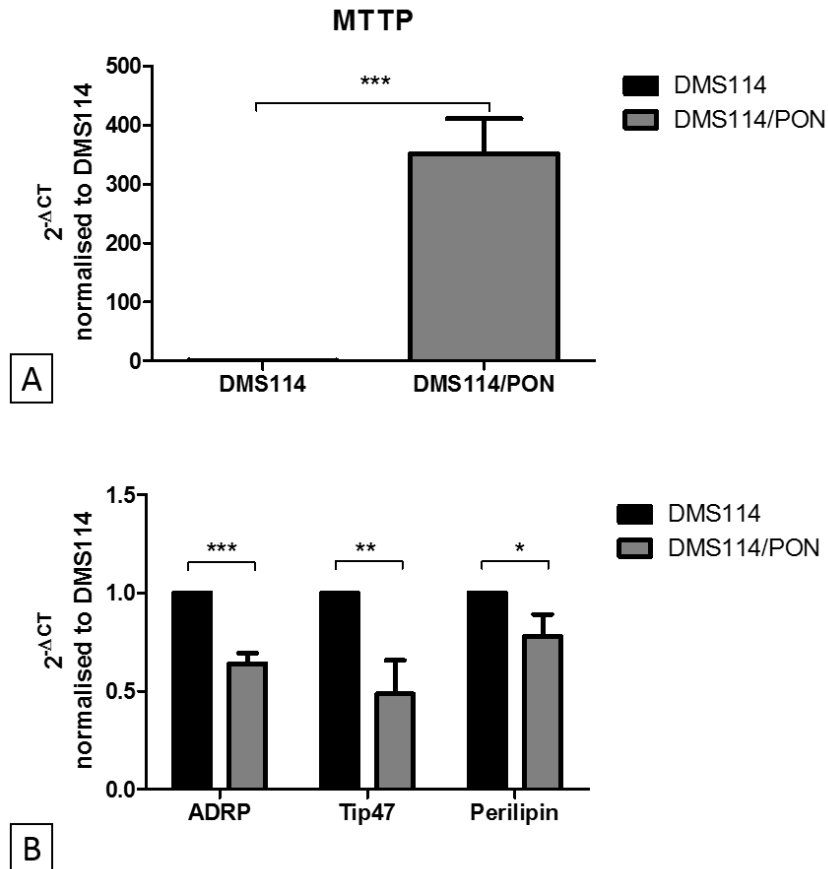


Figure 35: Massive upregulation of *MTPP* in ponatinib-resistant lung cancer cells. mRNA expression levels of A) *MTPP* and B) *PLIN1* (Perilipin), *PLIN2* (ADRP), *PLIN3* (Tip47) in DMS114 and DMS114/PON cells were quantified by qRT-PCR. Respective expression levels were normalized to the housekeeping gene β -actin (ΔCT) and converted to a linear form using $2^{-\Delta\text{CT}}$ and further normalized to DMS114 by dividing the values with $2^{-\Delta\text{CT}}$ from DMS114. Significance was calculated using student's t-test (**= $p < 0.001$; **= $p < 0.01$ and *= $p < 0.05$).

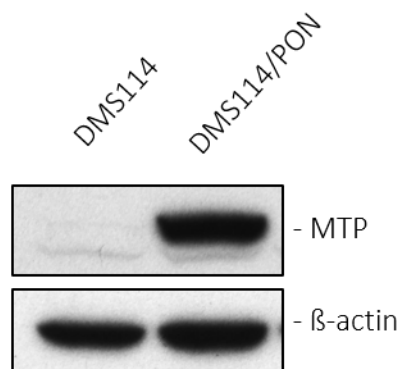


Figure 36: MTP overexpression on a protein level in ponatinib-resistant lung cancer cells. MTP expression in DMS114 and DMS114/PON cells was determined by Western blot. β -actin served as loading control.

To investigate whether upregulated expression of MTP is the link to enhanced LD formation and thus mediates a cellular-adaptive response of DMS114/PON cells towards ponatinib, *MTTP* gene expression of DMS114/PON cells was transiently knocked down with MTP siRNA. Decreased expression of MTP was verified on a protein level 48 and 72 h after knockdown. (Figure 37).

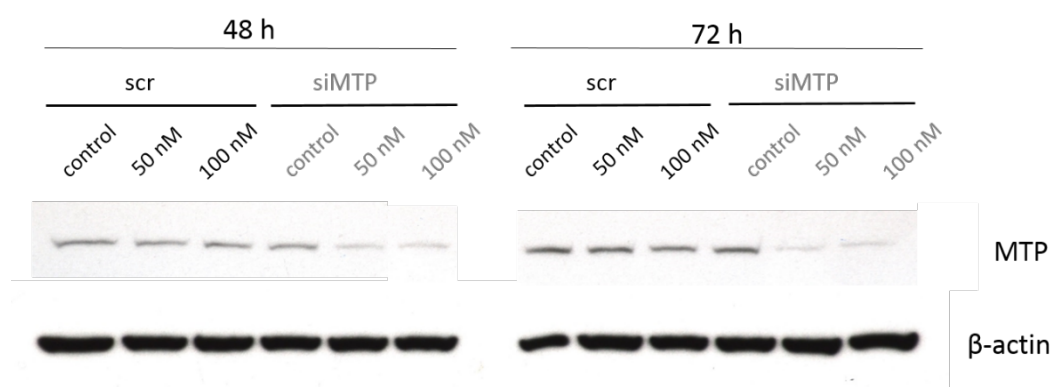


Figure 37: Decreased expression of MTP in ponatinib-resistant lung cancer cells after *MTTP* knockdown. DMS114/PON cells were transfected with scrambled and MTP-siRNA using Xfect transfection reagent. MTP expression in DMS114/PON cells was determined by Western blot, 48 and 72 h after MTP knockdown. β -actin served as loading control.

Surprisingly, cell viability assays showed increased resistance of *MTTP* knockdown cells towards ponatinib, when compared to both untransfected and scrambled siRNA-treated DMS114/PON cells (Figure 38A). In addition, flow cytometry experiments revealed marginally, and non-significantly increased LD- as well as ponatinib content in *MTTP* knockdown cells (Figure 38B).

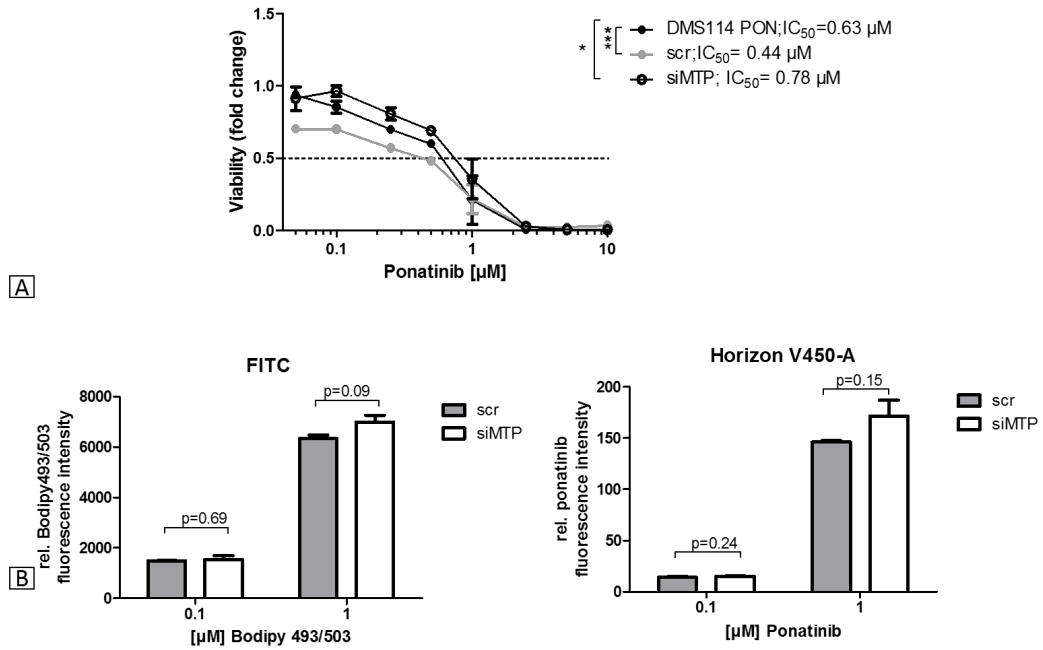


Figure 38: *MTTP* knockdown increases resistance towards ponatinib and marginally increases LD- and ponatinib content in ponatinib-resistant lung cancer cells. DMS114/PON cells were transfected with scrambled and MTP siRNA using Xfect transfection reagent. A) Cells were exposed to increasing concentrations of ponatinib for 72 h. Viability was determined with MTT assay. Each data point represents the mean \pm SD of triplicate values of a representative experiment, performed in three times. Significance was calculated using two-way ANOVA with Bonferroni post-test (*= $p < 0.05$; ***= $p < 0.001$). B) Intracellular LD and ponatinib content was quantified by flow cytometry of trypsinized cells, using FITC and Horizon V450-A channel, respectively. Cells were exposed to ponatinib or Bodipy 493/503 for 30 min. Bodipy 493/503 served as LD marker. Significance was calculated using student's t-test.

To further define the role of MTP concerning LD formation, MTP was also pharmacologically inhibited with its specific inhibitor lomitapide. This FDA- and European Medicines Agency (EMA)-approved compound blocks the assembly process of very low density lipoprotein (VLDL) on ER membranes [81]. In cell viability assays, lomitapide was more cytotoxic in DMS114 than DMS114/PON cells (Figure 39A). Further MTT assays, combining ponatinib and lomitapide, revealed no synergistic or additive effects of these drugs (Figure 39B).

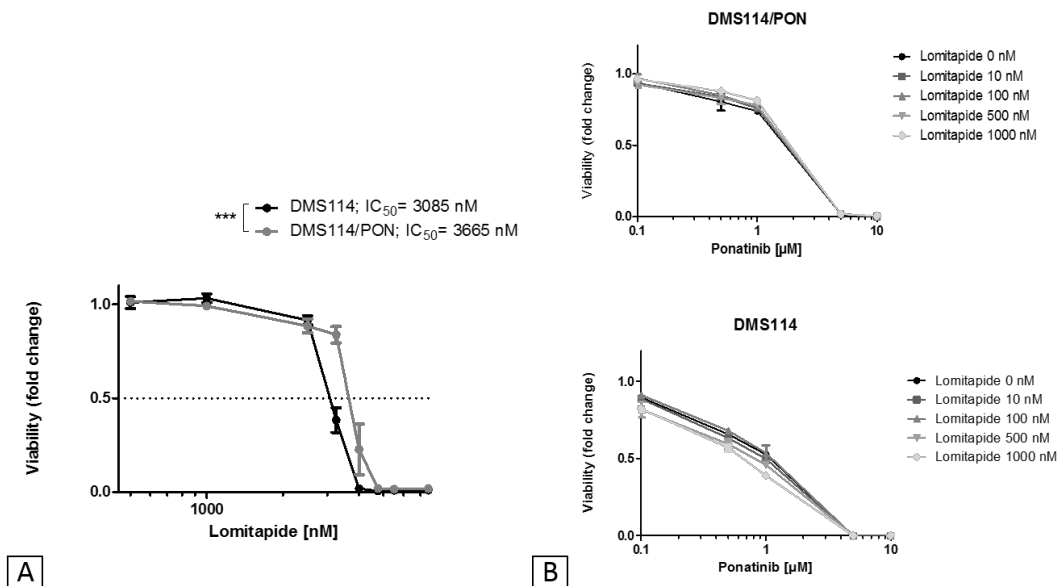


Figure 39: Ponatinib-resistant lung cancer cells show increased resistance towards lomitapide. DMS114 and DMS114/PON cells were exposed to increasing concentrations of lomitapide only (A) or in combination with ponatinib (B) for 72 h. DMS114/PON cells were exposed to 10 μ M of ponatinib in constant intervals. Viability was determined with MTT assay. Each data point represents the mean \pm SD of triplicate values of a representative experiment, performed in three times. Significance was calculated using two-way ANOVA with Bonferroni post-test (**= p <0.001).

Interestingly, pre-treatment with 2 μ M of lomitapide for 72 h resulted in an increased content of both LDs and ponatinib in DMS114/PON cells, as compared to lomitapide-untreated DMS114/PON cells. As expected, lomitapide addition had only minor effects in DMS114 cells (Figure 40A). Further, lomitapide pre-treatment had no impact on cell viability assays in parental DMS114 cell resistance towards ponatinib. Interestingly, in DMS114/PON cells, pre-treatment with lomitapide decreased the sensitivity towards ponatinib (Figure 40B).

Subcellular analysis with CLSM revealed a distinct LD induction in DMS114/PON cells upon addition of lomitapide for 24 h, as compared to DMS114 cells (Figure 41-42). Furthermore, as expected, OA treatment led to increased intracellular LD levels in both cell lines. However, when OA was combined with lomitapide, this resulted in massive LD induction in DMS114/PON cells, while a similar effect was not observed in parental cells. This suggests a crucial role of MTP upregulation as adaptive mechanism enhancing lipid export (Figure 41-42).

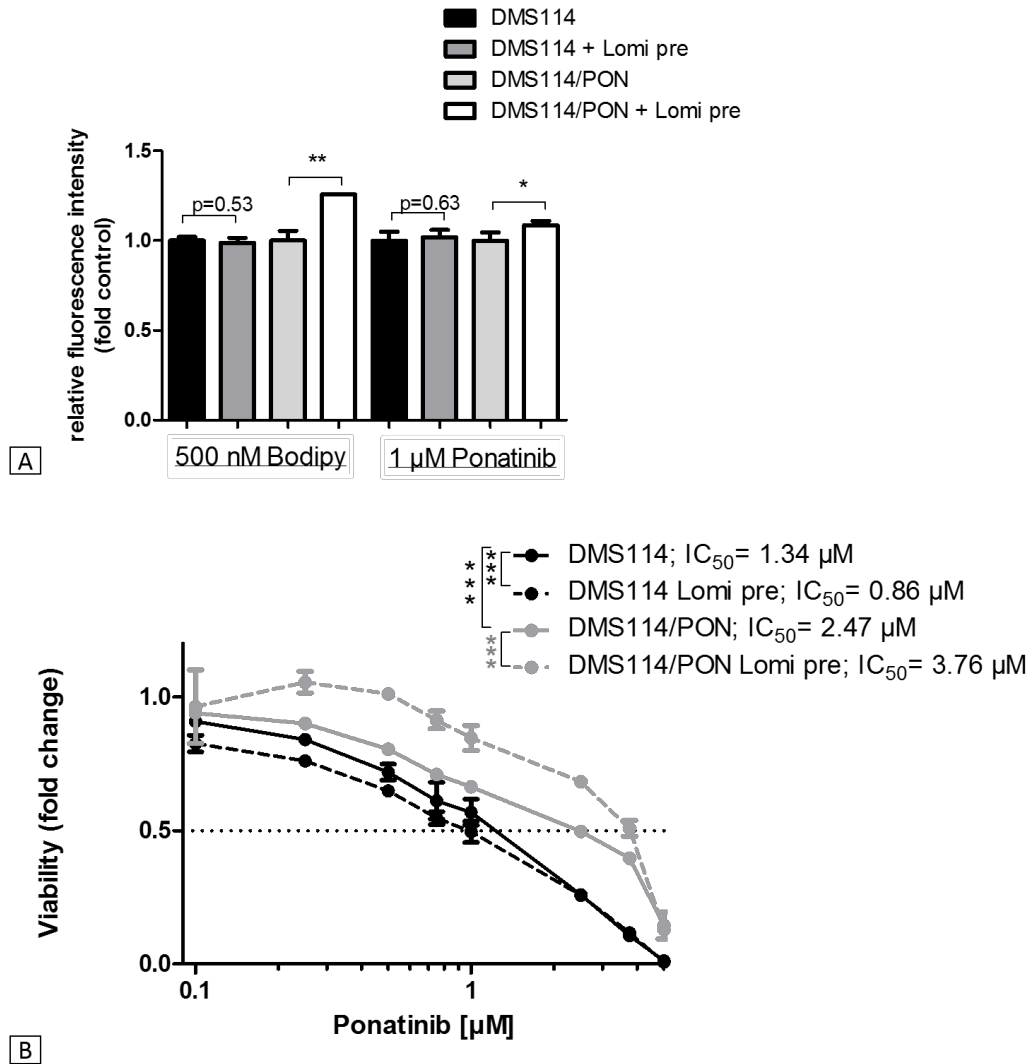


Figure 40: Pre-incubation with lomitapide increases LD- and ponatinib content, and contributes to an increased resistance towards ponatinib in ponatinib-resistant lung cancer cells. A) DMS114 and DMS114/PON cells were pre-incubated with 2 μM of lomitapide for 72 h. Cells were exposed to 500 nM of Bodipy 493/503 for 15 min or to 1 μM of ponatinib for 30 min. Intracellular LD- and ponatinib content was quantified by flow cytometry of trypsinized cells, using FITC and DAPI channels, respectively. Bodipy 493/503 served as LD marker. Significance was calculated using student's t-test (**=p<0.01 and *=p<0.05). B) DMS114 and DMS114/PON cells were pre-incubated with 2 μM for 72 h and compared to lomitapide-untreated DMS114/PON and DMS114 cells. All cells were exposed to increasing concentrations of ponatinib for 72 h. Viability was determined with MTT assay. Each data point represents the mean ± SD of triplicate values of a representative experiment, performed in three times. Significance was calculated using two-way ANOVA with Bonferroni post-test (***=p<0.001).

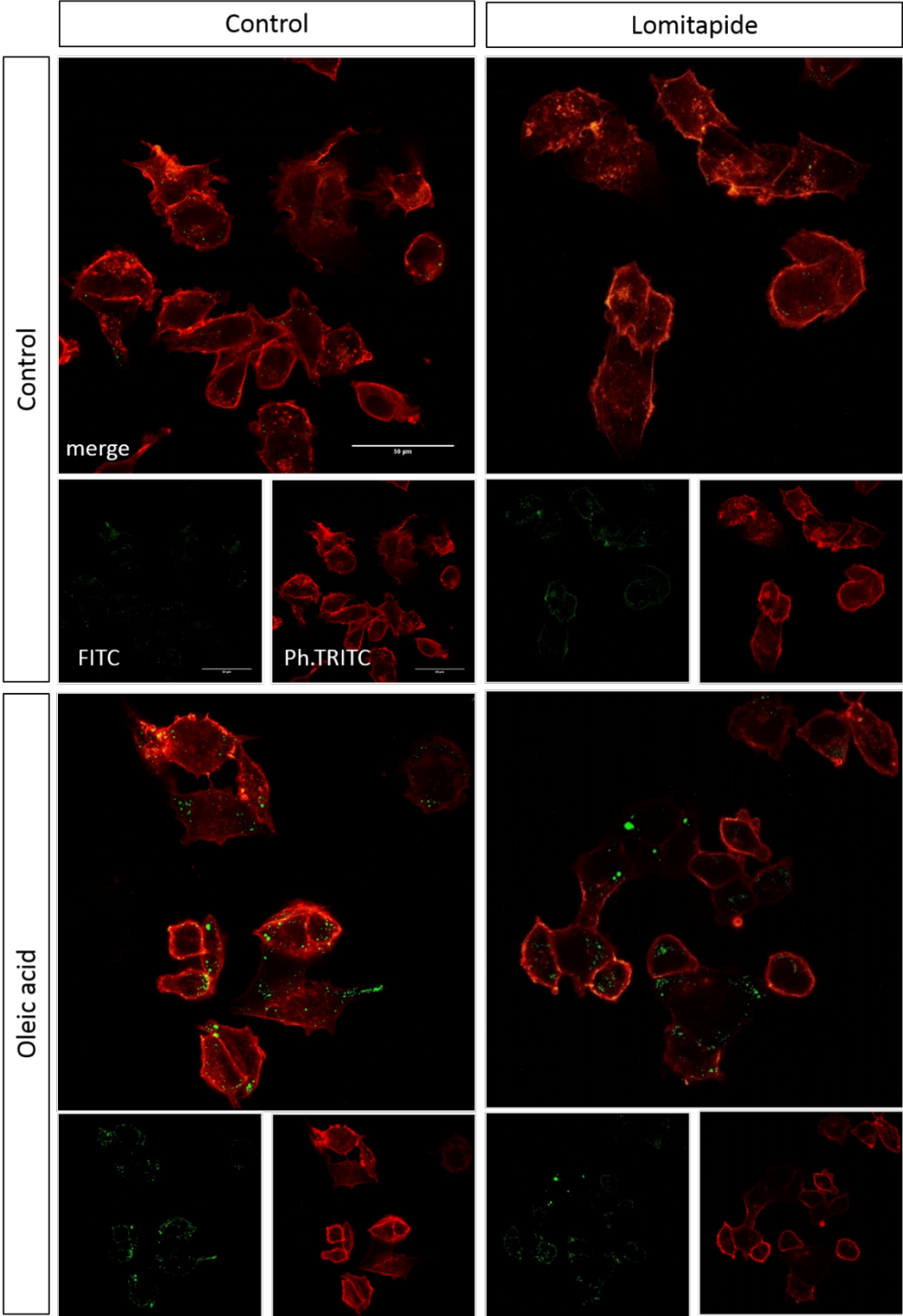


Figure 41: Treatment with OA, but not with lomitapide increases LD accumulation in lung cancer cells. DMS114 cells were treated with 2 μM of lomitapide and/or 100 μM of OA for 24 h. Subcellular LD accumulation was analyzed by CLSM using FITC and Phalloidin-TRITC channels. Bodipy 493/503 served as LD marker, phalloidin-TRITC as actin staining. Scale bars indicate 50 μM .

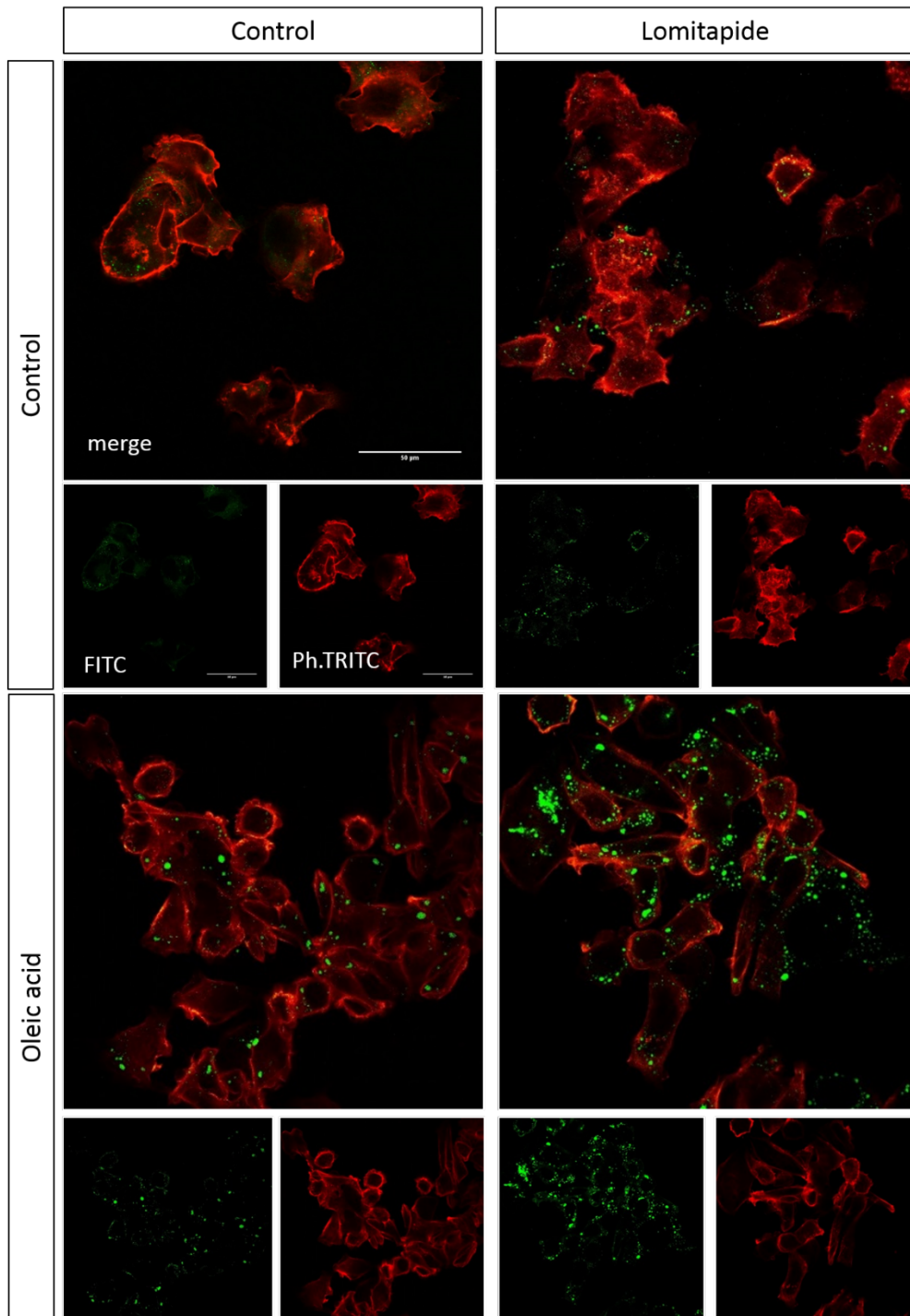


Figure 42: Simultaneous treatment with lomitapide and OA massively increases LD accumulation in ponatinib-resistant lung cancer cells. DMS114/PON cells were treated with 2 μM of lomitapide and/or 100 μM of OA for 24 h. Subcellular LD accumulation was analyzed by CLSM using FITC and Phalloidin-TRITC channels. Bodipy 493/503 served as LD marker, phalloidin-TRITC as actin staining. Scale bars indicate 50 μM .

4.3. Characterization of ponatinib derivatives

In cooperation with the Institute for Inorganic Chemistry at the University of Vienna, various derivatives of ponatinib were designed and synthesized in order to investigate the effects of structural alterations on lipophilicity, subcellular distribution or toxicity on DMS114, NCI-H520 and NCI-H1703 lung cancer cells. Design and synthesis of derivatives were performed by Dipl.-Ing. Marlene Mathuber from the Institute for Inorganic Chemistry and the following results will also be given in her dissertation.

4.3.1. Effect of chemical modifications on ponatinib toxicity

The derivatives MMAT057-2, MMAT077-3, MMAT066-2, MMAT040-3 and MMAT081-1 bear in common a replacement of the methylpiperazine, whereas derivative MMAT095-6 is missing the trifluoromethyl group (Figure 43). Viability assays revealed a huge impact of structural modification on the toxicity of ponatinib, illustrated by the fact that none of the derivatives were as cytotoxic as the parental compound. In general, the killing potential of all derivatives varied between the cell lines (DMS114, NCI-H520 and NCI-H1703). Nevertheless, derivative MMAT081-1 was effective in all three cell lines, whereas MMAT057-2 had the weakest toxicity in all three cell lines (Figure 44).

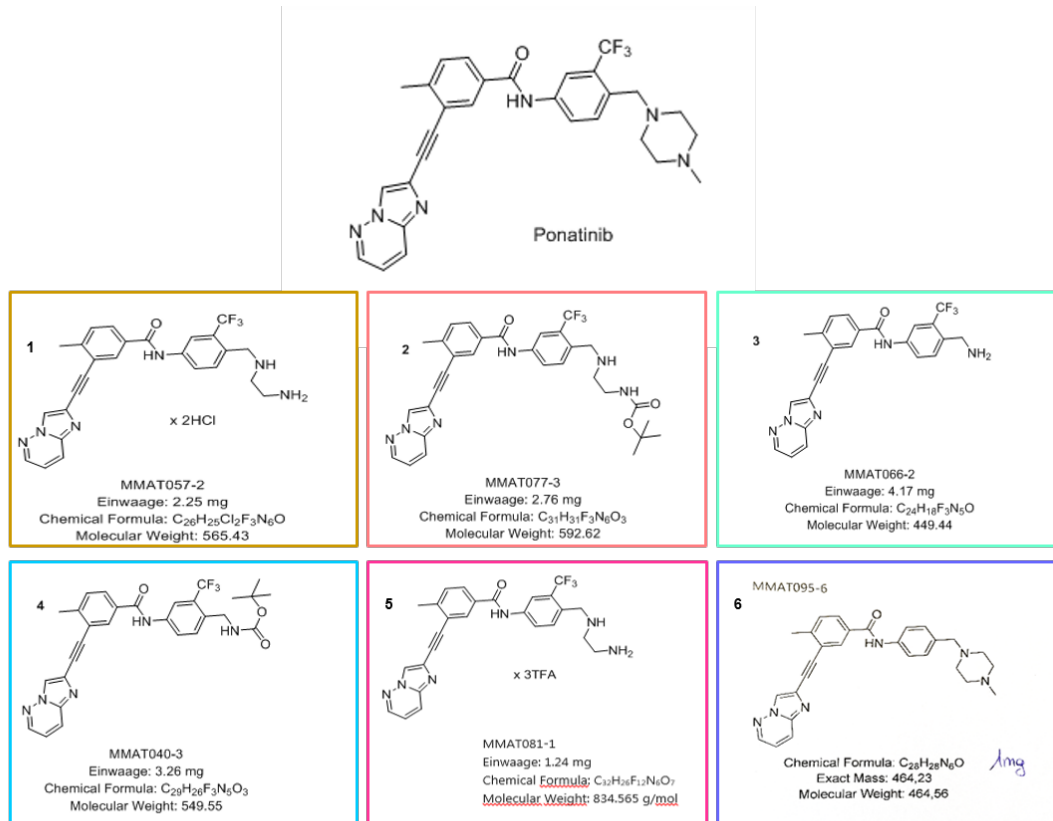


Figure 43: Molecular structure, formula and weight of ponatinib and all six derivatives. All derivatives were designed and synthesized by Dipl. Ing. Marlene Mathuber.

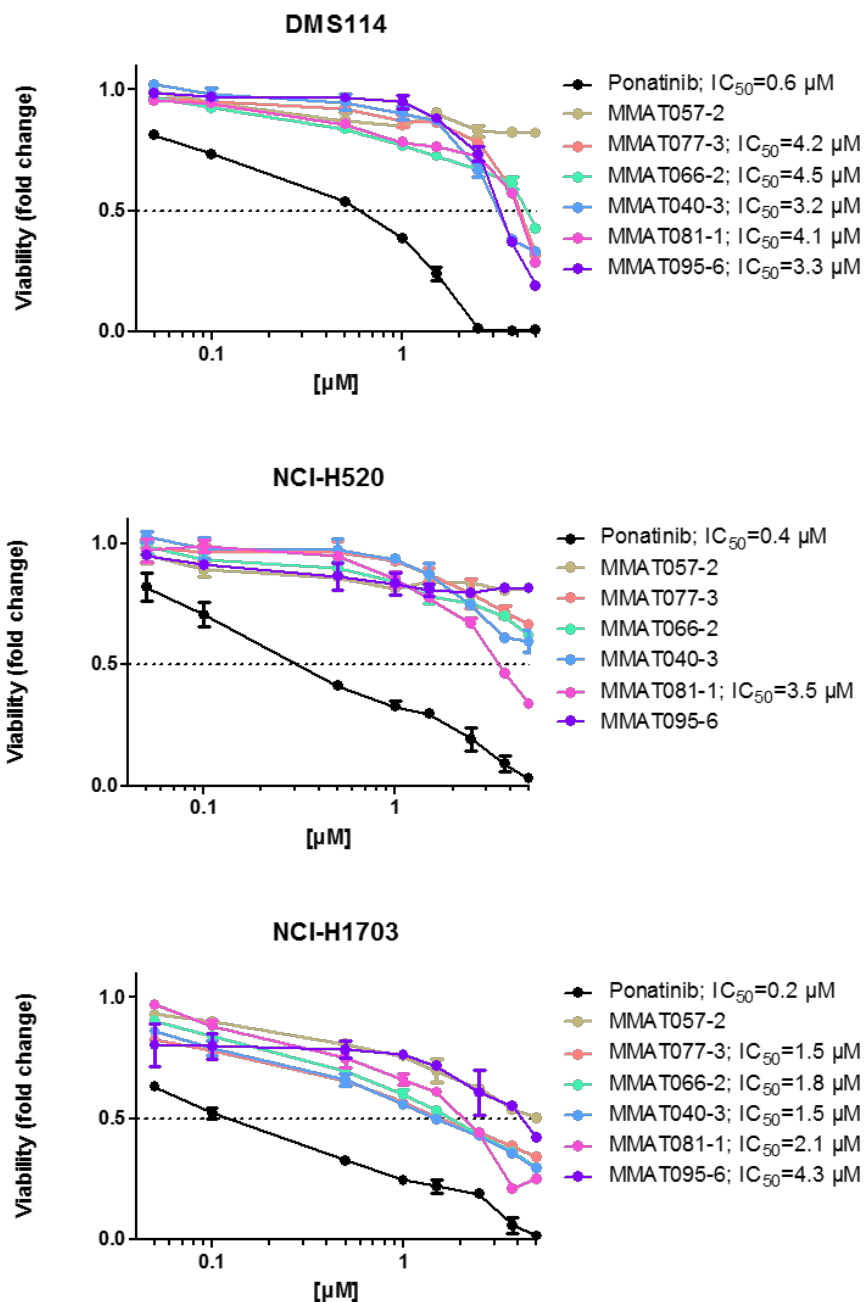


Figure 44: Structural modifications impair the cytotoxic activity of ponatinib. Cytotoxicity of ponatinib and synthesized derivatives of ponatinib: MMAT057-2, MMAT077-3, MMAT066-2, MMAT040-3, MMAT081-1 and MMAT095-6 in DMS114, NCI-H520 and NCI-H1703 cells. Cells were exposed to increasing drug concentrations for 72 h. Viability was determined with MTT assay. Each data point represents the mean \pm SD of triplicate values of a representative experiment, performed in three times.

4.3.2. Effect of chemical modifications on subcellular distribution of ponatinib

In order to gain insights into the subcellular distribution of all ponatinib derivatives, CLSM was performed. Therefore, all derivatives were checked in a prior step for their intracellular fluorescence. Flow cytometry in NCI-H1703 cells revealed elevated fluorescence for MMAT081-1 when compared to ponatinib in the Horizon V450 channel. All the other derivatives showed less fluorescence intensities than ponatinib. Especially the derivatives MMAT057-2, MMAT077-3 and MMAT040-3 demonstrated massively reduced fluorescence intensities (Figure 45). These results were similar for the DAPI and Qdot 605 channel (data not shown). In contrast, for FITC, PE-A, PE-Texas Red, PE-Cy5, PE-Cy7, APC-Cy7, Indo-1, APC-A, Qdot 605 and Alexa Fluor channels no differences were detectable (data not shown).

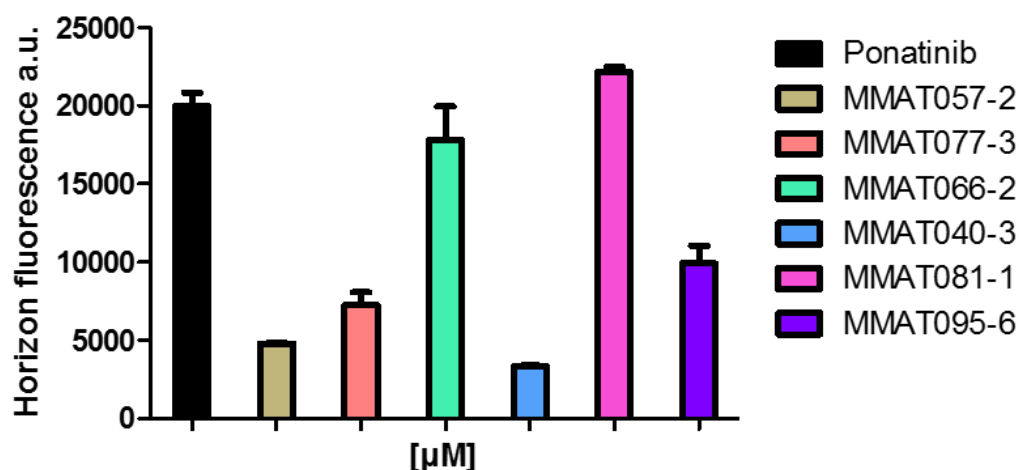


Figure 45: Structural modifications alter the fluorescence intensity of ponatinib. Intracellular fluorescence of ponatinib and ponatinib derivatives MMAT057-2, MMAT077-3, MMAT066-2, MMAT040-3, MMAT081-1 and MMAT095-6 in NCI-H1703 cells after 30 min of incubation. Ponatinib and ponatinib derivative fluorescence was quantified by flow cytometry of NCI-H1703 cells treated with 10 μM of respective drugs using the Horizon V450 channel.

In CLSM experiments, the derivatives MMAT057-2 and MMAT081-1 showed no similarities with ponatinib in terms of cellular distribution. They rather accumulated in proximity to the endoplasmic reticulum. On the contrary, derivative MMAT040-3 appeared to have a similar distribution like ponatinib

CHAPTER FOUR: RESULTS

indicated by overlapping signals with the LD marker Bodipy 493/503. Derivative MMAT095-6 had very low fluorescence signals in the DAPI channel. Thus, the laser intensity was increased 5-fold, in order to obtain representative pictures, which depicted to a little extent spatial overlap with Bodipy 493/503 (Figure 46). Because of high fluorescence signals of derivatives MMATT077-3 and MMAT066-2, a second confocal microscopy with a lower concentration was performed. While MMAT077-3 proved to be located in LDs similarly to ponatinib, MMAT066-2 had no overlap with Bodipy 493/503, however, remained in a speckled appearance, indicating accumulation in different intracellular organelles such as lysosomes (Figure 47). In conclusion, these experiments clearly demonstrate that structural compound modifications influence drug accumulation in LDs, probably by modifying key physiochemical parameters such as lipophilicity or tendency towards protonation.

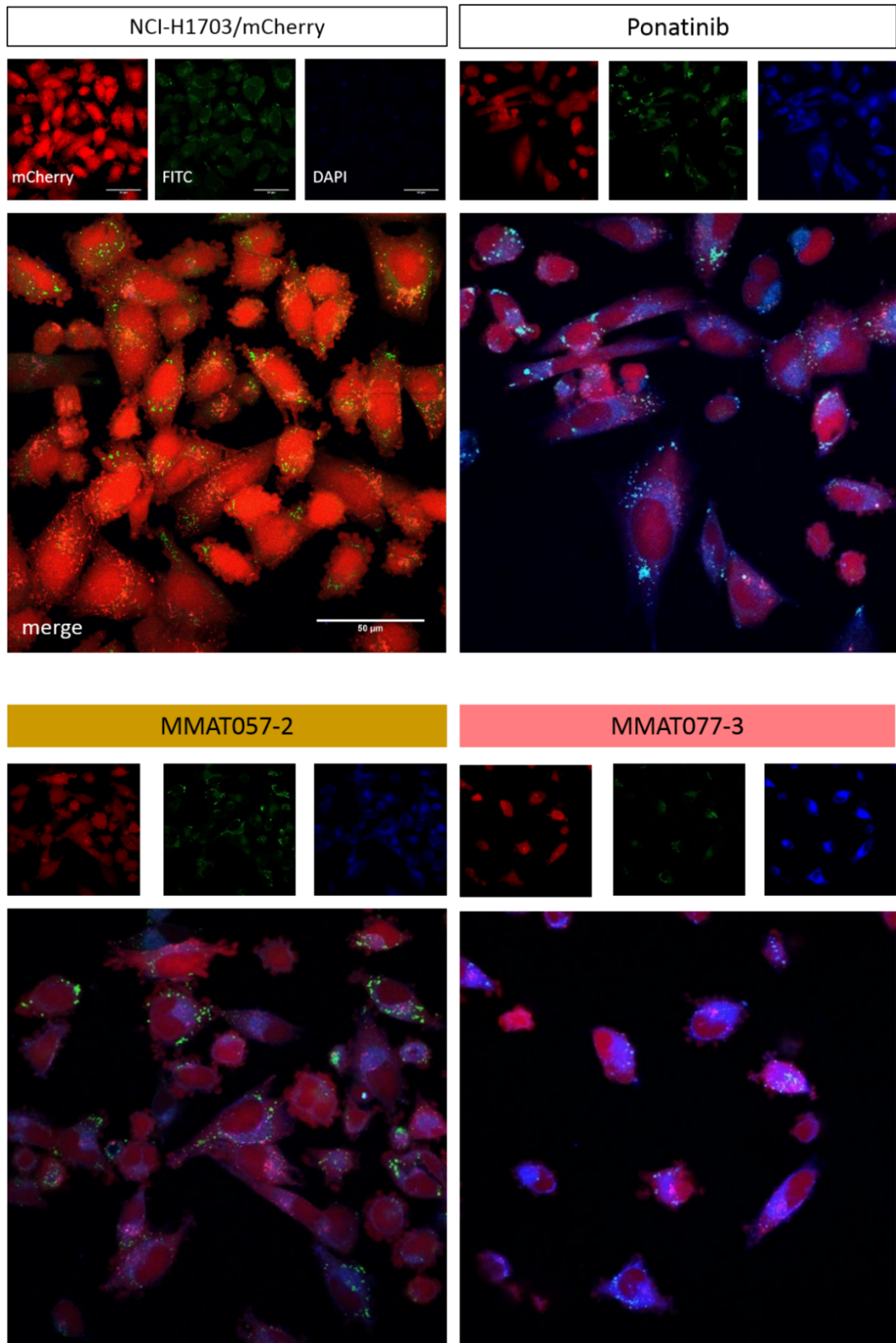


Figure 46: Chemical modification strongly influences the subcellular distribution of ponatinib. Subcellular localization of ponatinib and the ponatinib derivatives MMAT057-2, MMAT077-3, MMAT066-2, MMAT040-3, MMAT081-1 and MMAT095-6 in NCI-H1703/mCherry cells determined by CLSM using mCherry, FITC and DAPI channels. Bodipy 493/503 was used as marker for LDs. Cells were incubated with 10 μM of ponatinib or ponatinib derivatives for 1 h. Scale bars indicate 50 μM .

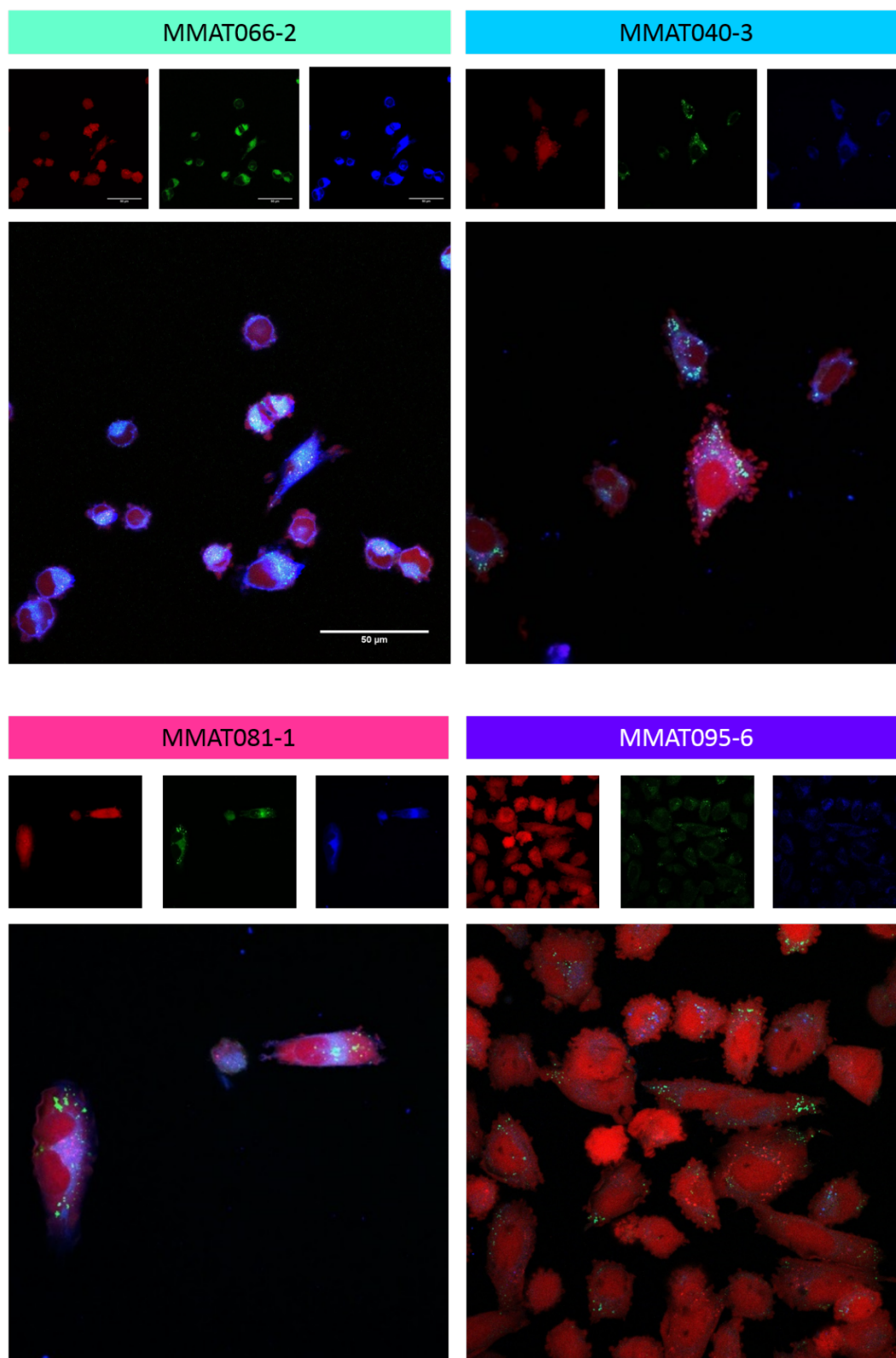


Figure 46 continued: Chemical modification strongly influences the subcellular distribution of ponatinib. Subcellular localization of ponatinib and the ponatinib derivatives MMAT057-2, MMAT077-3, MMAT066-2, MMAT040-3, MMAT081-1 and MMAT095-6 in NCI-H1703/mCherry cells determined by CLSM using mCherry, FITC and DAPI channels. Bodipy 493/503 was used as marker for LDs. Cells were incubated with 10 μM of ponatinib or ponatinib derivatives for 1 h. Scale bars indicate 50 μM.

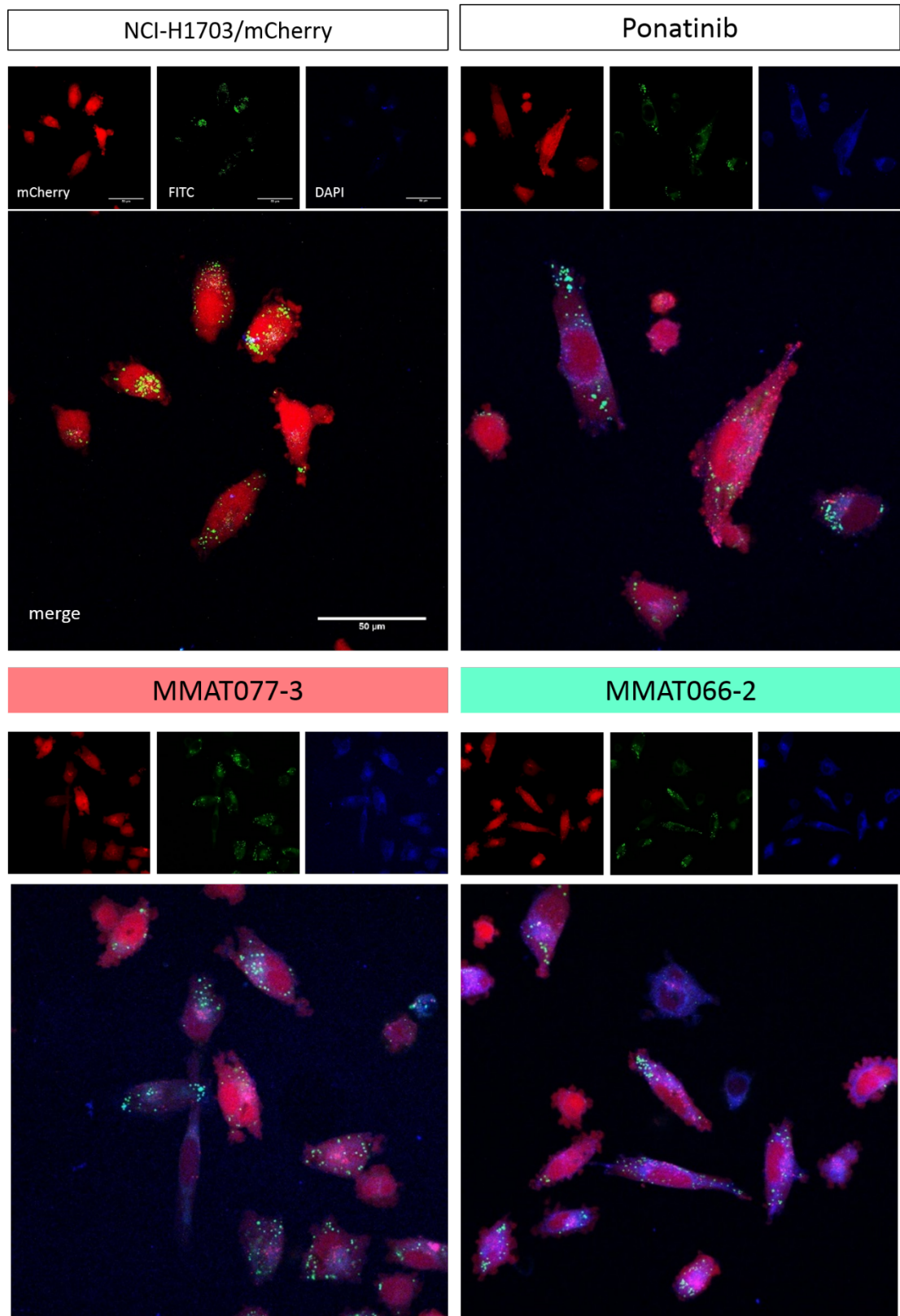


Figure 47: Chemical modification strongly influences the subcellular distribution of ponatinib. Subcellular localization of ponatinib and ponatinib derivatives MMAT057-2 and MMAT066-2 in NCI-H1703/mCherry cells determined by CLSM using mCherry, FITC and DAPI channels. Bodipy 493/503 was used as marker for LDs. Cells were incubated with 1 μM of ponatinib or ponatinib derivatives for 1 h. Scale bars indicate 50 μm .

4.4. LDs as resistance mechanism in other cancer cell lines

Viability assays revealed that not only ponatinib is losing its potency in LD-induced cancer cell lines, but also other anticancer compounds, e.g. gefitinib showed decreased activity in LD-enriched NCI-H1703 cells (Figure 48), suggesting for LDs as a contributing factor in cellular responsiveness to this drug.

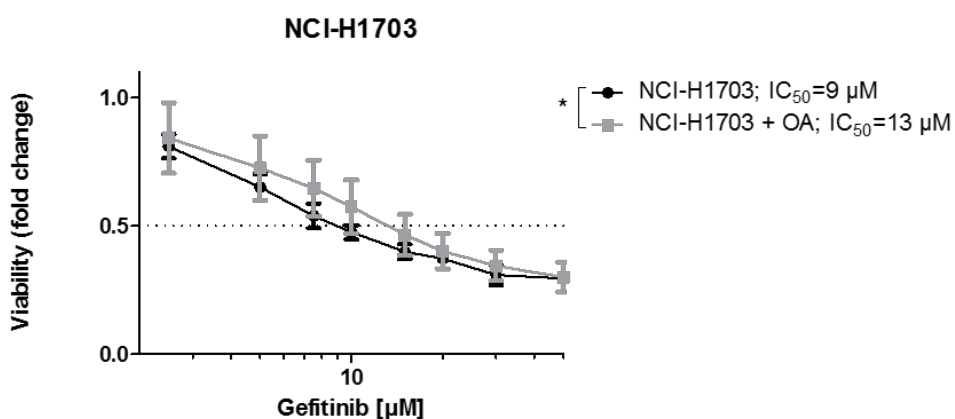


Figure 48: LDs reduce the sensitivity of lung cancer cells towards gefitinib. NCI-H1703 cells were exposed to increasing concentrations of gefitinib for 72 h. Induction of LDs was with 100 µM OA for 72 h. Viability was determined with MTT assay. Each data point represents the mean \pm SD of triplicate values of a representative experiment, performed in three times. Significance was calculated using two-way ANOVA (*= $p < 0.05$).

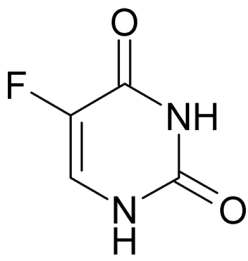

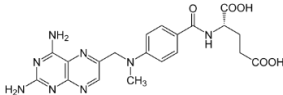
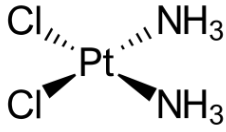
4.4.1. Drug-specific effects

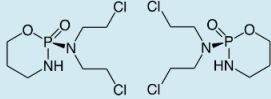
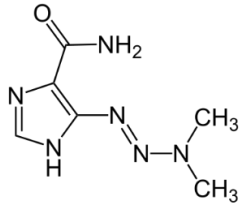
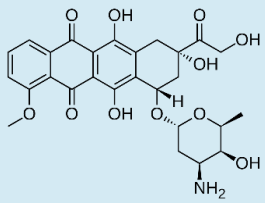
We further aimed at studying the impact of LDs on drug sensitivity also in other cell lines. Thus, we selected an extended cancer cell line panel, consisting of bladder, brain, breast, cervix, colon, liver, ovarian and prostate cancer cell lines (Table 1, except the human cancer cell lines DMS114, DMS114/PON, NCI-H520, NCI-H1703/PON, NCI-H1703/mCherry and the murine cell line 3T3-L1). Further, we chose compounds that are clinically approved in these entities (Table 14). LD formation was induced by OA. Subsequently, viability assays with clinically approved as well as pre-clinical drugs (Table 14), were conducted. Fold changes were defined by dividing the IC₅₀ values of the OA pre-treated cell line by the IC₅₀ values of the OA-naïve cell line. The obtained results revealed that some drugs showed decreased killing potential in OA pre-treated cells (indicated by a positive fold change, >1). Based on these findings, we were interested to compare this reduced drug activity with the lipophilicity of the compounds, in order to possibly

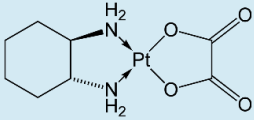
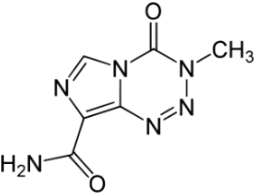
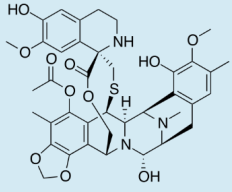
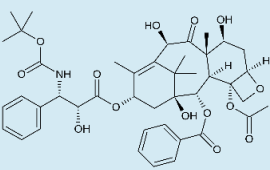
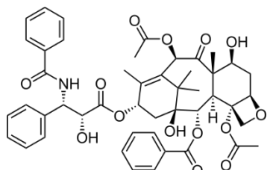
pinpoint a key parameter for LD accumulation of drugs. Therefore, the IC_{50} values of all drugs were plotted against the $\log P$ values of the drugs. Interestingly, a drug-specific, LD-dependently decreased activity in various cell lines was observed for several compounds including doxorubicin, paclitaxel and temozolomide, having a $\log P$ of 1.27, 3 and -2.8, respectively (Figure 49A, Table 14). The opposite was seen for irinotecan, with a $\log P$ of 3.2, which was in some cell lines even more active in the LD-enriched background (Figure 49B, Table 14). Thus, a unifying direct correlation between compound lipophilicity and decreased activity was not apparent from these analyses.

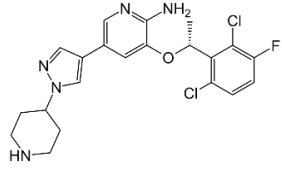
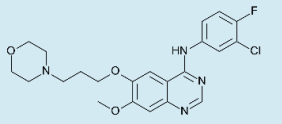
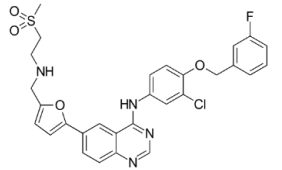
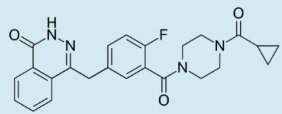
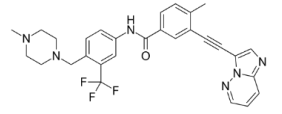
CHAPTER FOUR: RESULTS

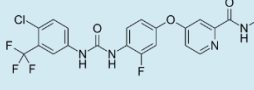
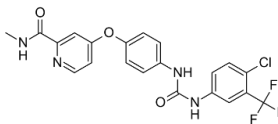
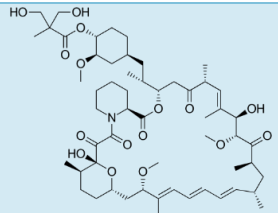
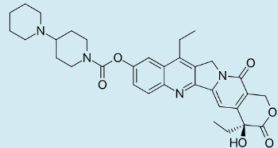
Table 14: List of drugs used in this study with their mode of action, approval, molecular structure and predicted or measured logP values.

Drug	Mode of action	Tumor type	Structure	LogP
Antimetabolites				
5-Fluorouracil (Adrucil)	an analogue of the antimetabolite nucleoside pyrimidine ^{a)}	approved for breast, colorectal, gastric and pancreatic cancer ^{b)}		-0.89 ^{c)}
Gemcitabine (Gemzar)	an analogue of the antimetabolite nucleoside deoxycytidine ^{a)}	approved for breast cancer; NSCLC; ovarian and pancreatic cancer ^{b)}		-1.4 ^{c)}
Methotrexate (Trexall)	an inhibitor of the enzyme dihydrofolate reductase, resulting in inhibition of purine nucleotide and thymidylate synthesis ^{a)}	approved for ALL; breast cancer; gestational trophoblastic disease; head and neck cancer; lung cancer; mycosis fungoides; NHL and osteosarcoma ^{b)}		-1.85 ^{c)}
DNA-interacting agents				
Cisplatin (Platinol)	forms highly reactive, charged, platinum complexes that bind to GC-rich sites in DNA ^{a)}	approved for bladder, ovarian and testicular cancer ^{b)}		-2.19 ^{c)}

Drug	Mode of action	Tumor type	Structure	LogP
DNA-interacting agents				
Cyclophosphamide (Cytophospane)	its active metabolites bind to DNA ^{a)}	approved for ALL; AML; breast cancer; CLL; CML; Hodgkin lymphoma; multiple myeloma; mycosis fungoides; neuroblastoma; NHL; ovarian cancer and retinoblastom ^{b)}		0.8 ^{c)}
Dacarbazine	alkylates and cross-links DNA during all phases of the cell cycle ^{a)}	approved for Hodgkin lymphoma and melanoma ^{b)}		-0.24 ^{c)}
Doxorubicin (Adriamycin)	inhibits topoisomerase II and intercalates between base pairs in the DNA helix ^{a)}	Approved for ALL; AML; breast cancer; gastric cancer; Hodgkin lymphoma; neuroblastoma; NHL; ovarian cancer; SCLC; soft tissue and bone sarcomas; thyroid cancer; transitional cell bladder cancer and Wilms tumor ^{b)}		1.27 ^{c)}

Drug	Mode of action	Tumor type	Structure	LogP
DNA-interacting agents				
Oxaliplatin (Eloxatin)	active oxaliplatin derivatives alkylate macromolecules, forming both inter- and intra-strand platinum-DNA crosslinks ^{a)}	approved for colorectal and stage III colon cancer ^{b)}		-0.47 ^{c)}
Temozolomide (Temodar)	induces methylation of DNA at guanine positions ^{a)}	approved for anaplastic astrocytoma and glioblastoma multiform ^{b)}		-2.8 ^{c)}
Trabectedin (Yondelis)	binds to the minor groove of the DNA ^{a)}	approved for liposarcoma and leiomyosarcoma ^{b)}		2.04-3.99 ^{c)}
Spindle poisons				
Docetaxel (Taxotere)	binds to and stabilizes tubulin ^{a)}	approved for adenocarcinoma; breast cancer; NSCLC, prostate cancer and squamous cell carcinoma of the head and neck ^{b)}		2.4 ^{c)}
Paclitaxel (Taxol)	binds to tubulin and inhibits the disassembly of microtubules ^{a)}	approved for AIDS-related Kaposi sarcoma; breast cancer; NSCLC and ovarian cancer ^{b)}		3 ^{c)}

Drug	Mode of action	Tumor type	Structure	LogP
Targeted agents				
Crizotinib (Xalkori)	inhibits the receptor tyrosine kinase ALK and the c-Met/hepatocyte growth factor receptor (HGFR) a)	approved for NSCLC ^{b)}		1.83 ^{c)}
Gefitinib (Iressa)	inhibits the catalytic activity of numerous tyrosine kinases including EGFR ^{a)}	approved for NSCLC ^{b)}		3.2 ^{c)}
Lapatinib (Tykerb)	reversibly blocks phosphorylation of EGFR, ErbB2, and the Erk-1 and-2 and AKT kinases ^{a)}	approved for breast cancer ^{b)}		5.4 ^{c)}
Olaparib (Lynparza)	Inhibits PARP ^{a)}	approved for ovarian cancer; ovarian, epithelial, fallopian tube or primary peritoneal cancer ^{b)}		2.32-2.68 ^{c)}
Ponatinib (Iclusig)	inhibits unmutated and all mutated forms of BCR-ABL; VEGFR and FGFR kinases ^{a)}	approved for ALL and chronic myelogenous leukemia ^{b)}		3.94-4.97 ^{c)}

Drug	Mode of action	Tumor type	Structure	LogP
Targeted agents				
Regorafenib (Stivarga)	inhibits VEGFRs 2 and 3, and Ret, Kit, PDGFR and Raf kinases ^{a)}	approved for colorectal cancer; gastrointestinal stromal tumor and hepatocellular carcinoma ^{b)}		4.49-4.53 ^{c)}
Sorafenib (Nexavar)	blocks Raf kinase and inhibits the VEGFR-2/PDGFR-beta signaling cascade ^{a)}	approved for hepatocellular carcinoma; renal cell carcinoma and thyroid cancer ^{b)}		3.8 ^{c)}
Temsirolimus (Torisel)	inhibits the mammalian target of rapamycin (mTOR) ^{a)}	approved for renal cell carcinoma ^{b)}		4.39-7.13 ^{c)}
Topoisomerase inhibitor				
Irinotecan (Camptosar)	its active metabolite inhibits topoisomerase I activity ^{a)}	approved for colorectal cancer ^{b)}		3.2 ^{c)}

^{a)} NCI drug dictionary. (2018, April). Retrieved from

<https://www.cancer.gov/publications/dictionaries/cancer-drug>

^{b)} A to Z list of cancer drugs. (2018, April). Retrieved from <https://www.cancer.gov/about-cancer/treatment/drugs>

^{c)} Drugbank (2018, April). Retrieved from <https://www.drugbank.ca/>

AIDS: Acquired immunodeficiency syndrome

ALK: Anaplastic lymphoma kinase

ALL: Acute lymphoblastic leukemia

AML: Acute myeloid leukemia

CLL: Chronic lymphocytic leukemia

CML: Chronic myelogenous leukemia

EGFR: Epidermal growth factor receptor

NHL: Non-Hodgkin lymphoma

NSCLC: Non-small cell lung cancer

PARP: Poly (ADP-ribose) polymerase

PDGFR: Platelet-derived growth factor receptor

Raf: Rapidly accelerated fibrosarcoma

SCLC: Small cell lung cancer

VEGFR: Vascular endothelial growth factor receptor

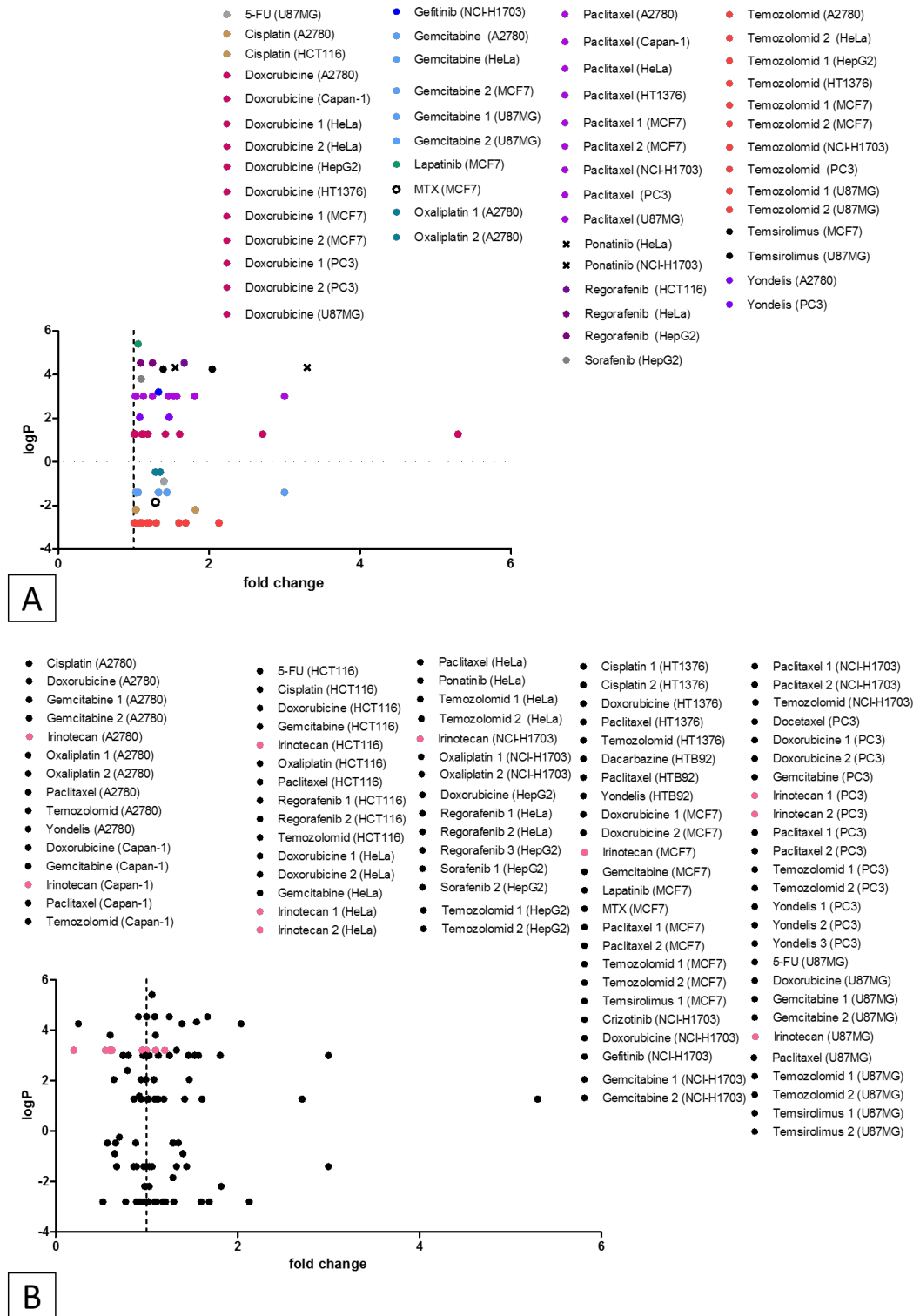


Figure 49: Oleic acid (OA) leads to A) decreased activity of several drugs, and B) increased activity of irinotecan in a selected cancer cell line panel. Lipophilicity is given in logP values. Cytotoxic activity is given as fold changes, dividing the IC₅₀ values of the oleic acid pre-treated cell line by the IC₅₀ values of the non-pre-treated cell line. Decreased cytotoxic activity is depicted by positive (>1) fold changes. OA pre-treatment was with 100 μM for 72 h.

4.4.2. Cell-specific effects

Interestingly, an OA-dependently increased resistance was observed for breast (MCF7), ovarian (A2780) and brain (U87MG) cell lines against multiple drugs, indicating cell-specific effects (Figure 50). Confoundingly, viability assays comparing naïve cells, cells with enriched or reduced LDs (TC pre-treated) revealed that LD-induced A2780 cells showed slightly more resistance towards temozolomide (Figure 51). However, this was not statistically significant. In contrast, this was not observed for MCF7 and U87MG cells. Figure 52 depicts some cell- and drug-specific effects observed with viability assays. Thus, at least for the ovarian, breast and brain tumor cell lines, these data suggest that targeting a lipogenic phenotype might synergize with compounds clinically approved for these cancer entities.

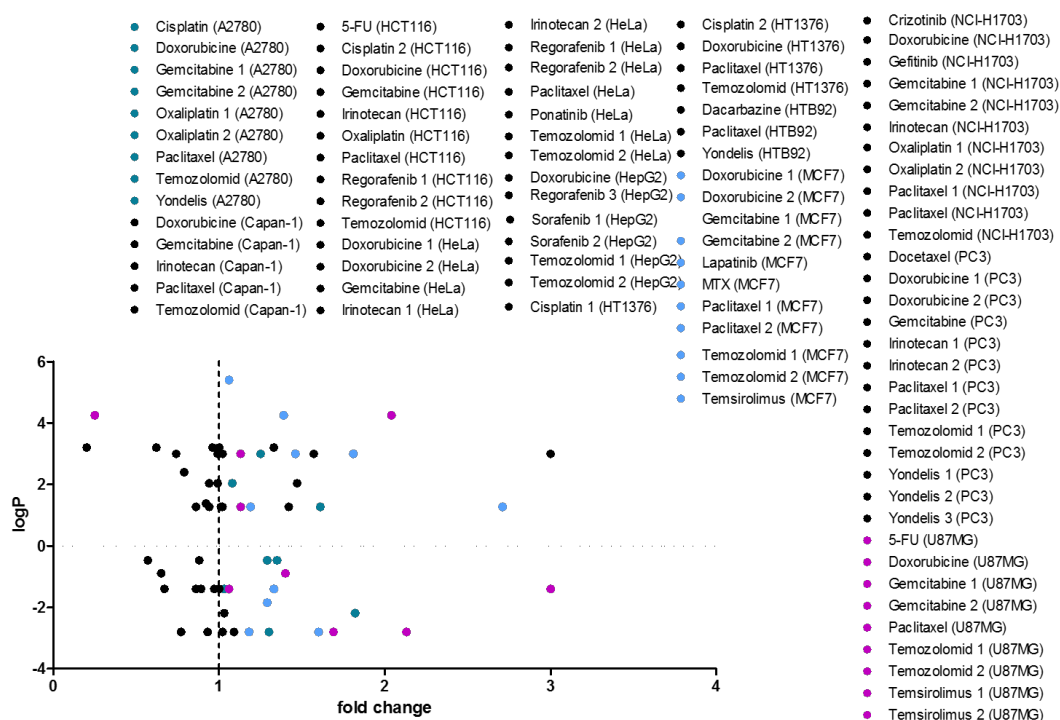


Figure 50: Breast, brain and ovarian cancer cell lines show increased, oleic acid (OA)-dependent resistance towards several drugs differing in their lipophilicity. Lipophilicity is given in log P values. Cytotoxic activity is given as fold changes, dividing the IC₅₀ values of the oleic acid pre-treated cell line by the IC₅₀ values of the non-pre-treated cell line. OA pre-treatment was with 100 µM for 72 h.

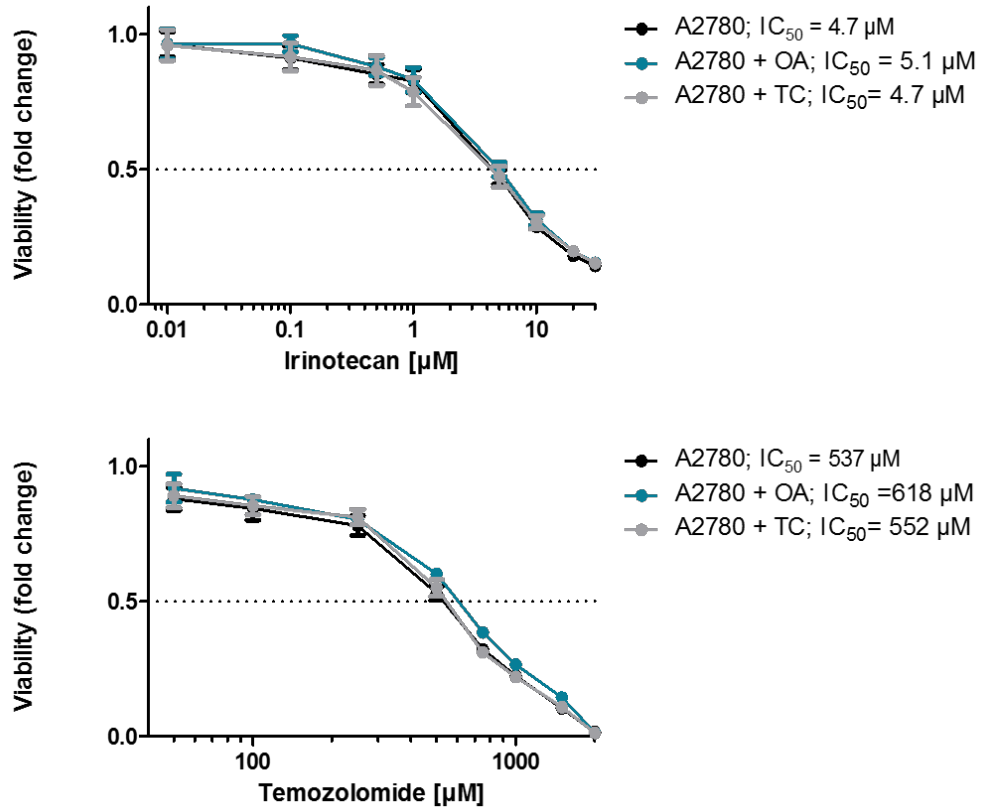


Figure 51: LD-induction marginally increases ovarian cancer cell viability towards temozolomide in contrast to irinotecan. A2780 cells were exposed to increasing concentrations of irinotecan and temozolomide for 72 h. LD-induction was with 100 μM OA, LD-depletion with 0.3 μM TC, each for 72 h.

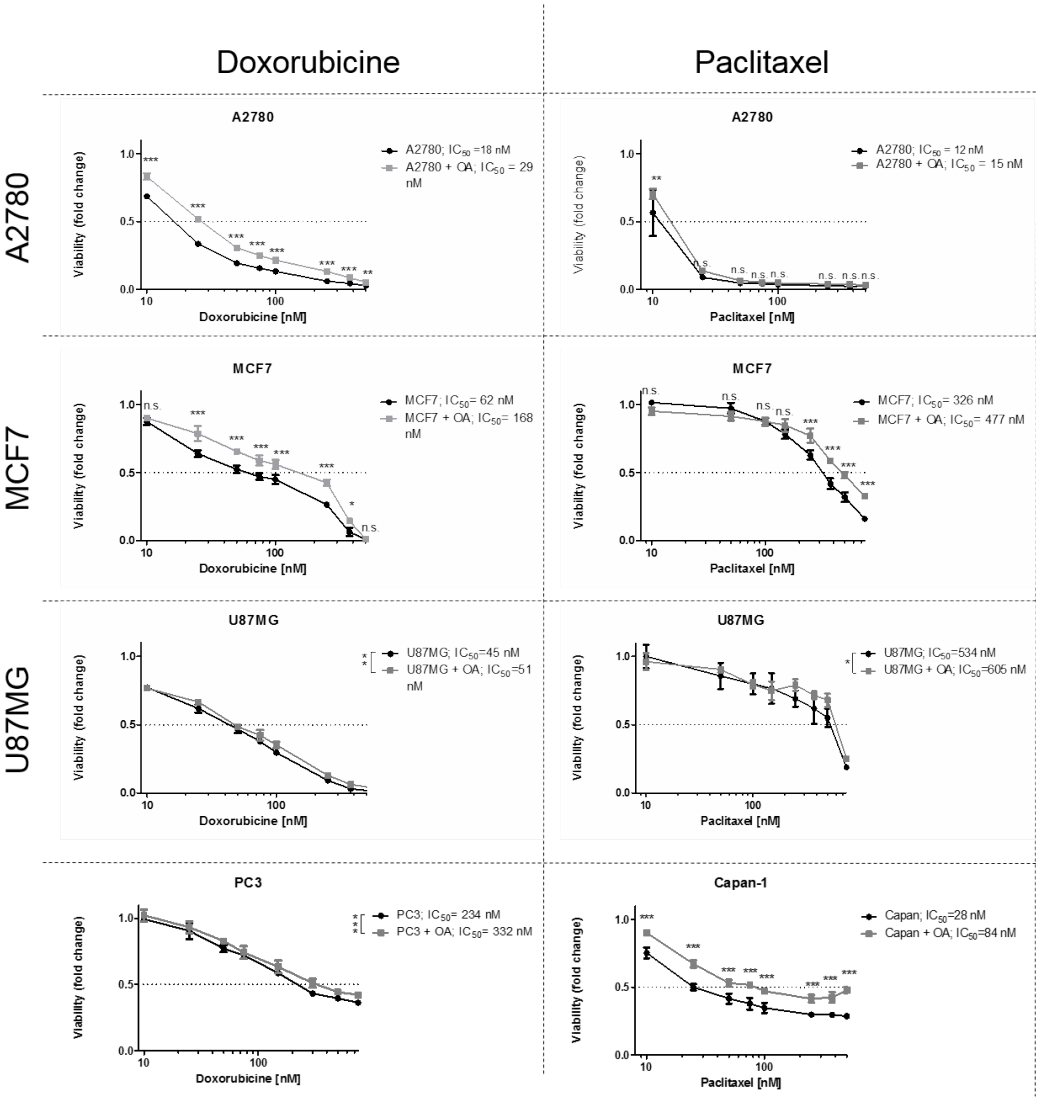


Figure 52: Cell- and drug-specific, oleic acid (OA)-dependent effects showing increased resistance of cells and decreased toxicity of drugs. Cancer cells were exposed to increasing concentrations of the respective drug for 72 h. Induction of LDs was with 100 μ M OA for 72 h. Viability was determined with MTT assay. Each data point represents the mean \pm SD of triplicate values of a representative experiment, performed in three times. Significance was calculated using two-way ANOVA (*= $p < 0.05$; **= $p < 0.01$, ***= $p < 0.001$).

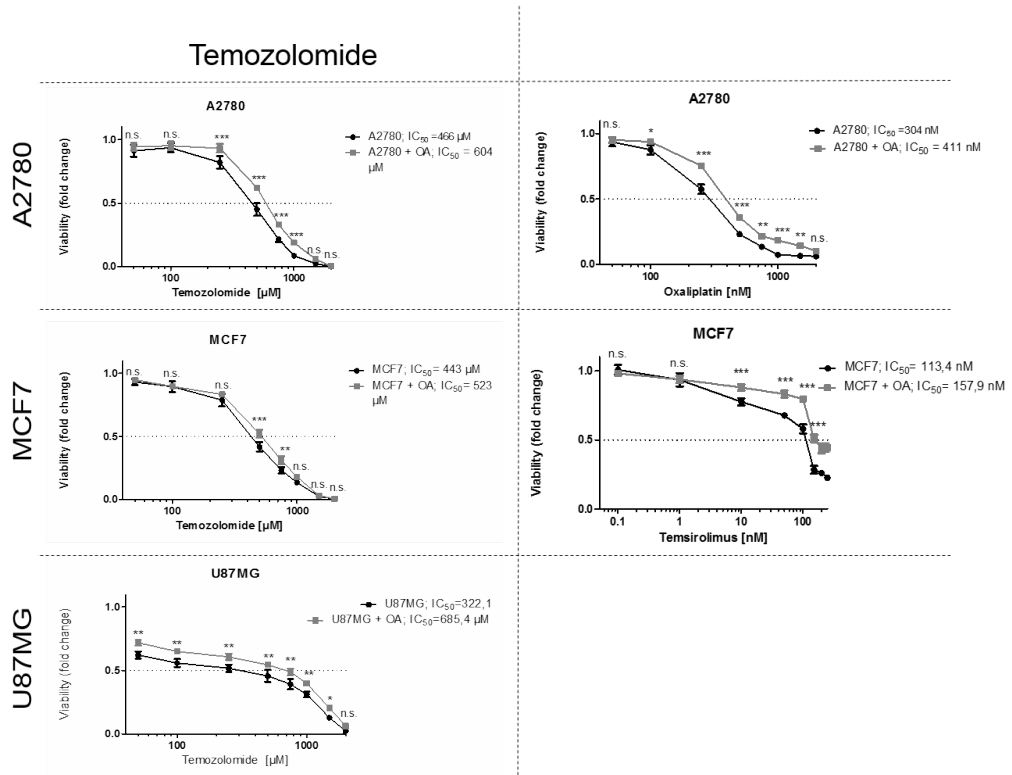


Figure 52 continued: Cell- and drug-specific, oleic acid (OA)-dependent effects showing increased resistance of cells and decreased toxicity of drugs. Cancer cells were exposed to increasing concentrations of the respective drug for 72 h. Induction of LDs was with 100 μM OA for 72 h. Viability was determined with MTT assay. Each data point represents the mean \pm SD of triplicate values of a representative experiment, performed in three times. Significance was calculated using two-way ANOVA (*= $p < 0.05$; **= $p < 0.01$, ***= $p < 0.001$).

5. Discussion

Resistance to chemotherapeutic and molecularly targeted drugs represents an enormous problem of cancer therapy. Both, intrinsic and acquired mechanisms limit the effectiveness of several drugs. Tumors are extremely adaptable and can acquire resistance through mutations (like a T315I mutation in BCR-ABL kinase), by upregulating the expression of the therapeutic target, or by activation of other, alternative pathways. In addition, cancer cells have been shown to increase drug efflux or alter the drug metabolism. Moreover, there is evidence that some drugs effectively kill only a certain cell population of the heterogenic tumor and, thus, miss a minor subpopulation that becomes, or is, intrinsically resistant. However, also the tumor microenvironment remarkably contributes to cancer therapy resistance [82].

For quite a while, LDs were simply regarded as intracellular fat depots. More recently, LDs were shown to play an important role in various cellular events like lipolysis, autophagy and cancer cell survival [50, 58].

Previous results from our lab at the Institute for Cancer Research revealed that lysosomal sequestration of two tyrosine kinase inhibitors (TKIs), nintedanib and PD173074, decreased their activity [83, 84]. Preliminary results from B. Englinger, MSc, PhD, pointed towards a selective accumulation of ponatinib, a multi-targeted, lipophilic TKI, into LDs. Inspired by these hints, we set out to identify the underlying molecular mechanisms driving this specific accumulation of ponatinib in intracellular LDs as resistance mechanism of lung cancer cells. Moreover, we studied the impact of a “lipoid” cell compartment on lung cancer cell survival upon ponatinib treatment. Also, we examined the chemical effect on the subcellular distribution and activity of ponatinib. In addition, we investigated the impact of LDs on the efficacy of other anticancer compounds and the role of LDs in other cancer entities.

5.1. Adipocytes reduce ponatinib availability and mediate cancer cell survival

Cancer cells need enormous amounts of lipids as biomass and building blocks and, thus, often act as metabolic “parasites” [58, 85]. Recently, the role of adipocytes in cancer is getting more and more evident. Pre-adipocytes and/or adipocytes are often found close to the tumor invasion sites [86]. In ovarian cancer, neighboring adipocytes were shown to foster homing to the omentum and further invasion of cancer cells [87]. In addition, adipocytes have been shown to promote proliferation of colon cancer cells [88]. Adipocytes or adipose tissue close to the tumor site present a factor of poor prognosis for breast, pancreas, kidney and colon cancer patients. Very often, the size of adipocytes at the tumor invasion site is reduced, indicating an increased lipolysis to generate FAs in order to fuel tumor cell proliferation [86]. Indeed, adipocytes have been shown to directly transfer lipids to ovarian and melanoma cancer cells in co-cultures [87, 89]. Another model suggests that cancer-associated adipocytes get de-differentiated into fibroblast-like cells. Many studies have shown that fibroblasts promote cancer development through structural and biochemical support [86].

Cell culture experiments in this presented study revealed diminished ponatinib content in NCI-H1703 cells that were directly cultured with adipocytes (3T3-L1/A) for short-time. Moreover, in co-culture experiments, survival of NCI-H520 cells in the presence of ponatinib was more potently stimulated by 3T3-L1/A cells than fibroblasts (3T3-L1/F). Additionally, in cell-conditioning experiments, DMS114, NCI-H520 and NCI-H1703 cells showed better colony formation capacity and less intracellular ponatinib levels when these cells were exposed to 3T3-L1/A-derived ponatinib-conditioned medium. However, it needs to be mentioned that in the case of DMS114 cells, adipocytes were transferred onto the cancer cells, challenging the reliability of quantification of the colony formation capacity (Figure 21). Nonetheless, these data provide evidence for adipocytes reducing ponatinib availability and, as a consequence, inducing lung cancer cell survival. This was further confirmed in a Western blot experiment, where DMS114 cells incubated with ponatinib-containing, 3T3-L1/A-conditioned media exhibited sustained phosphorylation of Erk in comparison to unconditioned, as well as fibroblast-conditioned media. All in all, these are interesting findings pointing towards a

crucial role of adipose cells influencing the activity and pharmacokinetics of ponatinib, consequently promoting cancer cell survival. These results are consistent with literature, reporting secretion of hormones, growth and inflammatory factors, as well as angiogenic factors by adipocytes [86, 88]. Further, breast cancer cells exposed to adipocyte culture medium were characterized by activated immune system- and wound healing-related genes [86]. In addition, melanoma cells had higher levels of phosphorylated Akt when co-cultured with adipocytes [89]. Importantly, breast cancer cells acquired trastuzumab resistance when they were cultured with adipocytes [85]. Also, there is evidence that adipocytes promote resistance towards vincristine, nilotinib, daunorubicin and dexamethasone in ALL by preventing apoptosis [90]. To our knowledge, the data presented in this thesis shows for the first time directly that adipocytes foster cancer cell survival by direct scavenging of lipophilic pharmacological agents (ponatinib).

These observations demonstrate that adipocytes should be considered as potent target in future rational therapeutic strategies in order to minimize tumor cell resistance-promoting effects in patients. Recently, such an approach in ovarian cancer was successful. Tebbe *et al.*, were able to inhibit the adipocyte tumor-promoting effects *in vitro* using metformin, a Type II diabetes drug [91].

5.2. Ponatinib uptake is detectable in cryosections

Tracking the intracellular distribution dynamics of a drug is of great importance as it provides a better understanding of the drug stability, metabolism, activity and cellular resistance mechanisms [83, 92]. Especially auto-fluorescent drugs are suitable for microscopic tracking approaches [92]. *In vivo* microscopy can give information on how drugs are delivered, work and fail. With *ex vivo* microscopy imaging can be performed at even higher resolution [93]. Cell and tissue penetration, as well as interactions of the compound with its target can be of great interest in order to reveal central processes of drug delivery [92]. Finally, microscopy can give possible reasons for drug failures, but also opportunities for improvement [93].

Orally administered drugs always pass through the intestine [94]. Drug absorption then happens to a large extent in the small intestine, where the lumen is decorated with epithelial cells and, subsequently, to a smaller extent in the colon [95, 96]. In the literature, intestine (and accordingly the liver) are described as the two major areas where drugs enter the systemic circulation and further reach the intended sites of action [96, 97]. Especially for drugs targeting receptors located in tissues or acting inside the cell, tissue distribution is of great importance. However, studying tissue distribution is methodologically limited and complicated [98].

Preliminary results from our lab revealed intrinsic fluorescence of ponatinib *in vitro* when excited with a 405 nm laser. Hence, we decided to investigate the ponatinib fluorescence *in vivo*, particularly in tissue cryosections generated from orally treated mice. Strong fluorescence of ponatinib was detected in tissues from the small intestine, and to a lesser extent in colon and tumor tissues. These data confirm that ponatinib is, indeed, resorbed by the small intestine and, as expected, accumulates in lung cancer xenografts, the relevant target tissue. The distribution of a drug into tissues contributes to its pharmacological and clinical response, including toxic effects [98]. Thus, a better understanding of tissue distribution is important. While tissue distribution of a drug can be investigated by analytical chemistry methods in preclinical models, the dynamics of compounds within cells and organelles is often difficult [84]. Microscopy provides a detailed insight into drug distribution and a semi-quantitative approach [98, 99]. However, a fluorescent labeling of the drug is necessary, which bears the risk of changing the pharmacological activity [93]. Thus, the intrinsic, label-free fluorescence property of ponatinib provides a possible application of the drug in intravital microscopy to further study its (side) effects on vascularization and how stromal cells contribute to drug resistance.

5.3. Lung cancer cells acquire resistance to ponatinib via a lipogenic phenotype switch and overexpression of MTP

Several organelles are known to play a major role in cancer therapy resistance. Recently, LDs have been shown to contribute to resistance towards anti-cancer drugs in breast, prostate and ovarian cancer [61-63]. However, the underlying molecular mechanisms are not completely understood.

We were able to show that the ponatinib resistance of the NSCLC cell line NCI-H1703 highly depended on the LDs status. This LD mediated resistance was diminished with TC, an inhibitor of the long fatty acid acyl-CoA synthetase, and increased with OA. Treatment with OA localizes the ER resident DGAT2 to the surfaces on LDs [49]. Further, OA contains isoenzymes for TAG synthesis and thus promotes enlargement of LDs [55]. Our findings highlight the evidence of an adaptively mechanism of cancer cells to switch into a lipogenic phenotype and damp the efficacy of ponatinib. Further experiments supported this lipogenic-switch theory. The ponatinib resistant subline of NCI-H1703 was characterized by an increased total triglyceride content. A strong relationship between LDs and ponatinib resistance was also found for the ponatinib resistant subline of the SCLC cell line DMS114 (DMS114/PON). This resistant cell line showed increased levels of ponatinib and simultaneously elevated levels of LDs. Besides this, DMS114/PON had increased triglyceride and cholesterol levels. Given the fact that ponatinib leads to adverse reactions like vascular occlusion, and excess cholesterol is stored in LDs of macrophages leading to macrophage foam cells that are involved in atherosclerosis, this lipogenic switch might not only happen in cancer cells, but also in healthy tissues such as blood vessel walls. Thus, it might be conceivable that lipid metabolism-associated inflammatory reactions in the vasculature provide an explanation for ponatinib-related serious vascular side effects [41, 50, 56]. The fact that fatty acid uptake was not increased in DMS114/PON cells, suggests an anabolic metabolism that accounts for the observed increase of triglyceride and cholesterol levels in ponatinib-resistant lung cancer cells. Such a *de novo* lipogenesis was already identified as key factor in breast, prostate and lung cancer growth [100].

Whole-genome gene transcription analysis revealed a massive upregulation of MTP in DMS114/PON cells. MTP is required for the assembly of lipoproteins, especially for apoB-containing lipoproteins in enterocytes and hepatocytes, but MTP also imports triglycerides into the ER lumen. MTP is described to act like a shuttle, extracting lipids from one membrane and delivering them to a second membrane [101, 102]. MTP is surrounding LDs in brown and white adipose tissue and is suggested to play a role in LD maturation in adipocytes [101]. Further, decreased MTP expression in mice was associated with LDs of diminished size [103]. Thus, we were interested whether MTP represents a role in the adaptive lipid reprogramming of lung cancer cells and mediates LD induction as ponatinib resistance mechanism. Targeted suppression of MTP by siRNA-knockdown and pharmacologically inhibition with the MTP inhibitor lomitapide resulted in increased levels of LDs and ponatinib, together with an increased ponatinib resistance of lung cancer cells. These findings do not support the theory of MTP as driver in LD maturation. Rather in the opposite, it is likely that MTP plays a role in enhanced lipid- and concomitantly ponatinib export. This conclusion is underpinned by reports that mention hepatic accumulation of triglycerides - hepatic steatosis - as prominent adverse side effect of lomitapide treatment of hyperlipidemia [81]. This might be because of a lomitapide-triggered decrease of Apolipoprotein A-1 (ApoA-1) [104]. Under normal conditions, ApoA-1 binds to the cell membrane and promotes the transport of cholesterol and phospholipids to the outer cell surface. Once outside the cell, these substances are transported by high-density lipoprotein through the bloodstream to the liver and further distributed or removed [105]. Moreover, MTP knockout mice embryos showed dysfunctional lipid export of the yolk sac, characterized by accumulation of cytosolic fat [106]. Regarding this, it would be interesting, whether ApoA-1 is also upregulated in our ponatinib-resistant cell model, contributing to an MTP-mediated lipid export as ponatinib resistance mechanism.

5.4. Ponatinib derivatization strongly influences the intracellular distribution and impairs the cytotoxic activity of ponatinib

Ponatinib was rationally designed to circumvent the T315I (a change from threonine to isoleucine at codon 315) gatekeeper mutation of BCR-ABL. This bypass was achieved by a special triple carbon-carbon bond, a so-called ethenyl linkage, which ensures extremely stable binding of ponatinib to the inactive conformation of ABL kinase, unaffected by steric hindrance of 315 isoleucine [107]. It is thought, that this stable binding is mediated by the formation of multiple bonds to the kinase, so that an individual mutation of the kinase has little effect on its target affinity. This explains the strong activity of the compound for all mutated BCR-ABL forms. Ponatinib is the only clinically available active TKI for ALL and CML patients that have this T315I mutation [108]. Moreover, Ponatinib is not specific to BCR-ABL alone, and inhibits also kinase domains of VEGFR and FGFR [44]. However, ponatinib accounts for a high frequency of serious adverse vascular side effects [41].

According to our findings that ponatinib accumulates specifically in LDs, we decided to design derivatives of ponatinib with the aim to optimize the FGFR kinase target selectivity and subcellular distribution. Five derivatives bore in common a replacement of the methylpiperazine group, which is assumed not to be crucial for the binding affinity. One derivative was missing the trifluoromethyl (CF_3) group. This CF_3 group is known for adding lipophilicity to an aromatic ring [109]. To our surprise, all derivatives were far less cytotoxic. In addition, the chemical modifications strongly affected the intracellular distribution of ponatinib. While the compounds MMAT057-2, MMAT081-1 and MMAT066-2 showed no overlapping signals with the LD stain Bodipy 493/503, the derivatives MMAT040-3, MMAT077-3 and, unexpectedly, MMAT095-6, which was missing the CF_3 group, showed a similar distribution like ponatinib to LDs. These findings suggest that the lipophilic CF_3 group seems to have a minor impact on the LD affinity of ponatinib. In drug design, lipophilicity is an important factor determining the success of an oral drug and needs to be well controlled [110]. On the one hand, lipophilicity is essential for the drug to pass from the aqueous phase through cell membranes, having hydrophilic heads on the outside and a panel of lipophilic chains in between [110, 111]. Furthermore, the majority of protein binding sites

is hydrophobic. On the other hand, the more lipophilic a drug, the higher is the risk for non-specific binding, poor solubility and metabolic clearance [110]. Thus far, two lipophilic drugs have been reported to be sequestered into LDs (compare chapter 5.5 Drug- and cell-specific LD-dependent resistance) [112, 113].

5.5. Drug- and cell-specific LD-dependent resistance

The physicochemical properties of a compound can lead to adverse outcomes. A better understanding of this relationship is of great interest in drug development. The promiscuity of a compound is characterized by off-target pharmacologies that lead to unknown responses. Especially, one physicochemical parameter, lipophilicity, is often linked with binding of the drug to unknown molecular targets. The lipophilicity, or also called hydrophobicity and non-polarity, of a compound is described as the compound's ability to dissolve in fats, oils, lipids and non-polar solvents. It can be assessed by determining the logP value of the compound. The lipophilicity of a compound affects not only its solubility, but also the absorption, permeability and binding properties, and, as mentioned before, can lead to non-specific binding or accumulation. There exists a positive correlation of the lipophilicity of a compound with its promiscuity [114].

Fungi were shown to trap self-produced (endogenous) as well as exogenous lipophilic toxins in LDs as self-protecting and resistance mechanism, respectively [115]. Recently, there is more and more evidence that also cancer cells trap anti-cancer compounds in LDs. Curcumin, a lipophilic drug with a logP value around 4, was suggested to localize into LDs in glioblastoma cells [116, 117]. By LD reduction the therapeutic effect of curcumin was enhanced [117]. Further, progesterin induced LDs and protected breast cancer cells from docetaxel, which has a logP value of 2.4 [112, 118].

We analyzed the impact of LDs on the efficacy of other anticancer compounds in an extended cancer cell line panel. Bladder, brain, breast, cervix, colon, liver, ovarian and prostate cancer cells were incubated with OA for 72 hours in order to induce LDs. Rohwedder *et al.*, showed that short-time incubation with OA stimulated LD induction and enlargement, while after long-time incubation OA was directly incorporated into LD-associated lipids in hepatoma cells [119]. We

were able to reveal that several drugs, including doxorubicin, paclitaxel and temozolomide, showed decreased activity in LD-induced cancer cells. Recent studies already prepared evidence for a LD connection of these drugs. Mehdizadeh *et al.*, observed increased numbers of LDs after application of doxorubicin in colorectal cancer cells and hepatocellular carcinoma [120]. Also, for paclitaxel a LD-enhancing effect was identified in both sensitive and resistant cervical cell lines [62]. However, temozolomide is a hydrophilic drug, demonstrating that the LD-dependent decreased drug activities in this thesis project were independent of the compound's lipophilicity. Recently, also the group of Cotte *et al.*, observed accumulation in LDs for the non-lipophilic drugs, 5-fluorouracil and oxaliplatin, further enabling colorectal cancer cell resistance [113]. Hence, the logP value of a compound represents no predictable factor for intracellular incorporation of the drug in LDs. However, we found a cell-specific, LD-dependent increased resistance in breast, glioblastoma and ovarian cancer cell lines, thus confirming the work of others which reported LD accumulation as resistance mechanism in these cancer entities [117]. Taken together, these data support LD accumulation as a hallmark in breast, glioblastoma and ovarian cancer cell resistance.

List of Figures

Figure 1: The ten hallmarks of cancer with their respective therapeutic targeting strategies. Illustration of the six hallmarks postulated in 2000 as well as the enabling characteristics and emerging hallmarks defined in 2011. Drugs that target these hallmarks are depicted [7].	4
Figure 2: Estimated number of new cases (left) and deaths (right) worldwide in 2018 related to all cancer types, sexes and ages. Adapted from Globocan 2018 [9].	5
Figure 3: Illustration of environmental and lifestyle factors as major contributors to lung cancer development by Russel Cobb. Adapted from [26].	9
Figure 4: Estimated number of cancer-caused deaths worldwide in 2018 related to tissue of origin. Adapted from Globocan 2018 [9].	10
Figure 5: Fibroblast growth factor (FGF) signaling pathways. FGFs bind to FGF receptor (FGFR) and induce receptor dimerization, cross-phosphorylation of the kinase domains and binding of several proteins that activate downstream pathways (RAS-RAF-MAPK, PI3-AKT, STAT and PLC γ). Adapted from [47].	14
Figure 6: Structural composition of lipid droplets (LDs). LDs have a phospholipid monolayer decorated with proteins e.g. perilipin (termed PLIN proteins) and a core containing neutral lipids (triglycerides and sterol esters). Adapted from [50].	18
Figure 7: Lipolysis of lipid droplets (LDs). Triacylglyceride (TAG) hydrolysis is catalyzed by adipose triglyceride lipase (ATGL), which leads to release of free fatty acids (FA) and diacylglycerol (DAG). Subsequently, DAG hydrolysis is catalyzed by hormone-sensitive lipase (HSL), which leads to free FA and monoacylglycerol (MAG). In turn, MAG lipase (MGL) hydrolyses MAG into free FA and glycerol. Adapted from [51].	20
Figure 8: Assembly and secretion of very-low density lipoprotein (VLDL). Apolipoprotein B (ApoB) is lipidated in the endoplasmic reticulum (ER) by the microsomal triglyceride transfer protein (MTP) to form primordial lipoprotein (pre-VLDL). Pre-VLDL is further lipidated and exits the ER. In the ER Golgi intermediate compartment (ERGIC) the VLDL2 is sorted and further promoted to enter the secretory pathway. Cytosolic lipid droplets (LDs) provide triglycerides for further lipidation to VLDL1 before it is secreted. Adapted from [52].	21
Figure 9: Cell conditioning experiment processing scheme.	35
Figure 10: Co-culture assembling scheme.	38
Figure 11: The order (top to bottom) of filters, gel and membrane for Western blotting.	55
Figure 12: Transfection efficiency of NCI-H1703 cells with pQCXIP-mCherry-IRES-Puro plasmid DNA. Cells were exposed for 4 h to plasmid and Lipofectamine2000 reagents. Transfectants were constantly selected with 0.75 μ g/mL puromycin. A) Toxicity of puromycin in non-transfected NCI-H1703 cells. Cells were exposed to increasing concentrations of puromycin for 72 h and viability was determined with MTT assay. B)	

Transfection efficiency was determined 20 days after transfection by fluorescence microscopy using the RFP channel and brightfield.	58
Figure 13: Ponatinib fluorescence is detectable in cultured lung cancer cells.	
Fluorescence activity of ponatinib in NCI-H1703/mCherry cells was analyzed by CLSM using DAPI and mCherry channels. Cells were incubated with 1 μ M of ponatinib for 1 h. Scale bars indicate 10 μ M.	59
Figure 14: Ponatinib accumulates in LDs in cancer cells. Subcellular localization of ponatinib in NCI-H1703/mCherry cells was determined by CLSM using mCherry, FITC and DAPI channels. Cells were incubated with 5 μ M of ponatinib for 1 h. 500 nM Bodipy 493/503 was used as marker for LDs. Scale bars indicate 10 μ M.	60
Figure 15: Changes of morphology of fibroblast (3T3-L1/F) upon differentiation into mature adipocytes (3T3-L1/A). 3T3-L1 mouse embryonic fibroblasts were thawed in Dulbecco's modified Eagle's Medium supplemented with 10 % fetal calf serum (FCS) and allowed to differentiate for 23 days. Composition of the differentiation media is listed in Table 8.	61
Figure 16: NCI-H1703/mCherry lung cancer cells do not tolerate long-time co-culturing with 3T3-L1/A cells. NCI-H1703/mCherry cells were co-cultured with fibroblasts or adipocytes. Photographs were taken in brightfield, DAPI and RFP settings, using a live-cell imaging system with 20x objective. Indicated are time points 20 min and 100 h representing the start and end of the experiment.	62
Figure 17: Ponatinib uptake in cancer cells is diminished in the presence of adipocytes. NCI-H1703/mCherry cells were exposed to ponatinib short-time in the presence of 3T3-L1/F or 3T3-L1/A cells. A) Photomicrographs were taken by CLSM using FITC, mCherry and DAPI channels. Bodipy 493/503 was used as marker for LDs. Cells were incubated with 2.5 μ M of ponatinib for 1 h. Scale bars indicate 50 μ M. Regions of interests (ROIs) were created by marking mCherry-positive areas in ImageJ. B) Ponatinib was quantified by measuring pixel intensities in the DAPI channel of each mCherry-positive ROI, subtracting the fluorescence of the respective untreated control images. Significance was calculated using D'Agostino and Pearson omnibus normality test, followed by Mann-Whitney test (**=p<0.0001).	64
Figure 18: Adipocytes mediate cancer cell survival. A) NCI-H520 cells were cultured in transwells in a co-culture assay with ponatinib containing medium or ponatinib-exposed 3T3-L1/F or 3T3-L1/A cells and stained after 5 days with crystal violet. B) Relative viability of NCI-H520 cells determined by measuring re-dissolved crystal violet absorbance at 560 nm. Results were normalized according to the corresponding untreated controls, set to 1. Significance was calculated using two-way ANOVA with Bonferroni post-test (**=p<0.001).	65
Figure 19: NCI-H1703 cells do not tolerate direct co-culturing with adipocytes in transwell chambers. A) NCI-H1703 cells were cultured in transwells in a co-culture assay with ponatinib containing medium or ponatinib-exposed 3T3-L1/F or 3T3-L1/A cells and stained	

after 5 days with crystal violet. B) Relative viability of NCI-H1703 cells determined by measuring re-dissolved crystal violet absorbance at 560 nm. Results were normalized according to the corresponding untreated controls, set to 1. Significance was calculated using two-way ANOVA with Bonferroni post-test (**=p<0.001).66

Figure 20: Adipocyte pre-exposure diminishes the cytotoxic activity of ponatinib towards cancer cells. Effect of ponatinib containing medium or fibroblast/adipocyte-pre-exposed supernatant on NCI-H520 cancer cell survival. A) Colony formation capacity of NCI-H520 cells upon conditioning with medium or supernatant of ponatinib treated 3T3-L1/F and 3T3-L1/A cells. Ponatinib incubation of fibroblasts/adipocytes was for 24 h, conditioning of NCI-H520 cells lasted for 4 days. B) Cell quantification was performed by measuring re-dissolved crystal violet absorbance at 560 nm. Results were normalized according to the corresponding untreated controls, set to 1. Significance was calculated using two-way ANOVA with Bonferroni post-test (**=p<0.001).68

Figure 21: Adipocyte pre-exposure diminishes the cytotoxic activity of ponatinib towards cancer cells. Effect of ponatinib containing medium or fibroblast/adipocyte-pre-exposed supernatant on DMS114 cancer cell survival. A) Colony formation capacity of DMS114 cells upon conditioning with medium or supernatant of ponatinib treated 3T3-L1/F and 3T3-L1/A cells. Ponatinib incubation of fibroblasts/adipocytes was for 24 h, conditioning of DMS114 cells lasted for 4 days. B) Cell quantification was performed by measuring re-dissolved crystal violet absorbance at 560 nm. Results were normalized according to the corresponding untreated controls, set to 1. Significance was calculated using two-way ANOVA with Bonferroni post-test (**=p<0.001). C) Ponatinib inhibitory potential on MAPK and Akt signaling pathways in DMS114 cells following 24 h pre-exposure to fibroblasts/adipocytes was determined by Western blot. β -actin served as loading control.69

Figure 22: Intracellular ponatinib fluorescence is decreased in NCI-H1703/mCherry cells exposed to adipocyte-conditioned media. Ponatinib incubation of medium, 3T3-L1/F or 3T3-L1/A cells lasted for 24 h, followed by exposure to NCI-H1703/mCherry cells for 1 h. Ponatinib fluorescence was quantified by flow cytometry, using the Horizon V450 channel. Significance was calculated using two-way ANOVA with Bonferroni post-test (**=p<0.001).70

Figure 23: Ponatinib uptake is detectable in colon cryosections from orally treated mice. SCID mice, bearing lung tumor xenografts, were treated orally with 30 mg ponatinib per kg weight for 2 h. Mice were sacrificed and consecutive cryosections were generated. Ponatinib fluorescence was imaged by CLSM using DAPI and PI channels. Propidium iodide (PI) was used as nuclear counterstain. H/E staining was used as histologically control.72

Figure 24: Ponatinib uptake is detectable in small intestine cryosections from orally treated mice. SCID mice, bearing lung tumor xenografts, were treated orally with 30 mg ponatinib per kg weight for 2 h. Mice were sacrificed and consecutive cryosections were

generated. Ponatinib fluorescence was imaged by CLSM using DAPI and PI channels. Propidium iodide (PI) was used as nuclear counterstain. H/E staining was used as histologically control.	73
Figure 25: Ponatinib uptake is detectable in liver cryosections from orally treated mice.	
SCID mice, bearing lung tumor xenografts, were treated orally with 30 mg ponatinib per kg weight for 2 h. Mice were sacrificed and consecutive cryosections were generated. Ponatinib fluorescence was imaged by CLSM using DAPI and PI channels. Propidium iodide (PI) was used as nuclear counterstain. H/E staining was used as histologically control.	74
Figure 26: Ponatinib uptake is detectable in tumor cryosections from orally treated mice.	
SCID mice, bearing lung tumor xenografts, were treated orally with 30 mg ponatinib per kg weight for 2 h. Mice were sacrificed and consecutive cryosections were generated. Ponatinib fluorescence was imaged by CLSM using DAPI and PI channels. Propidium iodide (PI) was used as nuclear counterstain. H/E staining was used as histologically control.	74
Figure 27: Ponatinib imaging in adipose tissue cryosections is hampered by tissue auto-fluorescence.	
SCID mice, bearing lung tumor xenografts, were treated orally with 30 mg ponatinib per kg weight for 2 h. Mice were sacrificed and consecutive cryosections were generated. Ponatinib fluorescence was imaged by CLSM using DAPI and PI channels. Propidium iodide (PI) was used as nuclear counterstain.	75
Figure 28: Strong ponatinib-fluorescence intensity is detectable in simulated single cells of small intestine.	
SCID mice, bearing lung tumor xenografts, were treated orally with 30 mg ponatinib per kg weight for 2 h. Mice were sacrificed and consecutive cryosections were generated. Ponatinib fluorescence was quantified with Tissue Studio software. A) The DAPI channels of small intestine, colon and tumor 8-bit images were divided and colored in respect to the measured intensity ranges, given below the figure. B) Quantification of ponatinib fluorescence intensity in simulated single cells of small intestine, colon and tumor cryosections. Significance was calculated using D'Agostino and Pearson omnibus normality test, followed by two-tailed Mann-Whitney test (***=p<0.001).	76
Figure 29: The LD status influences the sensitivity of two cancer cell lines towards ponatinib.	
A) NCI-H1703 lung cancer and B) HeLa cervix carcinoma cells were exposed to increasing concentrations of ponatinib for 72 h. Depletion of LDs was with 0.1 μ M TC for 72 h, induction of LDs was with 100 μ M OA for 72 h. Viability was determined with MTT assay. Each data point represents the mean \pm SD of triplicate values of a representative experiment, performed in three times. Significance was calculated using two-way ANOVA with Bonferroni post-test (**=p<0.01; ***=p<0.001).	77
Figure 30: Ponatinib-resistant sublines of lung cancer cells show increased resistance towards ponatinib.	
DMS114 and NCI-H1703 parental- and ponatinib-resistant cells were exposed to increasing concentrations of ponatinib for 72 h. DMS114/PON and NCI-H1703/PON cells were exposed to ponatinib (10 μ M and 3 μ M, respectively) in constant	

intervals. Viability was determined with MTT assay. Each data point represents the mean \pm SD of triplicate values of a representative experiment, performed in three times.

Significance was calculated using two-way ANOVA with Bonferroni post-test (*= $p < 0.05$; ***= $p < 0.001$).....78

Figure 31: Ponatinib-resistant lung cancer cells show alterations in lipid content and fatty acid uptake.

A) Lipid droplet content of trypsinized DMS114 and ponatinib-resistant DMS114/PON cells was quantified by flow cytometry, using FITC channel. Bodipy 493/503 served as LD marker. DMS114/PON cells were exposed to 10 μ M of ponatinib in constant intervals. Significance was calculated using student's t-test (*= $p < 0.05$). B) Fatty acid uptake of DMS114 and DMS114/PON cells was measured by GC analysis. C) Total triglyceride and cholesterol content in ponatinib-naïve, -pretreated and -resistant DMS114 cells was determined by GC analysis. Ponatinib pre-treatment was with 1 μ M for 1 h. DMS114/PON cells were exposed to 10 μ M of ponatinib in constant intervals and also pre-treated 5 days prior to GC analysis with 1 μ M of ponatinib. Significance was calculated using student's t-test (**= $p < 0.01$). D) Total triglyceride content in ponatinib-resistant NCI-H1703 and ponatinib-naïve NCI-H1703 cells was determined by GC analysis. Ponatinib pre-treatment was with 1 μ M for 1 h. NCI-H1703/PON cells were exposed to 3 μ M of ponatinib in constant intervals and also pre-treated 5 days prior to GC analysis with 1 μ M of ponatinib. Significance was calculated using student's t-test (**= $p < 0.05$).....79

Figure 32: Ponatinib-resistant lung cancer cells show an increased ponatinib uptake.

DMS114 and DMS114/PON cells were exposed to 1 μ M of ponatinib for 30 min. Intracellular ponatinib content of DMS114 and DMS114/PON cells was quantified by flow cytometry of trypsinized cells, using Horizon V450-A channel. Significance was calculated using student's t-test.....80

Figure 33: Elevated levels of MTP and NR2F2 expression in ponatinib-resistant lung cancer cells.

A) Whole-genome gene expression revealed upregulated expression (16-fold) of MTP in DMS114/PON cells. B) Array comparative genomic hybridization (aCGH) showed normal copy number of *MTTP* (pink circle) on chromosome 4 (4q23) in DMS114/PON cells. C) Listed up- and deregulated alternative transcription factors for *MTTP* promotor region in DMS114/PON cells. D) Whole-genome gene expression revealed upregulated expression (4-fold) of NR2F2 in DMS114/PON cells, indicated by the blue line. aCGH and whole-genome expression array were performed by Bernhard Englinger, MSc, PhD.....81

Figure 34: MTP has a central role in cellular lipid homeostasis. *MTTP* gene expression in

DMS114/PON vs. DMS114 cells and the relation to lipoprotein homeostasis. The "fat digestion and absorption" KEGG pathway was colored using the Search&Color KEGG pathway mapping tool. The red color illustrates upregulated *MTTP* expression in DMS114/PON cells as compared to DMS114 cells.82

Figure 35: Massive upregulation of *MTTP* in ponatinib-resistant lung cancer cells. mRNA

expression levels of A) *MTTP* and B) *PLIN1* (Perilipin), *PLIN2* (ADRP), *PLIN3* (Tip47) in

DMS114 and DMS114/PON cells were quantified by qRT-PCR. Respective expression levels were normalized to the housekeeping gene β -actin (Δ CT) and converted to a linear form using $2^{-\Delta$ CT and further normalized to DMS114 by dividing the values with $2^{-\Delta$ CT from DMS114. Significance was calculated using student's t-test (**= $p < 0.001$; **= $p < 0.01$ and *= $p < 0.05$). 83

Figure 36: MTP overexpression on a protein level in ponatinib-resistant lung cancer cells.

MTP expression in DMS114 and DMS114/PON cells was determined by Western blot. β -actin served as loading control. 83

Figure 37: Decreased expression of MTP in ponatinib-resistant lung cancer cells after *MTTP* knockdown.

DMS114/PON cells were transfected with scrambled and MTP-siRNA using Xfect transfection reagent. MTP expression in DMS114/PON cells was determined by Western blot, 48 and 72 h after MTP knockdown. β -actin served as loading control. 84

Figure 38: *MTTP* knockdown increases resistance towards ponatinib and marginally increases LD- and ponatinib content in ponatinib-resistant lung cancer cells.

DMS114/PON cells were transfected with scrambled and MTP siRNA using Xfect transfection reagent. A) Cells were exposed to increasing concentrations of ponatinib for 72 h. Viability was determined with MTT assay. Each data point represents the mean \pm SD of triplicate values of a representative experiment, performed in three times. Significance was calculated using two-way ANOVA with Bonferroni post-test (*= $p < 0.05$; **= $p < 0.001$). B) Intracellular LD and ponatinib content was quantified by flow cytometry of trypsinized cells, using FITC and Horizon V450-A channel, respectively. Cells were exposed to ponatinib or Bodipy 493/503 for 30 min. Bodipy 493/503 served as LD marker. Significance was calculated using student's t-test. 85

Figure 39: Ponatinib-resistant lung cancer cells show increased resistance towards lomitapide.

DMS114 and DMS114/PON cells were exposed to increasing concentrations of lomitapide only (A) or in combination with ponatinib (B) for 72 h. DMS114/PON cells were exposed to 10 μ M of ponatinib in constant intervals. Viability was determined with MTT assay. Each data point represents the mean \pm SD of triplicate values of a representative experiment, performed in three times. Significance was calculated using two-way ANOVA with Bonferroni post-test (**= $p < 0.001$). 86

Figure 40: Pre-incubation with lomitapide increases LD- and ponatinib content, and contributes to an increased resistance towards ponatinib in ponatinib-resistant lung cancer cells.

A) DMS114 and DMS114/PON cells were pre-incubated with 2 μ M of lomitapide for 72 h. Cells were exposed to 500 nM of Bodipy 493/503 for 15 min or to 1 μ M of ponatinib for 30 min. Intracellular LD- and ponatinib content was quantified by flow cytometry of trypsinized cells, using FITC and DAPI channels, respectively. Bodipy 493/503 served as LD marker. Significance was calculated using student's t-test (**= $p < 0.01$ and *= $p < 0.05$). B) DMS114 and DMS114/PON cells were pre-incubated with 2 μ M for 72 h and compared to lomitapide-untreated DMS114/PON and DMS114 cells. All cells were exposed to increasing concentrations of ponatinib for 72 h. Viability was

determined with MTT assay. Each data point represents the mean \pm SD of triplicate values of a representative experiment, performed in three times. Significance was calculated using two-way ANOVA with Bonferroni post-test (**= $p < 0.001$).	87
Figure 41: Treatment with OA, but not with lomitapide increases LD accumulation in lung cancer cells. DMS114 cells were treated with 2 μ M of lomitapide and/or 100 μ M of OA for 24 h. Subcellular LD accumulation was analyzed by CLSM using FITC and Phalloidin-TRITC channels. Bodipy 493/503 served as LD marker, phalloidin-TRITC as actin staining. Scale bars indicate 50 μ M.....	88
Figure 42: Simultaneous treatment with lomitapide and OA massively increases LD accumulation in ponatinib-resistant lung cancer cells. DMS114/PON cells were treated with 2 μ M of lomitapide and/or 100 μ M of OA for 24 h. Subcellular LD accumulation was analyzed by CLSM using FITC and Phalloidin-TRITC channels. Bodipy 493/503 served as LD marker, phalloidin-TRITC as actin staining. Scale bars indicate 50 μ M.	89
Figure 43: Molecular structure, formula and weight of ponatinib and all six derivatives. All derivatives were designed and synthesized by Dipl. Ing. Marlene Mathuber.	91
Figure 44: Structural modifications impair the cytotoxic activity of ponatinib. Cytotoxicity of ponatinib and synthesized derivatives of ponatinib: MMAT057-2, MMAT077-3, MMAT066-2, MMAT040-3, MMAT081-1 and MMAT095-6 in DMS114, NCI-H520 and NCI-H1703 cells. Cells were exposed to increasing drug concentrations for 72 h. Viability was determined with MTT assay. Each data point represents the mean \pm SD of triplicate values of a representative experiment, performed in three times.....	92
Figure 45: Structural modifications alter the fluorescence intensity of ponatinib. Intracellular fluorescence of ponatinib and ponatinib derivatives MMAT057-2, MMAT077-3, MMAT066-2, MMAT040-3, MMAT081-1 and MMAT095-6 in NCI-H1703 cells after 30 min of incubation. Ponatinib and ponatinib derivative fluorescence was quantified by flow cytometry of NCI-H1703 cells treated with 10 μ M of respective drugs using the Horizon V450 channel.	93
Figure 46: Chemical modification strongly influences the subcellular distribution of ponatinib. Subcellular localization of ponatinib and the ponatinib derivatives MMAT057-2, MMAT077-3, MMAT066-2, MMAT040-3, MMAT081-1 and MMAT095-6 in NCI-H1703/mCherry cells determined by CLSM using mCherry, FITC and DAPI channels. Bodipy 493/503 was used as marker for LDs. Cells were incubated with 10 μ M of ponatinib or ponatinib derivatives for 1 h. Scale bars indicate 50 μ M.....	95
Figure 47: Chemical modification strongly influences the subcellular distribution of ponatinib. Subcellular localization of ponatinib and ponatinib derivatives MMAT057-2 and MMAT066-2 in NCI-H1703/mCherry cells determined by CLSM using mCherry, FITC and DAPI channels. Bodipy 493/503 was used as marker for LDs. Cells were incubated with 1 μ M of ponatinib or ponatinib derivatives for 1 h. Scale bars indicate 50 μ M.	97
Figure 48: LDs reduce the sensitivity of lung cancer cells towards gefitinib. NCI-H1703 cells were exposed to increasing concentrations of gefitinib for 72 h. Induction of LDs was	

with 100 μ M OA for 72 h. Viability was determined with MTT assay. Each data point represents the mean \pm SD of triplicate values of a representative experiment, performed in three times. Significance was calculated using two-way ANOVA (*= p <0.05). 98

Figure 49: Oleic acid (OA) leads to A) decreased activity of several drugs, and B) increased activity of irinotecan in a selected cancer cell line panel. Lipophilicity is given in logP values. Cytotoxic activity is given as fold changes, dividing the IC₅₀ values of the oleic acid pre-treated cell line by the IC₅₀ values of the non-pre-treated cell line. Decreased cytotoxic activity is depicted by positive (>1) fold changes. OA pre-treatment was with 100 μ M for 72 h. 105

Figure 50: Breast, brain and ovarian cancer cell lines show increased, oleic acid (OA)-dependent resistance towards several drugs differing in their lipophilicity. Lipophilicity is given in log P values. Cytotoxic activity is given as fold changes, dividing the IC₅₀ values of the oleic acid pre-treated cell line by the IC₅₀ values of the non-pre-treated cell line. OA pre-treatment was with 100 μ M for 72 h..... 106

Figure 51: LD-induction marginally increases ovarian cancer cell viability towards temozolomide in contrast to irinotecan. A2780 cells were exposed to increasing concentrations of irinotecan and temozolomide for 72 h. LD-induction was with 100 μ M OA, LD-depletion with 0.3 μ M TC, each for 72 h..... 107

Figure 52: Cell- and drug-specific, oleic acid (OA)-dependent effects showing increased resistance of cells and decreased toxicity of drugs. Cancer cells were exposed to increasing concentrations of the respective drug for 72 h. Induction of LDs was with 100 μ M OA for 72 h. Viability was determined with MTT assay. Each data point represents the mean \pm SD of triplicate values of a representative experiment, performed in three times. Significance was calculated using two-way ANOVA (*= p <0.05; **= p <0.01, ***= p <0.001). 108

List of Tables

<i>Table 1: List of distinct human cancer cell lines and the murine cell line utilized during this study.</i>	24
<i>Table 2: Chemicals utilized for differentiation of 3T3-L1 fibroblasts into adipocytes, for lowering lipids and induction or reduction of lipid droplet formation in different cell lines.</i>	25
<i>Table 3: siRNAs and plasmids used for transfection of cancer cells.</i>	26
<i>Table 4: List of transfection reagents used for this study and their respective provider.</i>	27
<i>Table 5: Fluorescent dyes that were used for specific staining of cells.</i>	27
<i>Table 6: Classification of drugs used in this study and their respective provider.</i>	28
<i>Table 7: Human cell lines and the murine cell lines with their respective culture media used in this study.</i>	32
<i>Table 8: Composition of the culture media for differentiation of 3T3-L1 fibroblasts into adipocytes.</i>	33
<i>Table 9: Used solutions for hematoxylin/eosin staining of organ slices in their applied order, including washing steps in-between. All solutions were prepared by the Filipits lab group.</i>	48
<i>Table 10: Composition of the master mix for mRNA transcription.</i>	51
<i>Table 11: List of used primers.</i>	53
<i>Table 12: SDS-PAGE ingredient recipe for a stacking (4.5 %) and separation gel (10%). Polymerization of each gel lasted for 30 min.</i>	55
<i>Table 13: List of primary antibodies that were used for Western blot analysis.</i>	56
<i>Table 14: List of drugs used in this study with their mode of action, approval, molecular structure and predicted or measured logP values.</i>	100

Abbreviations

°C	Degree Celsius
*	Significance level $p < 0.05$
**	Significance level $p < 0.01$
***	Significance level $p < 0.001$
µg	Micro gram
µL	Micro liter
µM	Micro molar
3T3-L1/A	Adipocytes
3T3-L1/F	Mouse embryonic fibroblasts
a.u.	Arbitrary unit
aCGH	Array comparative genomic hybridization
ADRP	Adipose differentiation related protein
AIDS	Acquired immunodeficiency syndrome
Akt	Protein Kinase B
ALK	Anaplastic lymphoma kinase
ALL	Acute lymphoblastic leukemia
AML	Acute myeloid leukemia
AMP	Adenosine monophosphate
ANOVA	Analysis of variance
APC	Allophycocyanin
APGAT	Acylglycerolphosphate acyltransferase
ApoB	Apolipoprotein B
APS	Ammonium Persulfate
ATCC	American Type Culture Collection
ATGL	Adipose triglyceride lipase
ATP	Adenosine triphosphate
BCR-ABL	Fusion gene where ABL from chromosome 9 translocates to the breakpoint cluster region on chromosome 22
BSA	Bovine serum albumin
cAMP	Cyclic adenosine-monophosphate
CAR-T	Chimeric Antigen Receptor T-cells
CD19	Follicular B-cell antigen
cDNA	Complementary Deoxyribonucleic acid
CLL	Chronic lymphocytic leukemia
CLSM	Confocal laser scanning microscopy

CML	Chronic myelogenous leukemia
CO₂	Carbon dioxide
DAG	Diacylglycerol
DAPI	4,6-diamidino-2-phenylindole
ddH₂O	Bidistilled water
DGAT2	Diacylglycerol acetyltransferase 2
DMSO	Dimethylsulfoxid
DNA	Deoxyribonucleic acid
dNTP	Nucleoside triphosphate
dsDNA	double-stranded DNA
DTT	Dithiothreitol
e.g.	Exempli gratia
ECL	Electrochemiluminescent
ECM	Extracellular matrix
ECM	Extracellular matrix
EDTA	Ethylenediaminetetraacetic acid
EGFR	Epidermal growth factor receptor
EMA	European Medicines Agency
EMT	Epithelial-to-mesenchymal transition
ER	Endoplasmic reticulum
Erk	Extracellular-signal regulated kinase
FA	Fatty acid
Fc	Fragment crystallizable region of an antibody
FC	Fold change
FCS	Fetal calf serum
FDA	Food and Drug Administration
FELASA	Federation of Laboratory Animal Science Associations
FGF	Fibroblast growth factor
FGFR	Fibroblast growth factor receptor
FITC	Fluorescein isothiocyanate
FRS2	Fibroblast growth factor receptor substrate 2
g	Gram or gravitational force
GDP	Guanosine diphosphate
GFP	Green Fluorescent Protein
GPAT	Glycerol-r-phosphate acyltransferase
GRB2	Growth factor receptor bound protein 2
GSEA	Gene set enrichment analysis

GTP	Guanosine triphosphate
GTPase	Enzyme that cleaves GTP, usually generating GDP
h	Hour
H₂O	Water
HCl	Hydrogen chloride
HER2	Human epidermal growth factor receptor 2
HRP	Horseradish peroxidase
HSL	Hormone-sensitive lipase
IBMX	3-Isobutyl-1-Methylxanthine
IC₅₀	Half maximal inhibitory concentration
ICR	Institute for Cancer Research
IP3	inositol (1,4,5)-triphosphate
JAK	Janus kinase
kDa	Kilo Dalton
KEGG	Kyoto Encyclopedia of Genes and Genomes
L	Liter, Litre
LD	Lipid droplet
logP	Partition coefficient
MAG	Monoacylglycerol
MAPK	Mitogen-activated protein kinase
MAPKK	Mitogen-activated protein kinase kinase
MAPKKK	Mitogen-activated protein kinase kinase kinase
mCherry	pQCXIP-mCherry-IRES-Puro plasmid
MEK	MAPK/Erk kinase
mg	Milligram
MGL	Monoacylglycerol lipase
min	Minute
mL	Mililitre
mM	Milimolar
mRNA	Messenger ribonucleic acid
MTT	3-(4,5-dimethylthiazol-2-yl)-2,5diphenyltetrazolium bromide
MTTP, MTP	Microsomal triglyceride transfer protein
Na₂HPO₄	Disodium phosphate
NaCl	Sodium chloride
NADPH	Nicotinamide adenine dinucleotide phosphate
NaOH	Sodium hydroxide
NCI	National Cancer Institute

ng	Nano gram
NHL	Non-Hodgkin lymphoma
nm	Nano meters
nM	Nanomolar
n.s.	Non-significant
NSCLC	Non-small cell lung cancer
OA	Oleic acid
OCT	Optimal cutting temperature
pAKT/pAkt	phospho Akt
PAP	Phosphatidic acid phosphatase
PARP	Poly (ADP-ribose) polymerase
PAT	Perilipin, ADRP, Tip47 family
PBS	Phosphate buffered saline
PD1	Programmed cell death protein 1
PDGFR	Platelet-derived growth factor receptor
PDL1	Programmed death ligand 1
pERK/pErk	phospho Erk
PFA	Paraformaldehyde
Ph	Philadelphia chromosome
PH	Pleckstrin homology
PI	Propidium Iodide
PI3K	Phosphatidylinositol 3-kinase
PIP2	Phosphatidylinositol-(4,5)diphosphate
PIP3	Phosphatidylinositol (3,4,5)-triphosphate
PKA	cyclic-AMP-dependent protein kinase A
PLCγ	Phospholipase C- γ
PMSF	Phenylmethylsulfonyl fluoride
PON	Ponatinib
PVDF	Polyvinylidene difluoride
qRT-PCR	Quantitative Real-Time Polymerase Chain Reaction
Rab	Ras-related in brain protein belonging to GTPase family
Raf	Serine/threonine-specific protein kinase, Rapidly accelerated fibrosarcoma
Ras	Protein of ras oncogene
RFP	Red Fluorescent Protein
RNA	Ribonucleic acid
RPMI	Roswell Park Memorial Institute medium

SCID	Severe combined immunodeficient mice
SCLC	Small-cell lung cancer
SD	Standard Deviation
SDS	Sodium dodecyl sulfate
SDS-PAGE	Sodium dodecyl sulfate polyacrylamide electrophoresis
Sec	Seconds
siRNA	Small interfering RNA
SOS	Son of sevenless
Src	Sarc, short for sarcoma
STAT	Signal transducers and activators of transcription
TAG	Triacylglycerol, triacylglyceride, triglyceride
TBS	Tris-buffered saline
TBS-T	Tris-buffered saline/Tween
TC	Triacin C
TCGA	The Cancer Genome Atlas
TEMED	Tetramethylethylenediamine
Tip47	Tail-interacting protein of 47 kDa
TKI	Tyrosine kinase inhibitor
Tris	Tris(hydroxymethyl)aminomethane
TRITC	Tetramethylrhodamine
USA	United States of America
VEGFR	Vascular endothelial growth factor
VLDL	Very-low density lipoprotein
w/v	Weight per volume
WHO	World Health Organization
z.B.	Zum Beispiel

References

1. Weinberg, R.A., *The biology of cancer*. Second edition. ed. 2014, New York: Garland Science, Taylor & Francis Group. xx, 876, A 6, G 30, I 28 pages.
2. World Health Organisation. *Cancer Fact Sheet*. 2018 [27.11.2018]; Available from: <http://www.who.int/en/news-room/fact-sheets/detail/cancer>.
3. Hanahan, D. and R.A. Weinberg, *The hallmarks of cancer*. Cell, 2000. **100**(1): p. 57-70.
4. Lambert, A.W., D.R. Pattabiraman, and R.A. Weinberg, *Emerging Biological Principles of Metastasis*. Cell, 2017. **168**(4): p. 670-691.
5. Vineis, P. and C.P. Wild, *Global cancer patterns: causes and prevention*. Lancet, 2014. **383**(9916): p. 549-57.
6. Stewart, B.W., et al., *World cancer report 2014*. 2014, Lyon, France Geneva, Switzerland: International Agency for Research on Cancer WHO Press. xiv, 630 pages.
7. Hanahan, D. and R.A. Weinberg, *Hallmarks of cancer: the next generation*. Cell, 2011. **144**(5): p. 646-74.
8. Austria, S., *Trends der Entwicklung von Krebserkrankungen in Österreich. Eine Prognose bis 2030.*, B.f.G. (BMG), Editor. 2015, Bundesministerium für Gesundheit (BMG). p. 158.
9. Ferlay, J., et al., *Estimating the global cancer incidence and mortality in 2018: GLOBOCAN sources and methods*. Int J Cancer, 2018.
10. National Cancer Institute at the National Institute of Health. *Surgery to Treat Cancer*. 2018; Available from: <https://www.cancer.gov/about-cancer/treatment/types/surgery>.
11. National Cancer Institute at the National Institute of Health. *Chemotherapy to Treat Cancer*. 2018; Available from: <https://www.cancer.gov/about-cancer/treatment/types/chemotherapy>.
12. National Cancer Institute at the National Institute of Health. *A to Z list of cancer drugs*. . 2018; Available from: <https://www.cancer.gov/about-cancer/treatment/drugs>.
13. National Cancer Institute at the National Institute of Health. *NCI Drug Dictionary*. 2018; Available from: <https://www.cancer.gov/publications/dictionaries/cancer-drug>.
14. National Cancer Institute at the National Institute of Health. *Radiation Therapy to Treat Cancer*. 2018; Available from: <https://www.cancer.gov/about-cancer/treatment/types/radiation-therapy>.
15. Zhang, H. and J. Chen, *Current status and future directions of cancer immunotherapy*. J Cancer, 2018. **9**(10): p. 1773-1781.
16. Arteaga, C.L., et al., *Treatment of HER2-positive breast cancer: current status and future perspectives*. Nat Rev Clin Oncol, 2011. **9**(1): p. 16-32.
17. Tokarew, N., et al., *Teaching an old dog new tricks: next-generation CAR T cells*. Br J Cancer, 2018.
18. Pardoll, D.M., *The blockade of immune checkpoints in cancer immunotherapy*. Nat Rev Cancer, 2012. **12**(4): p. 252-64.

19. Tsao, A.S., et al., *Scientific Advances in Lung Cancer 2015*. J Thorac Oncol, 2016. **11**(5): p. 613-638.
20. The Nobel Prize, *The Nobel Prize in Physiology or Medicine 2018*. 2018.
21. National Cancer Institute at the National Institute of Health. *Hormone Therapy to Treat Cancer*. 2018; Available from: <https://www.cancer.gov/about-cancer/treatment/types/hormone-therapy>.
22. Risbridger, G.P., et al., *Breast and prostate cancer: more similar than different*. Nat Rev Cancer, 2010. **10**(3): p. 205-12.
23. Katoh, M., *Fibroblast growth factor receptors as treatment targets in clinical oncology*. Nat Rev Clin Oncol, 2019. **16**(2): p. 105-122.
24. Health, N.C.I.a.t.N.I.o., *Targeted Cancer Therapies Fact Sheet*. 2019.
25. National Cancer Institute at the National Institute of Health, *Targeted Therapy to Treat Cancer*. 2018.
26. Brody, H., *Lung cancer*. Nature, 2014. **513**(7517): p. S1.
27. Giangreco, A., K.R. Groot, and S.M. Janes, *Lung cancer and lung stem cells: strange bedfellows?* Am J Respir Crit Care Med, 2007. **175**(6): p. 547-53.
28. Doll, R. and A.B. Hill, *Smoking and carcinoma of the lung; preliminary report*. Br Med J, 1950. **2**(4682): p. 739-48.
29. Torre, L.A., R.L. Siegel, and A. Jemal, *Lung Cancer Statistics*. Adv Exp Med Biol, 2016. **893**: p. 1-19.
30. Thompson, C.A., et al., *Smoking and lung cancer: current trends in Austria*. Wien Klin Wochenschr, 2012. **124**(15-16): p. 493-9.
31. Chen, Z., et al., *Non-small-cell lung cancers: a heterogeneous set of diseases*. Nat Rev Cancer, 2014. **14**(8): p. 535-46.
32. Lehman, J.M., M.E. Gwin, and P.P. Massion, *Immunotherapy and Targeted Therapy for Small Cell Lung Cancer: There Is Hope*. Curr Oncol Rep, 2017. **19**(7): p. 49.
33. Weiss, J., et al., *Frequent and focal FGFR1 amplification associates with therapeutically tractable FGFR1 dependency in squamous cell lung cancer*. Sci Transl Med, 2010. **2**(62): p. 62ra93.
34. Pietanza, M.C. and M. Ladanyi, *Bringing the genomic landscape of small-cell lung cancer into focus*. Nat Genet, 2012. **44**(10): p. 1074-5.
35. Vignaud, J.M., et al., *The role of platelet-derived growth factor production by tumor-associated macrophages in tumor stroma formation in lung cancer*. Cancer Res, 1994. **54**(20): p. 5455-63.
36. Murdoch, C., et al., *The role of myeloid cells in the promotion of tumour angiogenesis*. Nat Rev Cancer, 2008. **8**(8): p. 618-31.
37. Quail, D.F. and J.A. Joyce, *Microenvironmental regulation of tumor progression and metastasis*. Nat Med, 2013. **19**(11): p. 1423-37.
38. Sabari, J.K., et al., *Unravelling the biology of SCLC: implications for therapy*. Nat Rev Clin Oncol, 2017. **14**(9): p. 549-561.
39. Reck, M., et al., *Pembrolizumab versus Chemotherapy for PD-L1-Positive Non-Small-Cell Lung Cancer*. N Engl J Med, 2016. **375**(19): p. 1823-1833.
40. Englinger, B., et al., *Metal Drugs and the Anticancer Immune Response*. Chem Rev, 2018.
41. *Ponatinib*. Aust Prescr, 2015. **38**(6): p. 221-2.
42. Gainor, J.F. and B.A. Chabner, *Ponatinib: Accelerated Disapproval*. Oncologist, 2015. **20**(8): p. 847-8.

43. Narasimhan, N.I., et al., *Effects of food on the pharmacokinetics of ponatinib in healthy subjects*. J Clin Pharm Ther, 2013. **38**(6): p. 440-4.
44. Musumeci, F., et al., *Recent Studies on Ponatinib in Cancers Other Than Chronic Myeloid Leukemia*. Cancers (Basel), 2018. **10**(11).
45. Li, X., et al., *Fibroblast growth factors, old kids on the new block*. Semin Cell Dev Biol, 2016. **53**: p. 155-67.
46. Babina, I.S. and N.C. Turner, *Advances and challenges in targeting FGFR signalling in cancer*. Nat Rev Cancer, 2017. **17**(5): p. 318-332.
47. Turner, N. and R. Grose, *Fibroblast growth factor signalling: from development to cancer*. Nat Rev Cancer, 2010. **10**(2): p. 116-29.
48. Hallinan, N., et al., *Targeting the fibroblast growth factor receptor family in cancer*. Cancer Treat Rev, 2016. **46**: p. 51-62.
49. Walther, T.C. and R.V. Farese, Jr., *The life of lipid droplets*. Biochim Biophys Acta, 2009. **1791**(6): p. 459-66.
50. Onal, G., et al., *Lipid Droplets in Health and Disease*. Lipids Health Dis, 2017. **16**(1): p. 128.
51. Thiam, A.R., R.V. Farese, Jr., and T.C. Walther, *The biophysics and cell biology of lipid droplets*. Nat Rev Mol Cell Biol, 2013. **14**(12): p. 775-86.
52. Olofsson, S.O., et al., *Lipid droplets as dynamic organelles connecting storage and efflux of lipids*. Biochim Biophys Acta, 2009. **1791**(6): p. 448-58.
53. Martin, S. and R.G. Parton, *Lipid droplets: a unified view of a dynamic organelle*. Nat Rev Mol Cell Biol, 2006. **7**(5): p. 373-8.
54. Guo, Y., et al., *Lipid droplets at a glance*. J Cell Sci, 2009. **122**(Pt 6): p. 749-52.
55. Schuldiner, M. and M. Bohnert, *A different kind of love - lipid droplet contact sites*. Biochim Biophys Acta Mol Cell Biol Lipids, 2017. **1862**(10 Pt B): p. 1188-1196.
56. Yu, J. and P. Li, *The size matters: regulation of lipid storage by lipid droplet dynamics*. Sci China Life Sci, 2017. **60**(1): p. 46-56.
57. Zechner, R., et al., *Lipolysis: pathway under construction*. Curr Opin Lipidol, 2005. **16**(3): p. 333-40.
58. Koizume, S. and Y. Miyagi, *Lipid Droplets: A Key Cellular Organelle Associated with Cancer Cell Survival under Normoxia and Hypoxia*. Int J Mol Sci, 2016. **17**(9).
59. Beloribi-Djefafia, S., S. Vasseur, and F. Guillaumond, *Lipid metabolic reprogramming in cancer cells*. Oncogenesis, 2016. **5**: p. e189.
60. Chen, Y.Y. and P. Li, *Fatty acid metabolism and cancer development*. Science Bulletin, 2016. **61**(19): p. 1473-1479.
61. Potcoava, M.C., et al., *Raman and coherent anti-Stokes Raman scattering microscopy studies of changes in lipid content and composition in hormone-treated breast and prostate cancer cells*. J Biomed Opt, 2014. **19**(11): p. 111605.
62. Zietkowski, D., et al., *Comparison of NMR lipid profiles in mitotic arrest and apoptosis as indicators of paclitaxel resistance in cervical cell lines*. Magn Reson Med, 2012. **68**(2): p. 369-77.
63. Montopoli, M., et al., *"Metabolic reprogramming" in ovarian cancer cells resistant to cisplatin*. Curr Cancer Drug Targets, 2011. **11**(2): p. 226-35.

64. Yosef, H.K., et al., *In vitro prediction of the efficacy of molecularly targeted cancer therapy by Raman spectral imaging*. Anal Bioanal Chem, 2015. **407**(27): p. 8321-31.
65. Riss, T.L., et al., *Cell Viability Assays*, in *Assay Guidance Manual*, G.S. Sittampalam, et al., Editors. 2004: Bethesda (MD).
66. van Tonder, A., A.M. Joubert, and A.D. Cromarty, *Limitations of the 3-(4,5-dimethylthiazol-2-yl)-2,5-diphenyl-2H-tetrazolium bromide (MTT) assay when compared to three commonly used cell enumeration assays*. BMC Res Notes, 2015. **8**: p. 47.
67. Rafehi, H., et al., *Clonogenic assay: adherent cells*. J Vis Exp, 2011(49).
68. Goers, L., P. Freemont, and K.M. Polizzi, *Co-culture systems and technologies: taking synthetic biology to the next level*. J R Soc Interface, 2014. **11**(96).
69. Mathieu, V., et al., *Aggressiveness of human melanoma xenograft models is promoted by aneuploidy-driven gene expression deregulation*. Oncotarget, 2012. **3**(4): p. 399-413.
70. Green, H. and M. Meuth, *An established pre-adipose cell line and its differentiation in culture*. Cell, 1974. **3**(2): p. 127-33.
71. Brown, M. and C. Wittwer, *Flow cytometry: principles and clinical applications in hematology*. Clin Chem, 2000. **46**(8 Pt 2): p. 1221-9.
72. Frigault, M.M., et al., *Live-cell microscopy - tips and tools*. J Cell Sci, 2009. **122**(Pt 6): p. 753-67.
73. Paddock, S.W., *Confocal laser scanning microscopy*. Biotechniques, 1999. **27**(5): p. 992-6, 998-1002, 1004.
74. Laszlo, V., et al., *Epigenetic down-regulation of integrin alpha7 increases migratory potential and confers poor prognosis in malignant pleural mesothelioma*. J Pathol, 2015. **237**(2): p. 203-14.
75. Puujalka, E., et al., *Opposing Roles of JNK and p38 in Lymphangiogenesis in Melanoma*. J Invest Dermatol, 2016. **136**(5): p. 967-77.
76. Ritchie, M.E., et al., *limma powers differential expression analyses for RNA-sequencing and microarray studies*. Nucleic Acids Res, 2015. **43**(7): p. e47.
77. Gadkar, V. and M. Fillion, *New Developments in Quantitative Real-time Polymerase Chain Reaction Technology*. Curr Issues Mol Biol, 2014. **16**: p. 1-6.
78. Navarro, E., et al., *Real-time PCR detection chemistry*. Clin Chim Acta, 2015. **439**: p. 231-50.
79. Kim, T.K. and J.H. Eberwine, *Mammalian cell transfection: the present and the future*. Anal Bioanal Chem, 2010. **397**(8): p. 3173-8.
80. Jensen, E.C., *The basics of western blotting*. Anat Rec (Hoboken), 2012. **295**(3): p. 369-71.
81. Goulooze, S.C., A.F. Cohen, and R. Rissmann, *Lomitapide*. Br J Clin Pharmacol, 2015. **80**(2): p. 179-81.
82. Holohan, C., et al., *Cancer drug resistance: an evolving paradigm*. Nat Rev Cancer, 2013. **13**(10): p. 714-26.
83. Englinger, B., et al., *Intrinsic fluorescence of the clinically approved multikinase inhibitor nintedanib reveals lysosomal sequestration as resistance mechanism in FGFR-driven lung cancer*. J Exp Clin Cancer Res, 2017. **36**(1): p. 122.

84. Englinger, B., et al., *Lysosomal Sequestration Impairs the Activity of the Preclinical FGFR Inhibitor PD173074*. *Cells*, 2018. **7**(12).
85. Hoy, A.J., S. Balaban, and D.N. Saunders, *Adipocyte-Tumor Cell Metabolic Crosstalk in Breast Cancer*. *Trends Mol Med*, 2017. **23**(5): p. 381-392.
86. Rio, M.C., N. Dali-Youcef, and C. Tomasetto, *Local adipocyte cancer cell paracrine loop: can "sick fat" be more detrimental?* *Horm Mol Biol Clin Investig*, 2015. **21**(1): p. 43-56.
87. Nieman, K.M., et al., *Adipocytes promote ovarian cancer metastasis and provide energy for rapid tumor growth*. *Nat Med*, 2011. **17**(11): p. 1498-503.
88. Tabuso, M., et al., *Role of tissue microenvironment resident adipocytes in colon cancer*. *World J Gastroenterol*, 2017. **23**(32): p. 5829-5835.
89. Kwan, H.Y., et al., *Subcutaneous adipocytes promote melanoma cell growth by activating the Akt signaling pathway: role of palmitic acid*. *J Biol Chem*, 2014. **289**(44): p. 30525-37.
90. Sheng, X. and S.D. Mittelman, *The role of adipose tissue and obesity in causing treatment resistance of acute lymphoblastic leukemia*. *Front Pediatr*, 2014. **2**: p. 53.
91. Tebbe, C., et al., *Metformin limits the adipocyte tumor-promoting effect on ovarian cancer*. *Oncotarget*, 2014. **5**(13): p. 4746-64.
92. White, N.S. and R.J. Errington, *Fluorescence techniques for drug delivery research: theory and practice*. *Adv Drug Deliv Rev*, 2005. **57**(1): p. 17-42.
93. Miller, M.A. and R. Weissleder, *Imaging of anticancer drug action in single cells*. *Nat Rev Cancer*, 2017. **17**(7): p. 399-414.
94. Shitara, Y., T. Horie, and Y. Sugiyama, *Transporters as a determinant of drug clearance and tissue distribution*. *Eur J Pharm Sci*, 2006. **27**(5): p. 425-46.
95. Clive G. Wilson, P.J.C., *Controlled Release in Oral Drug Delivery*, ed. Springer US. 2011. 414.
96. Artursson, P. and S.D. Knight, *Structural biology. Breaking the intestinal barrier to deliver drugs*. *Science*, 2015. **347**(6223): p. 716-7.
97. Estudante, M., et al., *Intestinal drug transporters: an overview*. *Adv Drug Deliv Rev*, 2013. **65**(10): p. 1340-56.
98. Lanao, J.M. and M.A. Fraile, *Drug tissue distribution: study methods and therapeutic implications*. *Curr Pharm Des*, 2005. **11**(29): p. 3829-45.
99. Davies, C.L., et al., *Effect of gamma-linolenic acid on cellular uptake of structurally related anthracyclines in human drug sensitive and multidrug resistant bladder and breast cancer cell lines*. *Eur J Cancer*, 1999. **35**(10): p. 1534-40.
100. Schug, Z.T., et al., *Acetyl-CoA synthetase 2 promotes acetate utilization and maintains cancer cell growth under metabolic stress*. *Cancer Cell*, 2015. **27**(1): p. 57-71.
101. Swift, L.L., et al., *Microsomal triglyceride transfer protein expression in adipocytes: a new component in fat metabolism*. *FEBS Lett*, 2005. **579**(14): p. 3183-9.
102. Hussain, M.M., J. Shi, and P. Dreizen, *Microsomal triglyceride transfer protein and its role in apoB-lipoprotein assembly*. *J Lipid Res*, 2003. **44**(1): p. 22-32.

103. Swift, L.L., et al., *Microsomal triglyceride transfer protein contributes to lipid droplet maturation in adipocytes*. PLoS One, 2017. **12**(8): p. e0181046.
104. Liu, X., et al., *Efficacy and Safety of Lomitapide in Hypercholesterolemia*. Am J Cardiovasc Drugs, 2017. **17**(4): p. 299-309.
105. U.S. National Library of Medicine. *APOA1 gene*. Genetics Home Reference 2019; Available from: <https://ghr.nlm.nih.gov/gene/APOA1>.
106. Raabe, M., et al., *Knockout of the abetalipoproteinemia gene in mice: reduced lipoprotein secretion in heterozygotes and embryonic lethality in homozygotes*. Proc Natl Acad Sci U S A, 1998. **95**(15): p. 8686-91.
107. O'Hare, T., et al., *AP24534, a pan-BCR-ABL inhibitor for chronic myeloid leukemia, potently inhibits the T315I mutant and overcomes mutation-based resistance*. Cancer Cell, 2009. **16**(5): p. 401-12.
108. Frankfurt, O. and J.D. Licht, *Ponatinib--a step forward in overcoming resistance in chronic myeloid leukemia*. Clin Cancer Res, 2013. **19**(21): p. 5828-34.
109. Smith, D.A. and Royal Society of Chemistry (Great Britain), *Metabolism, pharmacokinetics and toxicity of functional groups : impact of the building blocks of medicinal chemistry in ADMET*. RSC drug discovery. 2010, Cambridge, UK: RSC Pub. xiv., 530 p.
110. Leeson, P.D. and B. Springthorpe, *The influence of drug-like concepts on decision-making in medicinal chemistry*. Nat Rev Drug Discov, 2007. **6**(11): p. 881-90.
111. T. E. Peck, S.A.H., M. Williams,, *Pharmacology for Anaesthesia and Intensive Care, Third Edition*, ed. C.U. Press. Cambridge University Press. 378.
112. Schlaepfer, I.R., et al., *Progesterin modulates the lipid profile and sensitivity of breast cancer cells to docetaxel*. Mol Cell Endocrinol, 2012. **363**(1-2): p. 111-21.
113. Cotte, A.K., et al., *Lysophosphatidylcholine acyltransferase 2-mediated lipid droplet production supports colorectal cancer chemoresistance*. Nat Commun, 2018. **9**(1): p. 322.
114. Price, D.A., et al., *Physicochemical drug properties associated with in vivo toxicological outcomes: a review*. Expert Opin Drug Metab Toxicol, 2009. **5**(8): p. 921-31.
115. Chang, W., et al., *Trapping toxins within lipid droplets is a resistance mechanism in fungi*. Sci Rep, 2015. **5**: p. 15133.
116. Drugbank. *Curcumin*. 2019; Available from: <https://www.drugbank.ca/drugs/DB11672>.
117. Zhang, I., et al., *Pharmacological inhibition of lipid droplet formation enhances the effectiveness of curcumin in glioblastoma*. Eur J Pharm Biopharm, 2016. **100**: p. 66-76.
118. Drugbank. *Docetaxel*. 2019; Available from: <https://www.drugbank.ca/drugs/DB01248>.
119. Rohwedder, A., et al., *Lipid droplet formation in response to oleic acid in Huh-7 cells is mediated by the fatty acid receptor FFAR4*. Journal of Cell Science, 2014. **127**(14): p. 3104-3115.
120. Mehdizadeh, A., et al., *Common chemotherapeutic agents modulate fatty acid distribution in human hepatocellular carcinoma and colorectal cancer cells*. Bioimpacts, 2017. **7**(1): p. 31-39.

